

The Texas Medical Center Library

DigitalCommons@TMC

The University of Texas MD Anderson Cancer
Center UTHealth Graduate School of
Biomedical Sciences Dissertations and Theses
(Open Access)

The University of Texas MD Anderson Cancer
Center UTHealth Graduate School of
Biomedical Sciences

8-2010

NHERF1 – New Modifier of Colorectal Cancer Progression

Yuho Hayashi

Follow this and additional works at: https://digitalcommons.library.tmc.edu/utgsbs_dissertations



Part of the [Cancer Biology Commons](#)

Recommended Citation

Hayashi, Yuho, "NHERF1 – New Modifier of Colorectal Cancer Progression" (2010). *The University of Texas MD Anderson Cancer Center UTHealth Graduate School of Biomedical Sciences Dissertations and Theses (Open Access)*. 71.

https://digitalcommons.library.tmc.edu/utgsbs_dissertations/71

This Dissertation (PhD) is brought to you for free and open access by the The University of Texas MD Anderson Cancer Center UTHealth Graduate School of Biomedical Sciences at DigitalCommons@TMC. It has been accepted for inclusion in The University of Texas MD Anderson Cancer Center UTHealth Graduate School of Biomedical Sciences Dissertations and Theses (Open Access) by an authorized administrator of DigitalCommons@TMC. For more information, please contact digitalcommons@library.tmc.edu.

The
TMC LIBRARY
Health Sciences Resource Center

**NHERF1 – NEW MODIFIER OF COLORECTAL CANCER
PROGRESSION**

A

DISSERTATION

**Presented to the Faculty of
The University of Texas
Health Science Center at Houston
and
The University of Texas
M. D. Anderson Cancer Center
Graduate School of Biomedical Sciences
in Partial Fulfillment**

of the Requirements

for the Degree of

DOCTOR OF PHILOSOPHY

by

**Yuho Hayashi, M.Sc.
Houston, Texas**

August, 2010

DEDICATION

To my parents; my sisters; and to the memory of my furry little friend, Raki.

ACKNOWLEDGMENTS

I would like to first acknowledge my mentor, Dr. Maria-Magdalena Georgescu, for working with me to make this dissertation possible. I learned a great deal from Maria over these past three years, not just about science but many things about life, too. I especially thank her for always standing by me with her full and cheerful support. She also always extended me her hand whenever I was in trouble; and, often, shared with me many little good news to celebrate with her. I was inspired by the many ways she approaches work – her discipline, strength, enthusiasm, persistence, and all-out effort. I thank her very much for all her help, all her teachings, and all her encouragement through today; I will always take a lot of pride in having been a student in her lab.

Drs. Gil Cote, Benoit de Crombrughe, Pierre McCrea, and Carolyn Van Pelt – these are my thesis committee, incredibly nice and supportive people, too. I would like to thank them tremendously for all their time, their help, advice, and support for me.

Drs. Fabiana Morales, Erica Kreimann, Yoko Takahashi, Jennifer Molina, Nitin Agarwal; and Safan Momin – these are the past and present members of Dr. Georgescu's lab that I had the privilege of working with. I especially thank Fabiana and Safan for working with me as I started in the lab; they walked me through many protocols, and gave me many nice hints about how to make things not just good, but better.

Mr. Hank Adams taught me a great deal of microscopy. My work is half as colorful without him and his microscope. Dr. Stan Hamilton provided us with, and helped me analyze, the special CRC specimens; Drs. Alan Hall and Noriko Kaji, our collaborators in New York, taught me how to culture Caco-2 cells in 3D and stain them. I would like to thank the GSBS deans Drs. Jon Wiener, Tom Goka, and Vicky Knutson for all their tremendous help throughout my program in GSBS. I also thank my GSBS friend, Ben Chou, for his company in the lab, and Drs. Michael Barratt and Shang-Jin Shi for many years of their friendship in the space sector, and for the inspirations that they give me through their work.

“Only as high as I reach can I grow, only as far as I seek can I go, only as deep as I look
can I see, only as much as I dream can I be.”

- Karen Ravn

NHERF1 – NEW MODIFIER OF COLORECTAL CANCER PROGRESSION

Publication No. _____

Yuho Hayashi, M.Sc.

Supervisory Professor: Maria-Magdalena Georgescu, M.D., Ph.D.

Colorectal cancer (CRC) develops from multiple progressive modifications of normal intestinal epithelium into adenocarcinoma. Loss of cell polarity has been implicated as an early event in this process, but the molecular players involved are not well known. NHERF1 (Na⁺/H⁺ Exchanger Regulatory Factor 1) is an adaptor protein with apical membrane localization in polarized epithelia. In this study, we tested our hypothesis that NHERF1 plays a role in CRC. We examined surgical CRC resection specimens for changes in NHERF1 expression, and modeled these changes in two- and three-dimensional (2D and 3D) Caco-2 CRC cell systems. NHERF1 had significant alterations from normal to adenoma and carcinoma transitions ($\chi^2=38.5$, d.f.=4, $P<0.001$), displaying apical membrane localization in normal tissue but loss of expression in adenoma and ectopic overexpression in carcinoma. In Caco-2 cell models, NHERF1 depletion induced epithelial-mesenchymal-transition in 2D cell monolayers and disruption of apical-basal polarity in 3D cyst system. The mesenchymal phenotype of NHERF1-depleted cells was fully restored by re-expression of NHERF1 at the apical membrane. Cytoplasmic and nuclear NHERF1 re-expression not only failed to restore the epithelial phenotype but led to more aggressive phenotypes. Our findings suggest that membrane NHERF1 is an important regulator of epithelial morphogenesis, and that changes in NHERF1 expression correlate with CRC progression. NHERF1 loss and ectopic expression that induce massive disruption of epithelial cell polarity may, thereby, mark important steps in CRC development.

TABLE OF CONTENTS

	Page
LIST OF ILLUSTRATIONS	xi
LIST OF TABLES	xiv
ABBREVIATIONS	xv
LIST OF PUBLICATIONS	xvii
CHAPTER 1. INTRODUCTION	1
1.1 Colorectal cancer	2
1.2 Genomic instability in colorectal cancer	2
1.3 Loss of adenomatous polyposis coli	5
1.4 Loss of epithelial cell polarity	7
1.5 Na ⁺ /H ⁺ Exchanger Regulatory Factor 1 (NHERF1)	9
1.5.1 NHERF adaptor	9
1.5.2 NHERF1 in cells and tissues	10
1.5.3 NHERF in cancer	12
1.6 Phenotypes of NHERF1 deficiency in mice.....	13
1.7 Study objective	15
CHAPTER 2. MATERIAL AND METHODS	17
2.1 CRC resection specimens and tissue microarray	18
2.2 Tissue staining	18
2.2.1 H&E staining	18

	Page
2.2.2 Immunofluorescence (IF)	19
2.2.3 Immunohistochemistry (IHC)	19
2.3 Image acquisition	21
2.3.1 IF images	21
2.3.2 Brightfield images	23
2.4 Image analyses	23
2.4.1 IF/IHC signal intensity analysis	23
2.4.2 Nuclear localization analysis	23
2.5 Immunoblot analysis of frozen tissues	24
2.6 Cell culture	24
2.7 Plasmids	24
2.8 Transfection and retroviral infection	25
2.9 Epithelial morphogenesis assay	26
2.10 Cell morphology assay	28
2.11 Migration assay	28
2.12 Invasion assay	28
2.13 Gelatin zymography	29
2.14 Proliferation assay	30
2.15 Whole cell lysis	30
2.16 Immunoblotting	30
2.17 Immunofluorescence of cells (IF-C) in 2D monolayer culture	31

	Page
2.18 Statistical analysis	33
CHAPTER 3. RESULTS	35
3.1 CRC case study	36
3.1.1 Patient demographics and H&E analyses	36
3.1.2 IF and IHC analyses.....	36
<i>3.1.2.1 Altered NHERF1 expression in adenoma and carcinoma</i>	<i>36</i>
<i>3.1.2.2 Nuclear NHERF1 at the invasive front of carcinoma</i>	<i>40</i>
<i>3.1.2.3 NHERF1-positive T lymphocytes</i>	<i>40</i>
3.1.3 Immunoblot analysis	49
3.2 CRC tissue microarray	53
3.2.1 IHC analysis	53
<i>3.2.1.1 Analysis by three groups of tumor grade</i>	<i>53</i>
<i>3.2.1.2 Analysis by four groups of IHC-NHERF1 intensity scores</i>	<i>53</i>
<i>3.1.1.3 Serial analyses with b-catenin, E-cadherin, and cytokeratin</i>	<i>57</i>
3.2.2 IF analysis	61
<i>3.2.2.1 Nuclear localization analyses of NHERF1</i>	<i>61</i>
3.3 CRC cell study	72
3.3.1 Screening of human intestinal cells	72
3.3.2 NHERF1 knockdown in Caco-2 cells	72
3.3.3 Re-establishment of epithelial phenotypes by Myr-NHERF1	77

	Page
3.3.4 <i>Apical targeting of Myr-NHERF1 requires tail EB-region</i>	85
3.3.5 <i>NHERF1-depleted Caco-2 cysts</i>	91
3.3.6 <i>Polarized distributions of AKT and PTEN in Caco-2 cysts</i>	96
CHAPTER 4. DISCUSSION	100
4.1 Initial summary	101
4.2 NHERF1 and epithelial morphogenesis	101
4.3 NHERF1 loss and ectopic overexpression	104
4.4 Theoretical and clinical considerations	105
4.5 Future aims	106
4.5.1 Mechanism of NHERF1 loss in colorectal tumorigenesis	106
4.5.2 Role of cytoplasmic and nuclear NHERF1 in CRC invasion	107
4.5.3 Cooperation between NHERF1 & b-catenin in Apc ^{Min/+} mouse model ..	108
4.6 Conclusions	109
REFERENCES	111

LIST OF ILLUSTRATIONS

	Page
FIGURE 1.1 The risk of colorectal cancer by different age groups	3
FIGURE 1.2 Anatomy of the colon	4
FIGURE 1.3 A simplified two-step model of CRC development	6
FIGURE 1.4 Polarized organization of intestinal epithelium	8
FIGURE 1.5 NHERF family members and their domain structures	11
FIGURE 1.6 Apical membrane localization of NHERF1 in mouse colon	14
FIGURE 1.7 Intestinal microvilli of NHERF(+/+) and (-/-) mice	16
FIGURE 3.1 Post-CRC diagnosis survival status of patients in CRC case study	38
FIGURE 3.2 Normal, adenoma, and carcinoma areas in CRC resection specimens ...	39
FIGURE 3.3 Area comparisons of NHERF1 intracellular distribution	41
FIGURE 3.4 Loss of NHERF1 expression in carcinoma	42
FIGURE 3.5 Cytoplasmic overexpression of NHERF1 in carcinoma	43
FIGURE 3.6 Quantitative analysis of IF data for NHERF1 loss	44
FIGURE 3.7 Quantitative analysis of IF data for cytoplasmic NHERF1 overexpressi.	45
FIGURE 3.8 Nuclear NHERF1 at the leading edges of invasive tumor cells	46
FIGURE 3.9 More nuclear NHERF1 at the leading edges of invasive tumor cells	47
FIGURE 3.10 NHERF1-positive immune cells infiltrate the colonic mucosa	48
FIGURE 3.11 Characterization of NHERF1-positive immune cells	51
FIGURE 3.12 Low molecular weight form of NHERF1 in carcinoma	52
FIGURE 3.13 IHC-stained TMA section with NHERF1 antibody	54
FIGURE 3.14 Distribution of NHERF1 intensity scores in CRC TMA samples	56

	Page
FIGURE 3.15 IHC-NHERF1 intensity scores of TMA samples by groups	58
FIGURE 3.16 IHC-NHERF1 staining of TMA samples by groups	59
FIGURE 3.17 IHC- β -catenin intensity scores of TMA samples by groups	62
FIGURE 3.18 IHC-E-cadherin intensity scores of TMA samples by groups	63
FIGURE 3.19 IHC-cytokeratin intensity scores of TMA samples by groups	64
FIGURE 3.20 IHC- β -catenin staining of TMA samples by groups	65
FIGURE 3.21 IHC-E-cadherin staining of TMA samples by groups	66
FIGURE 3.22 IHC-cytokeratin staining of TMA samples by groups	67
FIGURE 3.23 Nuclear localization analysis of NHERF1 and β -catenin in TMA sam.	68
FIGURE 3.24 NHERF1 IF staining of TMA samples by groups	71
FIGURE 3.25 Screening of six CRC cell lines for NHERF1 expression	73
FIGURE 3.26 Subcellular localization of NHERF1 in Caco-2 cells	74
FIGURE 3.27 NHERF1 depletion by two shRNAs (sh1 and sh4) in Caco-2 cells	75
FIGURE 3.28 EMT for NHERF1-depleted Caco-2 cells	76
FIGURE 3.29 Nuclear β -catenin in NHERF1-depleted Caco-2 cells	78
FIGURE 3.30 Migration assay in NHERF1-depleted Caco-2 cells	79
FIGURE 3.31 Invasion assay in NHERF1-depleted Caco-2 cells	80
FIGURE 3.32 Gelatin zymography for NHERF1-depleted Caco-2 cells	81
FIGURE 3.33 Wild-type NHERF1 overexpression in NHERF1-depleted Caco-2 cell.	82
FIGURE 3.34 Myr-NHERF1 overexpression in NHERF1-depleted Caco-2 cells	83
FIGURE 3.35 NLS-NHERF1 overexpression in NHERF1-depleted Caco-2 cells	84

	Page
FIGURE 3.36 Epithelial-like morphology of Myr-NHERF1-reconstituted Caco-2	86
FIGURE 3.37 Migration assay of Myr-NHERF1-reconstituted Caco-2 cells	87
FIGURE 3.38 β -catenin redistribution in Myr-NHERF1-reconstituted Caco-2 cells ...	88
FIGURE 3.39 Apical vs. lateral distribution of Myr-NHERF1 and Myr-PDZ1-2	90
FIGURE 3.40 Confluent cell morphology with Myr-NHERF1 and Myr-PDZ1-2	89
FIGURE 3.41 Development of Caco-2 3D cyst	92
FIGURE 3.42 Apical PM formation in Caco-2 cysts	93
FIGURE 3.43 Loss of cell polarity in NHERF1-depleted Caco-2 spheroids	94
FIGURE 3.44 Nuclear b-catenin in NHERF1-depleted Caco-2 spheroids	95
FIGURE 3.45 Basal distribution of HA-AKT in Caco-2 cysts	97
FIGURE 3.46 Apical distribution of Myc-PTEN in Caco-2 cysts	99
FIGURE 4.1 Model of the NHERF1 role in CRC development	110

LIST OF TABLES

	Page
TABLE 2.1 Primary antibodies used for IF/IHC in N-A-C samples and TMA	20
TABLE 2.2 Primary antibodies used for IHC of NHERF1-positive immune cells	22
TABLE 2.3 Primary antibodies used for epithelial morphogenesis assay	27
TABLE 2.4 Primary antibodies used for immunoblotting	32
TABLE 2.5 Primary antibodies used for IF-C in 2D monolayer culture	34
TABLE 3.1 Demographic characteristics of patients in CRC case study	37
TABLE 3.2 IHC-NHERF1 intensity scores of TMA samples by tumor grade	55
TABLE 3.3 IHC-NHERF1 intensity scores of TMA samples by groups and patient	60

ABBREVIATIONS

CRC	colorectal cancer
APC	adenomatous polyposis coli
FAP	familial adenomatous polyposis
NHERF1	Na ⁺ /H ⁺ Exchanger Regulatory Factor 1
NHE	Na ⁺ /H ⁺ Exchanger
BBM	brush border membrane
ERM	ezrin-radixin-moesin
EBP50	ERM-binding phosphoprotein 50 kDa
PSD-95	Post-synaptic density-95 kDa
Dlg	Discs Large
ZO-1	Zonula occludin-1
PDZ	PSD-95/Dlg/ZO-1
EB	ERM-binding
IHC	immunohistochemistry
IF	immunofluorescence
ER	estrogen receptor
TCF	T-cell factor
LOH	loss of heterozygosity
IECs	intestinal epithelial cells
MEFs	mouse embryonic fibroblasts

ECM	extracellular matrix
TMA	tissue microarray
NLS	nuclear localization signal
2D	two-dimensional
EMT	Epithelial-mesenchymal transition
3D	three-dimensional
PIP3	phosphatidylinositol-3,4,5-triphosphate
PIP2	phosphatidylinositol-4,5-bisphosphate

LIST OF PUBLICATIONS

Yokoyama, T., Iwado, E., Kondo, Y., Aoki, H., **Hayashi, Y.**, Georgescu, M. M., Sawaya, R., Hess, K. R., Mills, G. B., Kawamura, H., *et al.* (2008a). Autophagy-inducing agents augment the antitumor effect of telomerase-sense oncolytic adenovirus OBP-405 on glioblastoma cells. *Gene Ther* 15, 1233-1239.

Yokoyama, T., Miyazawa, K., Naito, M., Toyotake, J., Tauchi, T., Itoh, M., Yuo, A., **Hayashi, Y.**, Georgescu, M. M., Kondo, Y., *et al.* (2008b). Vitamin K2 induces autophagy and apoptosis simultaneously in leukemia cells. *Autophagy* 4, 629-640.

Morales, F. C., Molina, J. R., **Hayashi, Y.**, De Orbeta-Cruz, J., and Georgescu, M. M. (2008). Emerging roles of NHERF1/EBP50 in cancer. In *Adaptor Proteins and Cancer* (Old City Publishing, Inc.), pp. 187-208.

Georgescu, M. M., Morales, F. C., Molina, J. R., and **Hayashi, Y.** (2008). Roles of NHERF1/EBP50 in cancer. *Curr Mol Med* 8, 459-468.

Morales, F. C., Molina, J. R., **Hayashi, Y.**, and Georgescu, M. M. (2010). Overexpression of ezrin inactivates NF2 tumor suppressor in glioblastoma. *Neuro Oncol* 12, 528-539.

Molina, J. R., **Hayashi, Y.**, Stephens, C., and Georgescu, M. M. (2010a). Invasive glioblastoma cells acquire stemness and increased Akt activation. *Neoplasia* 12, 453-463.

Molina, J. R., Morales, F. C., **Hayashi, Y.**, Aldape, K., and Georgescu, M. M. (2010b). Loss of PTEN binding adapter protein NHERF1 from plasma membrane in glioblastoma contributes to PTEN inactivation. *Cancer Res* *In press*.

Hayashi, Y., Molina, J. R., Hamilton, S. R., and Georgescu, M. M. (2010). NHERF1/EBP50 is a new marker in colorectal cancer. *Neoplasia* *In press*.

CHAPTER 1

INTRODUCTION

1.1 Colorectal cancer

Colorectal cancer (CRC), also known as large bowel cancer, is the fourth common type of cancer in the United States. The lifetime risk of CRC is 1 in 20 (5%) for both men and women. In 2009 alone, 147,000 new cases were diagnosed, as were 50,000 deaths due to CRC reported (Jemal et al., 2009). The etiology of CRC remains unclear, but multiple factors, including both hereditary and environmental influences, are posited to play roles. In particular, the incidence of CRC has long been recognized to increase steeply after middle age (FIGURE 1.1); and this has been thought to relate to the multi-stage theory of carcinogenesis as postulated over 50 years ago (Armitage and Doll, 1954; Foulds, 1954). On the basis of kinetic data that the incidence of human cancer is increased by 10^3 - 10^7 -folds over age, it has been taken to require three to seven rate-limiting events, or four to six decades of human lifetime, before cancer becomes clinically manifest (Vogelstein and Kinzler, 1993). The American Cancer Society (ACS) currently recommends men and women over age 50 to have screening colonoscopy every 10 years, or less invasive alternatives, such as sigmoidoscopy, CT (computed tomography) colonoscopy, and double-contrast barium enema every 5 years, for prevention and/or early detection of CRC (Walsh and Terdiman, 2003; Yeatman, 2003) (FIGURE 1.2).

1.2 Genomic instability in colorectal cancer

Most human CRC is considered a non-inherited condition, yet it shows many features of genetic abnormalities such as microsatellite instability, aneuploidy (changes

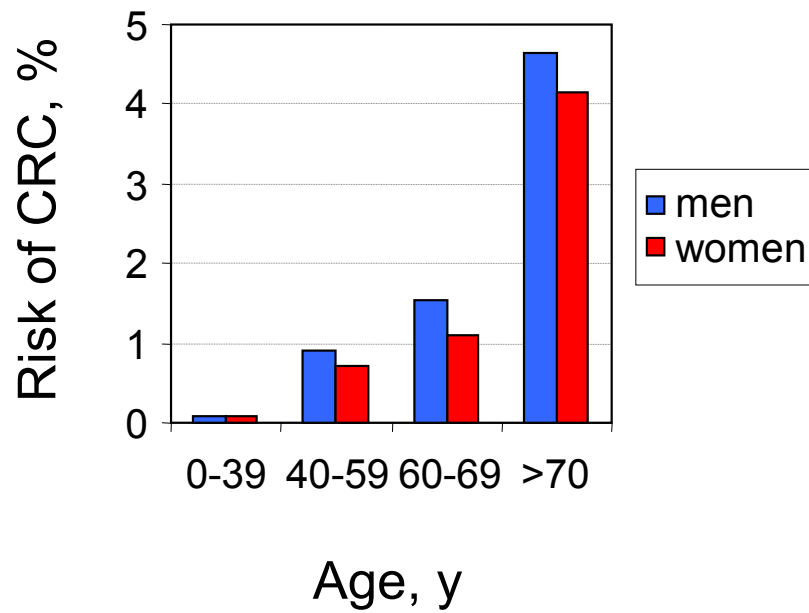


FIGURE 1.1 The risk of colorectal cancer by different age groups. Note steep increases in the risk of colorectal cancer (CRC) for both men and women after age 40-59 (Jemal et al., 2009).

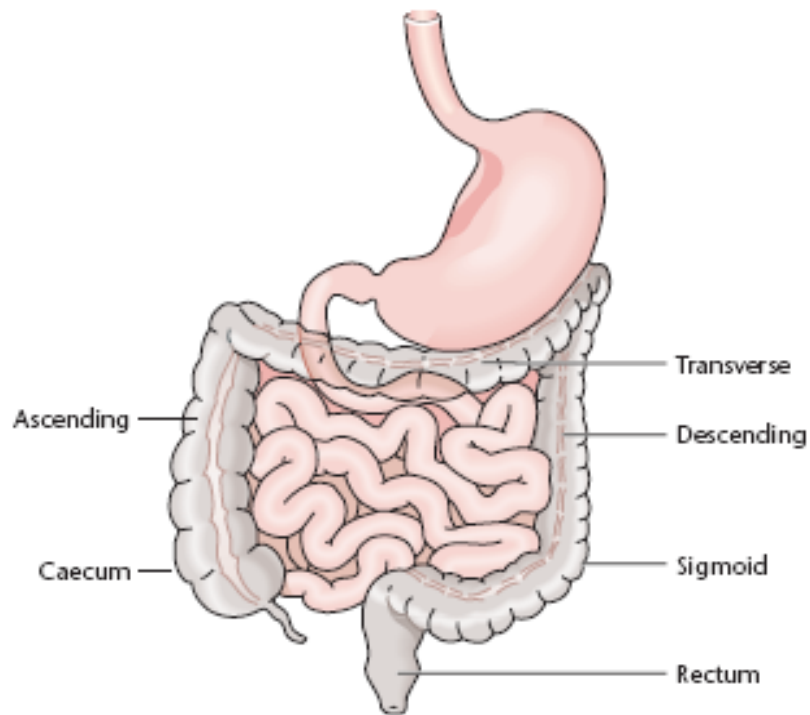


FIGURE 1.2 Anatomy of the colon. Four sections of the colon: caecum/ascending, transverse, descending, and sigmoid, are shown. Note the rectum at the most distal portion of the colon. In colonoscopy, colon is endoscopically examined with a CCD or fiber optic camera from the rectum up to the distal small intestine. Less invasive alternatives to colonoscopy is sigmoidoscopy, which examines only from the rectum up to the sigmoid section of the colon; CT colonography uses images reconstructed from CT scans; and double-contrast barium enema, the X-ray scans. Reprinted with permission from Yeatman, Encyclopedia of Life Sciences, Macmillan Publishers Ltd., 2001. Copyright © 2001 Macmillan Publishers Ltd.

in chromosome number), chromosome fusions, and gene amplifications (Lengauer et al., 1998). A long-standing postulate has been that these abnormalities represent a mutator phenotype that underlies the development of tumor growth (Loeb, 1991). In a landmark study by Vogelstein et al., colorectal tumor specimens ranging in the stages of neoplastic development were assayed for *KRAS* mutation and allelic deletions of chromosomes 5, 7, and 18 (Vogelstein et al., 1988). The results indicated that the frequency of *KRAS* mutation increased from 9% in adenomas <1 cm in size to 58% in those over 1 cm; on the other hand, deletions of chromosome 5, 17, and 18 were each observed in selected stages of adenoma or carcinoma. A multi-step genetic model of CRC development has since been proposed to consist both of activating mutations in an oncogene and of losses of multiple tumor suppressor genes (Fearon and Vogelstein, 1990). A simplified two-step model was re-drawn and presented in FIGURE 1.3.

1.3 Loss of adenomatous polyposis coli

One of the earliest altered genes in the development of CRC is the adenomatous polyposis coli (APC) (Fearon and Vogelstein, 1990; Powell et al., 1992). The *APC* gene localized on chromosome 5 (5q21) was initially identified as a chromosomal region deleted in rare familial adenomatous polyposis (FAP) syndrome (Bodmer et al., 1987; Leppert et al., 1987); incidentally, this locus is also frequently involved in the non-familial form of CRC (Ashton-Rickardt et al., 1989; Solomon et al., 1987; Vogelstein et al., 1988). Nucleotide sequence analyses of FAP and non-familial CRC tumor specimens suggested that somatic mutations of the *APC* gene initiated the development of tumor growth in both cases; over 60% of these mutations were clustered in a focal region in

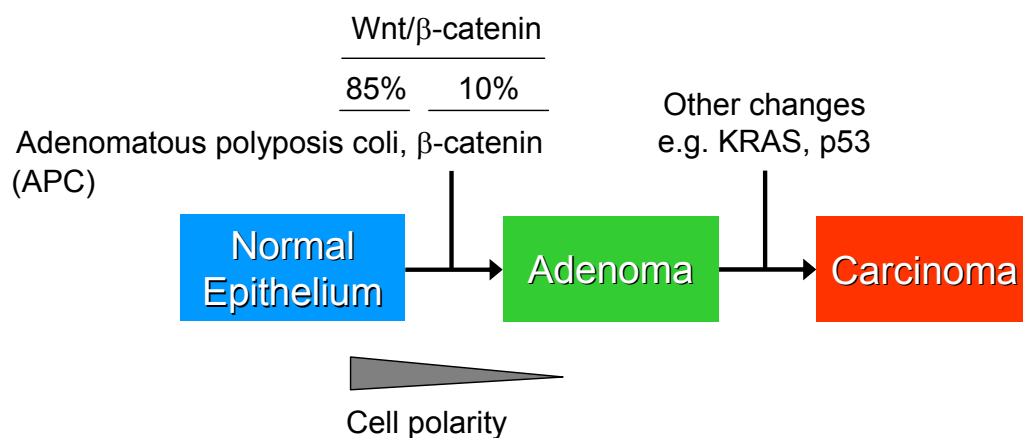


FIGURE 1.3 A simplified two-step model of CRC development. CRC is developed in two distinct steps. In first step, normal epithelium is transformed into (benign) adenoma. This process is believed to involve oncogenic activation of the Wnt/ β -catenin pathway; and, in most cases, occurs from inactivating mutation of the adenomatous polyposis coli (APC) gene. In some cases, however, activating mutation of β -catenin itself is also seen. In second step, other changes, such as mutation of KRAS and p53, promote transformation of adenoma into (invasive) carcinoma. Note also loss of cell polarity early in the transformation process.

exon 15, and were predicted to result in truncations of the cellular APC gene product (Miyoshi et al., 1992).

Currently the best known function of cellular APC protein is in acting as a negative regulator of β -catenin (Bienz and Clevers, 2000; Polakis et al., 1999). It appears that these two proteins closely interact, as has been shown that full-length, but not truncated, APC can be co-immunoprecipitated with β -catenin in CRC cells (Rubinfeld 1993, Su 1993). Cytoplasmic β -catenin level is seen to be elevated in CRC cells in the absence of wild-type APC, but can be reduced by forced expression of exogenous protein (Munemitsu et al., 1995). The elevated intracellular β -catenin level in the absence of wild-type APC has been further associated with constitutive activation of the β -catenin/T cell factor (TCF)-dependent transcription (Korinek et al., 1997; Morin et al., 1997). Among the target genes activated in this pathway are identified as c-Myc and cyclin D1 oncogenes (He et al., 1998; Tetsu and McCormick, 1999). A possible link between functional inactivation of APC, oncogenic activation of β -catenin, and the attending initiation of oncogenic growth was thereby implicated.

1.4 Loss of epithelial cell polarity

Intestinal epithelium has polarized structures, consisting of linearly arranged IECs with asymmetrically organized apical membrane, basolateral membrane, and tight junctions (zonula occludens) that separates them (FIGURE 1.4). There have been increasingly frequent mentions of the association between loss of epithelial polarity and the initiation of tumor growth (Aranda et al., 2008; Feigin and Muthuswamy, 2009;

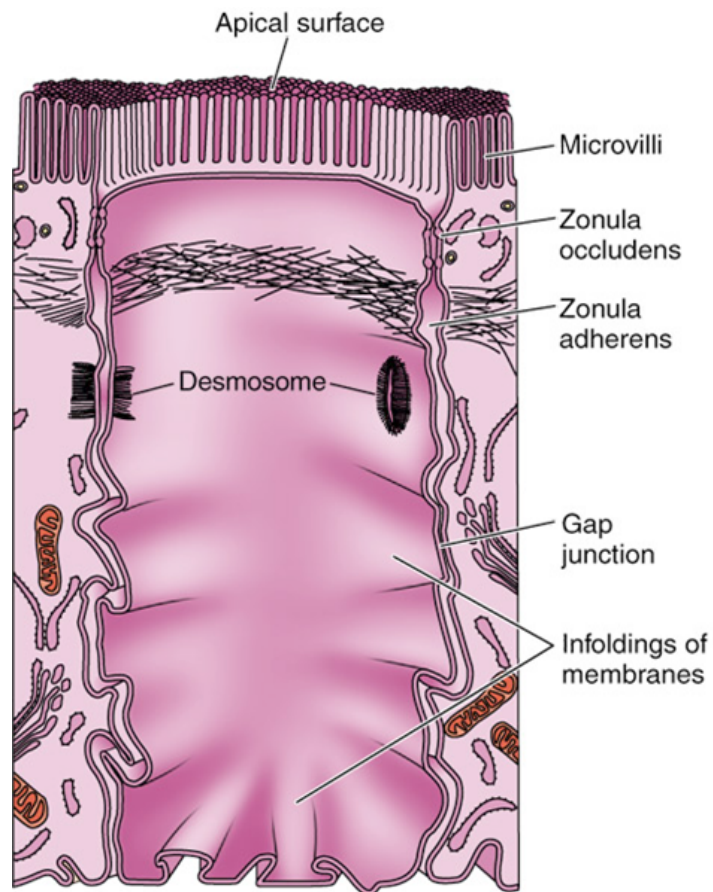


FIGURE 1.4 Polarized organization of intestinal epithelium. Intestinal epithelium has polarized structure. Note apical membrane, basolateral membrane, and tight junctions (zonula occludens) that separates the two membrane domains. Reprinted with permission from Junquiera and Carneiro, Basic Histology 11th edition, McGraw-Hill, 2005. Copyright © 2005 The McGraw-Hill Companies.

Huang and Muthuswamy, 2010; Lee and Vasioukhin, 2008; Mullin, 2004). Although molecular details of the relationship between cell polarity and tumor growth are still mostly missing, studies in *Drosophila* have implicated the role of three basolateral polarity proteins Lgl, Dlg, and Scrib in linking the cell polarity and growth pathways (Bilder et al., 2000). Others, more recently, indicated alterations in the members of apical polarity complex in human cancer, such as those of Par3, Par6, and aPKC (Nolan et al., 2008; Regala et al., 2005; Zen et al., 2009). Another apically localized protein, Na⁺/H⁺ exchanger regulatory factor 1 (NHERF1), will be the subject of this study, as below.

1.5 Na⁺/H⁺ exchanger regulatory factor 1 (NHERF1)

1.5.1 NHERF adaptors

NHERF1 (also known as NHE-RF) is a protein co-factor initially isolated for the regulation of Na⁺/H⁺ exchanger (NHE) activity from rabbit renal brush border membrane (BBM) (Weinman et al., 1993; Weinman et al., 1995). The cDNA analysis indicated that the *NHERF1* gene (*SLC9A3R1*) encoded a 358-residue protein, with two elements of repeat (amino acids 11-101 and 150-241) in predicted amino acid sequences (Weinman et al., 1995). Subsequently, ezrin-radixin-moesin (ERM)-binding phosphoprotein of 50 kDa (EBP50) was identified as the human homolog of NHERF1, and found to contain two elements of repeat over two-thirds of its full-length molecule (amino acids 11-97 and 149-236) (Reczek et al., 1997). Database searches on these elements gave a number of matched results; among included in this list were rat brain

post-synaptic density protein (PSD-95), *Drosophila* septate junction protein Discs Large (Dlg), and mouse tight junctions protein zonula occludin-1 (ZO-1). The repeat elements of NHERF1 were thereby identified as the PDZ (PSD-95/Dlg/ZO-1) domains. These are conserved protein modules that form a small binding pocket for short hydrophobic peptide sequences on the carboxyl-terminal end of their target proteins (Fanning and Anderson, 1996; Saras and Heldin, 1996).

Four members of the NHERF family, including NHERF1 (NHE-RF, EBP50), NHERF2 (E3KARP, SIP-1, TKA-1), NHERF3 (PDZK1, CLAMP, CAP70, DIPHOR-1, NaPi-CaP1), and NHERF4 (IKEPP, DIPHOR-2, NaPi-CaP2), have been identified to date (Donowitz et al., 2005). All four members have multiple PDZ domains, with an additional non-PDZ ERM-binding (EB) region for NHERF1 and NHERF2 but not the other two (Murthy et al., 1998; Reczek and Bretscher, 1998; Yun et al., 1998) (FIGURE 1.5). NHERF1 and NHERF2 also share over 35 common ligands (Shenolikar et al., 2004; Weinman et al., 2006); though, *in vivo*, the two proteins likely serve different functions. Their inter- and intra-tissue distributions do not appear to overlap (Fouassier et al., 2001; Ingraffea et al., 2002; Wade et al., 2003; Wade et al., 2001); neither is the deficiency of NHERF1 compensated by NHERF2 in the renal proximal tubules in mice *in vivo* (Shenolikar et al., 2002; Weinman et al., 2003).

1.5.2 NHERF1 in cells and tissues

Human NHERF1 mRNA is expressed at high levels in polarized epithelia, including liver, salivary gland, kidney, pancreas, trachea, adrenal glands, intestines,

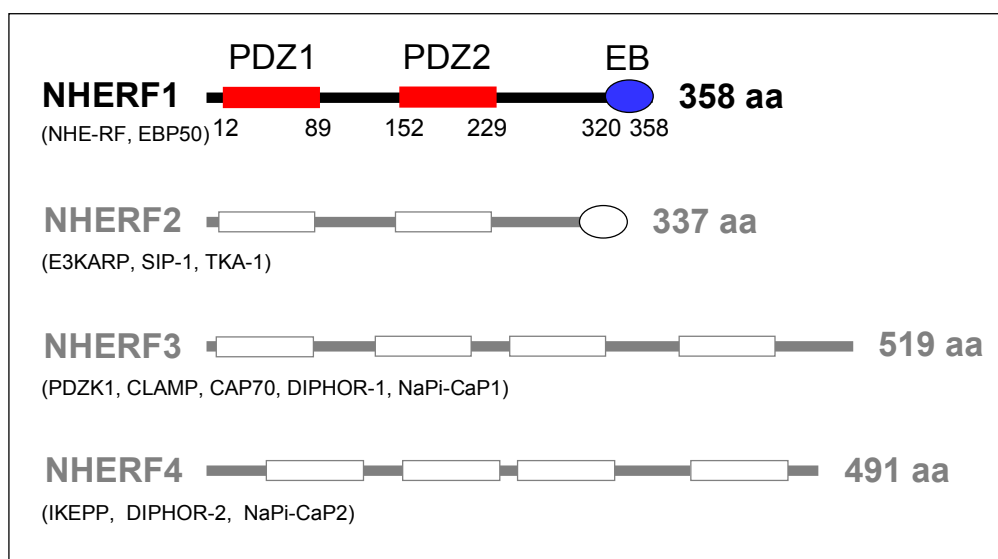


FIGURE 1.5 NHERF family members and their domain structures. Human NHERF1, a 358-residue protein, contains two PDZ (PSD-95/Dlg/ZO-1) domains (red) and a carboxyl-terminal ERM-binding region (EB, blue). Three other NHERF family members are also shown with multiple PDZ domains; their alternative names are noted in parentheses. The domain analysis was performed with NCBI Conserved Domain Database (CDD).

prostate, and mammary gland (Ediger et al., 1999). Immunohistochemistry (IHC) studies have shown that NHERF1 in many of these tissues is selectively localized at the apical membrane of absorptive cells, whereas secretory cells are negative for staining (Stemmer-Rachamimov et al., 2001). Immunofluorescence (IF) studies in mouse and rat tissues had corroborating results. NHERF1 has been detected in the apical microvilli of intestinal (Ingraffea et al., 2002; Reczek et al., 1997) and renal proximal tubule BBM (Reczek and Bretscher, 1998; Wade et al., 2001; Waite and Eng, 2002), in mesothelia of the stomach (Ingraffea et al., 2002), and at the canalicular (apical) membranes of both hepatocytes and cholangiocytes (Fouassier et al., 2001; Ingraffea et al., 2002).

1.5.3 NHERF1 in cancer

The role of NHERF1 in human cancer was first suggested in 2001 (Stemmer-Rachamimov et al., 2001). This pertained to the observation of a strong positive association between NHERF1 expression and estrogen receptor (ER) status in 18 breast cancer specimens. As NHERF1 had been earlier shown as an estrogen-inducible gene (Ediger et al., 1999), the elevated NHERF1 level in ER-positive tumors was posited as a predictable sequelae of estrogenic stimulation. Additional analyses of breast carcinoma specimens indicated that the association between NHERF1 expression and ER status indeed existed, but indications also were that NHERF1 was more likely accumulated in tumors of later than earlier disease stage, with lymph node-positive than -negative status and poorer than better prognosis index (Cardone et al., 2007; Song et al., 2007). Possible involvements of NHERF1 in breast cancer progression were thereby implicated.

A number of studies have since examined NHERF1 in this and several other human neoplasia. Of particular note is a study which reported NHERF1 interaction with β -catenin in hepatocellular carcinoma (Shibata et al., 2003). The additional indications were that NHERF1 accumulated in the cytoplasm and nucleus in these tumors, and that it promoted β -catenin/TCF-dependent transcription. NHERF1, in this context, appeared as an oncogenic protein. Two studies, however, have since presented a contrasting view that NHERF1 is rather a tumor suppressor protein. In the first of these two studies, allelic deletion of the *NHERF1* gene locus at 17q25.1 was described at 22-58% frequency in breast cancer cells and tissue specimens, with increased tumor aggressiveness with loss of heterozygosity (LOH) (Dai et al., 2004). In another study, NHERF1 was knocked down in ER-positive T47D and MCF7 breast cancer cells; this induced increased cell proliferation both *in vivo* and *in vitro*, indicating growth-suppressive role of NHERF1 in these two breast cancer cells (Pan et al., 2006). The current literature thus has conflicting data that are difficult to explain. Reconciliation has been offered, in that NHERF1 may have a dual functional role; and that its action as an oncogene or else as a tumor suppressor may be dictated by its subcellular localization (Georgescu et al., 2008).

1.6 Phenotypes of NHERF1 deficiency in mice

Our laboratory has generated NHERF1 (-/-) mice, and has found intestinal defects as among their main phenotypes. NHERF1, as others have found, is strongly expressed at the apical membrane of intestines in these mice (FIGURE 1.6). The observed

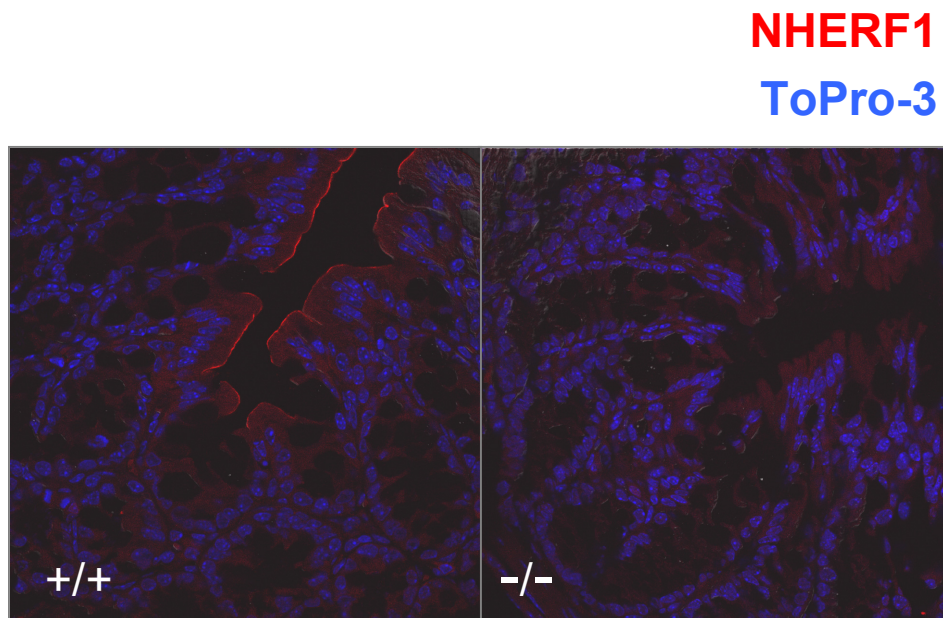


FIGURE 1.6 Apical membrane localization of NHERF1 in mouse colon. Confocal IF analysis of colon in six week-old C57BL/6J NHERF1 wild-type (+/+) and knockout (-/-) female mice is shown. Note strong apical membrane expression of NHERF1 (red). Nuclei were marked with ToPro-3 (blue).

defects included overt ultrastructural abnormalities in the intestinal microvilli of BBM (FIGURE 1.7); altered composition of intestinal epithelial cells (IECs) (Morales et al., 2004); and increased length of the intestinal tracts in both male and female mice at 18 months of age (data not shown). The additional finding was that NHERF1 (-/-) mouse embryonic fibroblasts (MEFs) but not their wild-type counterparts displayed anchorage-independent growth in soft agar colony assay (Kreimann et al., 2007). Taken altogether, the inferences from these mouse studies were that NHERF1 may have a role in the regulation of apical morphogenesis in the intestine *in vivo*; that it may regulate the growth of IECs; and that it acted as a tumor suppressor, at least in MEFs *in vitro*.

1.7 Study objective

Given the current literature that implicates the role of NHERF1 in cancer, and the results of our NHERF1 (-/-) mouse studies that indicated strong phenotypes in the intestine, the main objective of this study was to examine if NHERF1 plays a role in human CRC. Specifically, we hypothesized that NHERF1 may act as a tumor suppressor in normal human colon and that it may be lost or altered in CRC. The three-part study consisted of the following: (1) NHERF1 expression and subcellular localization were examined in normal human colonic mucosa, adenoma, and carcinoma specimens (Chapter 3.1); (2) NHERF1 expression and subcellular localization were examined in CRC tissue microarray (TMA) (Chapter 3.2); and (3) NHERF1 alterations in CRC were modeled in cultured 2D and 3D Caco-2 CRC cell systems (Chapter 3.3).

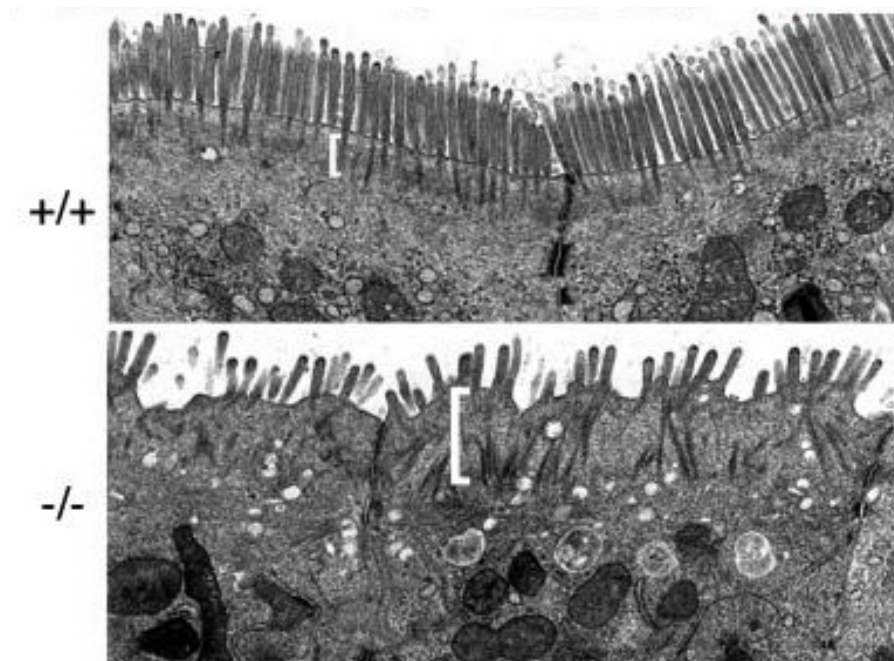


FIGURE 1.7 Intestinal microvilli of NHERF1(+/+) and (-/-) mice. Transmission electron microscopy of ileum from 5-week-old littermates. Note ordered, rod-like microvilli emerging from a structured terminal web region (bracket) in EBP50(+/+), contrasting with the EBP50(-/-) disorganized microvilli and thick terminal web. x12,000. Reprinted with permission from Morales et al., Proc Natl Acad Sci USA, 2004; 101(51): 17705-17710. Copyright © 2004 National Academy of Sciences, U.S.A.

CHAPTER 2

MATERIAL AND METHODS

2.1 CRC resection specimens and tissue microarray

Eleven paraffin-embedded surgical CRC resection specimens and seven additional liquid nitrogen-frozen specimens were obtained from the Institutional Tumor Bank at M. D. Anderson Cancer Center. Surgeries for all cases had been performed in a 15-year period between 1992 and 2007, with no patient receiving prior treatment. All paraffin-embedded specimens contained areas of normal mucosa, adjacent adenoma, and carcinoma on the same slide. Frozen specimens had pathologist-annotated vials of normal mucosa, deep-tumor, and tumor-edge as normal, carcinoma, and adenoma, respectively. The TARP (Tissue Array Research Program) colon and lung (T-CL-1) TMA was obtained from the U.S. National Cancer Institute-Center for Cancer Research (NIH-CCR) (http://ccr.cancer.gov/tech_initiatives/tarp/). This array by design contained 89 CRC specimens with 0.6-mm cores space at 0.8 mm. Approximately three-quarters of the samples (74-83% of 89 samples) had actually usable tissues.

2.2 Tissue staining

2.2.1 H&E staining

Paraffin-embedded sections were serially treated in xylene (10 min x3), graded ethanol: 100% (10 min x2), 95% (10 min x1), 70% (10 min x1), and ddH₂O (10 min x1); and were stained with hematoxylin (Fisher Scientific, #23-245-651) for 3 min. After a rinse in ddH₂O for 2 min, the sections were blued in tap water for 5 min; de-stained in 0.2% acid alcohol (70% ethanol with 0.2% HCl) for 30 sec; and rinsed in ddH₂O for 2 min. The sections were then stained with eosin (Fisher Scientific, #323-314-631) for 30

sec; rinsed in ddH₂O for 2 min; and dehydrated in graded ethanol: 95% (2 min x1) and 100% (2 min x1). The sections were cleared in xylene; and Permount (Fisher Scientific, #SP15-100) was used to mount the slides.

2.2.2 Immunofluorescence (IF)

Sections were deparaffinated and hydrated as above (see section 2.2.1); and heat-induced antigen retrieval was performed in a vegetable steamer for 20 min in 1/10x Target Retrieval Solution (Dako, #S1699). All sections were cooled for 10 min at room temperature; then rinsed in ddH₂O for 5 min three times. Blocking was performed with 20-50% donkey serum (Sigma, #G9023) in PBS for 30 min at room temperature. The primary antibodies (listed in TABLE 2.2) were applied in PBS in a humidified chamber at 4°C overnight. Next day, the sections were washed in PBS for 5 min three times; and one or both of the secondary antibodies Alexa Fluor 488 donkey anti-rabbit IgG and Alexa Fluor 555 donkey anti-mouse IgG (Molecular Probes, #A21206 and #A31570, respectively) was applied at 1:500 for 45 min, covered with aluminum foil. After three 5-min washes of the sections in PBS, ToPro-3 iodide (Molecular Probes, #T3605) was applied at 1:2000 in PBS for 20 min. After two final 5-min washes in PBS, Slowfade Gold antifade reagent (Invitrogen, #S36936) was applied to mount the slides.

2.2.3 Immunohistochemistry (IHC)

Manual staining. Sections were deparaffinated and hydrated as above (see section 2.2.1); and endogenous hydrogen peroxidase activity was quenched by treatment

<u>Antibody</u>	<u>Use</u>	<u>Product</u>	<u>Dilution</u>
NHERF1	IF, IHC	Affinity BioReagents, #PA1-090	1:300
β -catenin	IF, IHC	BD Biosciences, #C19220	1:300
E-cadherin	IHC	BD Biosciences, #C20820	1:100
Cytokeratin	IHC	Sigma, #C1801	1:100

TABLE 2.1 Primary antibodies used for manual IF/IHC tissue staining.

of the sections in 3% hydrogen peroxide in methanol for 10 min at room temperature. After three 2-min washes of the sections in PBS, heat-induced antigen retrieval was performed for 20 min as described above (see section 2.2.2). Blocking was performed using 1A and 1B solutions of the Histomouse-Max kit (Zymed Laboratories, #87-9551) for 30 min and 10 min at room temperature, respectively. The primary antibodies (listed in TABLE 2.2) were then applied in PBS at 4°C overnight. Next day, the sections were washed in PBS for 2 min three times; and 3,3'-diaminobenzidine (DAB) staining and nuclear hematoxylin counterstaining were performed per manufacturer's instructions of the Histomouse-Max kit. The sections were dehydrated in graded ethanol: 70% (5 min x1), 95% (5 min x1), 100% (5 min x2); cleared in xylene; and mounted using Histomount of the kit.

Automated staining. Five sections of CRC specimens were submitted to an American Society of Clinical Pathology/Texas Society of Histotechnology (ASCP/TSH)-certified Clinical Histology Laboratory, on-site at M. D. Anderson Cancer Center. The following primary antibodies: CD3, CD4, CD8, CD20, CD68 (listed in TABLE 2.3) were used to perform IHC staining in an automated Leica Bond-I system.

2.3 Image acquisition

2.3.1 IF images

Multi-channel IF images were acquired using the Zeiss LSM 510 confocal laser scanning microscope, with excitation laser lines of 488 nm (green), 543 nm (red), and 633 nm (far red); and differential interference contrast (DIC). For all images, the

<u>Antibody</u>	<u>Marker</u>	<u>Product</u>	<u>Dilution</u>
CD3	T cell	Dako, #A0452	1:100
CD4	Helper T cell	Novacastra, #NCL-L-368	1:80
CD8	Cytotoxic T cell	Dako, #MS-457-S	1:20
CD20	B cell	Dako, #M0755	1:1400
CD68	Macrophage	Dako, #M0814	1:500

TABLE 2.2 Primary antibodies used for automated IHC tissue staining.

40x/1.30 NA (numerical aperture) objective lens with oil immersion was used. All images were processed with the LSM 510 software, version 4.2.

2.3.2 Brightfield images

H&E and IHC images were acquired using the Nikon 80i upright microscope and Nikon DS-U2/L2 USB camera, with the 4x/0.2, 10x/0.45, an 20x/0.75 NA dry objective lenses. All images were processed with the NIS Elements AR software, version 3.1.

2.4 Image analyses

2.4.1 IF/IHC signal intensity analysis

Quantitative signal intensity analysis of selected IF/IHC images was performed in an 8-bit ($2^8 = 256$) gray densitometry scale from 0 (black) to 255 (white). The sample region of interest was circled using the NIH Image J software, version 1.34s; mean signal intensity was measured; and signal intensity score, x , was computed as $x = [255 - (\text{mean intensity reading})]$.

2.4.2 Nuclear localization analysis

Nuclear localization analysis of the triple IF-stained TMA samples was performed using co-localization analysis mode of the Bitplane AG Imaris x64 software, version 6.3.0. Data outputs were tallied as %Alexa 488 (green)/ToPro-3 co-localized voxels (nuclear *green*); %Alexa 568 (red)/ToPro-3 co-localized voxels (nuclear *red*);

and %Alexa 488/Alexa 568/ToPro-3 co-localized voxels (nuclear *green/red* co-localization).

2.5 Immunoblot analysis of frozen tissues

All tissues were stored at -80°C until use. The whole tissue lysates were prepared by homogenizing the samples with a motorized pestle (Kontes, #K749540-0000), in the same 1% Triton X-100 buffer and protease inhibitor cocktails as that used for whole cell lysis (see section 2.15). Protein concentration was measured and immunoblotting was performed as described (see sections 2.15 and 2.16).

2.6 Cell culture

The Caco-2 colon adenocarcinoma cells (a gift from Dr. Alan Hall, Memorial Sloan-Kettering Cancer Center, NY) were grown in a 50/50 mixture of Dulbecco modified Eagle's medium/Ham's F-12 nutrients (DMEM/F-12) supplemented with 10% fetal calf serum (FCS) (Hyclone, #SH30910-03) and 1/100x antibiotic-antimycotic (Invitrogen, #15240-062). The 293T human embryonic kidney cells were grown in DMEM, also supplemented with 10% FCS and 1/100x antibiotic-antimycotic.

2.7 Plasmids

NHERF1 shRNA#1 (ACCCATCCTAGACTTCAA) and shRNA#4 (GGGAAACT GACGAGTTTCGG) were cloned in the pSIREN-RetroQ retroviral vector (puromycin selection), as previously described (Kreimann et al., 2007). Wild-type

NHERF1 (358 residues) had been previously cloned in the pCX_b vector (Kreimann et al., 2007). The myristoylation signal of v-Src, MGSSKSKPKDPSQR, and the nuclear localization signal (NLS) of SV40 T antigen, PKKKRKV, were added N-terminally to the wild-type NHERF1 in the pCX_b vector, generating Myr-NHERF1 and NLS-NHERF1, respectively. The Myr signal was also added to the NHERF1 PDZ1-2 construct that lacks the terminal EB region. The retroviral constructs encoding AKT, PTEN, and ΔPDZ (former PTEN-401, (Georgescu et al., 1999a)) were obtained by inserting in the pCX_n vector (G418 selection) the cDNAs in frame with HA or Myc tags, respectively.

2.8 Transfection and retroviral infection

The 293T cells in 6-cm dishes (2.5×10^6 cells/dish, 16h post-plating) were co-transfected with 1 μg of retroviral construct and 1 μg of pCL-Ampho plasmid, with 6 μL of FuGENE (Roche #04-981- 057-001) in serum-free DMEM (Georgescu et al., 1999a). At 48h post-transfection, the medium containing retroviral particles was added on Caco-2 cells using a 0.45 μm-filter syringe (Corning, #09-754-21), and 8 μg/mL of Polybrene (Sigma, #28728-55-4) co-treatment. At 6h post-infection, the viral supernatant was removed from the Caco-2 cells and replaced with 10% FCS DMEM/F-12. At 48h post-infection, selection of the cells were begun with the growth medium containing 1 μg/mL of puromycin (Sigma, #P8833), 2.5 μg/mL of blasticidin (Invitrogen, #R210-01), and/or 1 μg/mL of G418 (Invitrogen, #11811-023). Selection lasted for approximately 5 days or until satisfactory expression of the retroviral constructs was obtained.

2.9 Epithelial morphogenesis assay

The single suspensions of Caco-2 cells were embedded in 40% growth factor-reduced Matrigel (BD Biosciences, #354230)/growth medium (v/v) with 20 mM HEPES (pH 7.4) (Invitrogen, #15630), to produce 3D cysts in 8-well chamber slides (Fischer Scientific, #12-565-8), as previously described (Jaffe et al., 2008). The cell-matrix mixture was overlaid with 400 μ L of Caco-2 growth medium, and re-fed on day 4 post-embedding. Prior to IF on day 2, 3, 4, or 8, cells were washed with PBS three times, fixed with 4% paraformaldehyde (PFA) for 30 min, and washed three times with 1/10x IF wash buffer containing 130 mM NaCl, 13 mM Na₂HPO₄ (Sigma, #S9390), 3.5 mM Na₂H₂PO₄ (Sigma, #S9368), 0.5% NaN₃, 1% bovine serum albumin (BSA) (Sigma, #A7888), 2% Triton X-100, and 0.5% Tween-20. Blocking was performed in 1% BSA in 1/10x IF wash buffer for 30 min. The primary antibodies (listed in TABLE 2.4) were applied in this blocking buffer overnight at 4°C. Next day, cells were washed with 1/10x IF wash buffer three times for 10 min; and the secondary antibodies Alexa Fluor 568 goat anti-rabbit IgG, Alexa Fluor 488 goat anti-mouse IgG, and/or rhodamine-phalloidin (Molecular Probes, #A11011, #A11001, and #R145, respectively) applied at 1:200 for 45 min at room temperature, covered with aluminum foil, and with ToPro-3 iodide (Molecular Probes, #T3605) co-incubation at 1:2000. Cells were washed again with 1/10x IF wash buffer for 10 min three times, then with PBS for 5 min three times. The Slowfade Gold antifade reagent (Invitrogen, #P36934) was used to mount the slides. Images were acquired with the Zeiss LSM 510 confocal microscope, using 63 x/1.40 NA objectives with oil immersion; and processed with the LSM 510 software, version 4.2.

<u>Antibody</u>	<u>Marker</u>	<u>Product</u>	<u>Dilution</u>
NHERF1	apical	Affinity BioReagents, #PA1-090	1:500
E-cadherin	basolateral	BD Biosciences, #C20820	1:250
Ezrin	apical	BD Biosciences, #610602	1:250
GM130	GA	BD Biosciences, #G65120	1:250
β -catenin	basolateral	Sigma, #C2206	1:500
Laminin	BM	Sigma, #L9393	1:500
ZO-1	TJ	Zymed Laboratories, #61-7300	1:250
aPKC (C-20)	apical	Santa Cruz Biotechnology, #sc-216	1:200
PTEN (A2B1)	apical	Santa Cruz Biotechnology, #sc-7974	1:200
Myc (9E10)	n/a	Santa Cruz Biotechnology, #sc-40	1:50
HA	n/a	Boehringer Mannheim, #1-583-816	1:200
P-HH3-S10	mitosis	Upstate Biotechnology, #06-570	1:500

TABLE 2.3 Primary antibodies used for epithelial morphogenesis assay. GA, Golgi apparatus; BM, basement membrane; TJ, tight junction.

2.10 Cell morphology assay

Cell morphology was assessed by plating 5×10^5 cells in duplicate in 2% FCS DMEM in 6-well dishes, and cultured for 10 days at 37°C. On Day 10, cells were washed with PBS twice; fixed with 10% acetic acid for 20 min; and stained with 0.1% crystal violet solution in methanol for 20 min. Phase-contrast images of the crystal-violet stained cells were obtained using 5x/0.12 and 20x/0.50 NA objectives of the Zeiss Axiovert 200 inverted microscope.

2.11 Migration assay

Cell migration was assessed by scratching a confluent cell monolayer in duplicate with sterile 2-200 μ L tip in serum-free DMEM. The scratch site was pen-marked and monitored once daily for closure: at 0, 24, and 48h. Phase-contrast images were obtained each day, using 10x/0.25 objective of the Zeiss Axiovert 200 inverted microscope. The widths of the scratch site were measured using Image J (NIH, version 1.34s). The distance of cell migration was computed as: (width of scratch site at 0h) – (width of scratch site at 48h).

2.12 Invasion assay

Cell invasion was assessed by suspending 1×10^6 cells in duplicate in 250 μ L of serum-free DMEM, in transwells with 8- μ m pore size polycarbonate filters (Corning #07-200-150) pre-coated with 100 μ L of 0.7 mg/mL Matrigel (BD Biosciences #354234). The wells below the polycarbonate filters were filled with 750 μ L of 10%

FCS DMEM to obtain a chemogradient across the transwell. At 48h post-plating, cells on the upper surface of the filter were removed with a cotton swab. Migratory cells remaining on the lower surface of the filter were fixed and stained with the HEMA3 stain set (Fisher, #22-122-911). Images were acquired using 5x/0.12 and 10x/0.25 NA objectives of the Zeiss Axiovert 200 inverted microscope. The number of cells in the fields was counted using Image J software (NIH, version 1.34s).

2.13 Gelatin zymography

To analyze the activities of secreted MMPs, 2.5×10^5 cells were plated in 10% FCS DMEM/F-12 in 12-well dishes. After overnight incubation to allow cell attachment to the dishes, growth medium was removed and replaced with serum-free DMEM. At 24h into serum starvation, the conditioned medium was collected and spun at 10,000 *g* for 5 min. The cell-free supernatant, normalized to cell numbers, was mixed with 1/4x sample buffer containing 0.25 M Tris (pH 6.8), 20% glycerol, 4% SDS, and 0.02% bromophenol blue; and loaded without boiling on 12% polyacrylamide gels copolymerized with 1 mg/mL gelatin (Sigma, #G6650). Following separation of the proteins by non-denaturing electrophoresis, the gel was washed twice for 30 min in wash buffer containing 2.5% Triton X-100, 50 mM Tris (pH 7.5), 5 mM CaCl_2 , 1 μM ZnCl_2 , and 0.02% NaN_3 . It was then equilibrated for 30 min at room temperature in the same buffer except with 1% Triton X-100, thereafter incubated in this buffer for 48h at 37°C. Coomassie Blue (Bio-Rad, #161-0436) was used to stain the gel for 30 min, and the white bands of gelatin-cleared areas were sought in the dark blue background.

2.14 Proliferation assay

1×10^4 cells were plated in triplicate in 2% FCS DMEM/F-12 in 24-well dishes. The increments in cell number were counted at 24h post-plating (D1) and subsequently every other 3 days up to D13, using Beckman-Coulter Vi-Cell analyzer.

2.15 Whole cell lysis

Cells removed from the growth medium were washed with PBS; scraped; and lysed in ice-cold cell lysis buffer containing 1% Triton X-100, 50 mM HEPES (pH 7.5), 100 mM NaCl, 10 mM EDTA, 10% glycerol, and protease inhibitor cocktails: 1 mM sodium orthovanadate (pH 10.0) (Sigma, S-6508), 0.1 mM sodium molybdate (Sigma, #S-6646), 1 mM phenylmethylsulfonyl fluoride (PMSF) (Sigma, P-7626), and 1% aprotinin (Sigma, #A-6279) (Georgescu et al., 1999b). After 15 min of incubation on ice, the samples were spun for 15 min at 16,000 g; and the cleared lysates were collected in new tubes. Protein concentrations of the lysates were then measured, using BSA standards (range: 0.5-20 $\mu\text{g/mL}$), and following manufacturer's instructions of the Micro BCA Protein Assay kit (Thermo Scientific, #PI-23223 and #PI-23224).

2.16 Immunoblotting

Protein samples were mixed with 1/6x sample buffer containing 125 mM Tris (pH 6.8), 10% SDS, 2.5% glycerol, 1.25% 2-mercaptoethanol, and 0.2% bromophenol blue. These were then boiled at 95°C for 5 min; and loaded on 8, 10, or 12% SDS-polyacromide gel. The proteins were separated by gel electrophoresis in 1x running

buffer containing 25 mM Tris, 200 mM glycine, and 0.1% SDS (w/v). Prestained *Rec* Protein ladder (Fisher BioReagents, #BP3603) was run with each gel. The proteins were then transferred to the Immobilon-P membrane (Millipore, #IPVH00010) using the Bio-Rad Trans-Blot SD Semi-Dry Trans Cell system at 5V for 2h, in 1x transfer buffer containing 25 mM Tris, 200 mM glycine, 20% methanol (v/v), and 0.375% SDS. Blocking of the membrane was performed with 3% BSA in 1x TBST buffer containing 50 mM Tris (pH 7.5), 150 mM NaCl, and 0.1% Tween-20 for 30 min. The primary antibodies (listed in TABLE 2.5), were applied in this blocking buffer for overnight at 4°C. Next day, the membrane was washed with 1x TBST for 5 min three times. The horseradish peroxidase (HRP)-conjugated mouse or rabbit secondary antibody (Jackson ImmunoResearch Laboratories, #115-035-071 and #711-036-152, respectively) was then applied at 1:40,000-1:10,000 for 45 min in 1x TBST; and the membrane was washed in 1x TBST for 5 min three times. The Western-Lightning Chemiluminescence Reagent (Perkin-Elmer, #NEL105001EA) was applied and the protein bands were visualized on autoradiography films.

2.17 Immunofluorescence of cells (IF-C) in 2D monolayer culture

The cells were grown to confluency in Permanox plastic 4-well chamber slides (Thermo Scientific, #12-565-2). After removal of the growth medium and a wash in PBS, the cells were fixed with 4% PFA for 20 min at room temperature. Next, the cells were washed with PBS three times; then permeabilized with 0.1% Triton X-100 in PBS for 10 min. After another three washes in PBS, few drops of Image-IT FX Signal Enhancer (Invitrogen, #I36933) were added for 30 min at room temperature. Blocking

<u>Antibody</u>	<u>MW, kDa</u>	<u>Product</u>	<u>Dilution</u>
NHERF1	50-53	BD Biosciences, #611160	1:1000
E-cadherin	120	BD Biosciences, #610181	1:1000
Fibronectin	240	BD Biosciences, #610077	1:1000
β -catenin	92	BD Biosciences, #610153	1:1000
GAPDH (0411)	37	Santa Cruz Biotechnology, #sc-47724	1:5000
Akt	60	Cell Signaling, #9272	1:1000
PTEN (A2B1)	55	Santa Cruz Biotechnology, #sc-7974	1:1000
Myc	n/a	Invitrogen, #R950-25	1:5000
HA	n/a	Boehringer Mannheim, #1-583-816	1:2000

TABLE 2.4 Primary antibodies used for immunoblotting.

was performed in 1% BSA in PBS for 30 min; and the primary antibodies (listed in TABLE 2.6), were applied in PBS for 2h at room temperature. The cells were washed with PBS for 10 min three times; and the secondary antibodies Alexa Fluor 568 goat anti-rabbit IgG and Alexa Fluor 488 goat anti-mouse IgG (Molecular Probes, #A11011 and #A11001, respectively) were applied at 1:500, with ToPro-3 iodide (Molecular Probes, #T3605) at 1:2000, for 1h. After final three washes of the cells in PBS for 10 min each time, the slides were mounted with Slowfade Gold antifade reagent (Invitrogen, #P36934). Images were acquired with the Zeiss LSM 510 confocal microscope, using 63x/1.40 NA objectives with oil immersion; and processed with the LSM 510 software, version 4.2.

2.18 Statistical analysis

All numerical data were examined for normality of distribution. Parametric or non-parametric methods of one- or two-way analysis of variance (ANOVA) and t-test were used, as appropriate, to analyze the differences between groups or groups by day. Tukey's test was used for multiple comparisons. A 3x3 contingency table of categorical data from CRC cases was analyzed by Fisher's exact test. For all tests, statistical significance was considered for $P < 0.05$. Unless otherwise indicated, data are presented as mean \pm standard error of the mean (SEM).

<u>Antibody</u>	<u>Marker</u>	<u>Product</u>	<u>Dilution</u>
NHERF1	apical	Affinity BioReagents, #PA1-090	1:500
E-cadherin	basolateral	BD Biosciences, #C20820	1:250
β -catenin	basolateral	Sigma, #C2206	1:500

TABLE 2.5 Primary antibodies used for IF-C.

CHAPTER 3

RESULTS

3.1 CRC case study

3.1.1 Patient demographics and H&E analyses

Patient demographic data for the 11 CRC cases are presented in TABLE 3.1. All patients were in their 50's, 60's or 70's, with comparable numbers of men and women. The most common primary tumor site was sigmoidal colon, with most common disease diagnosis being UICC (International Union Against Cancer) T2N0M0, or AJCC (American Joint Committee on Cancer) Stage I, CRC. Post-diagnosis median survival for this group of patients was 12 years (FIGURE 3.1). For all cases, H&E-stained slides were reviewed by a gastrointestinal pathologist at M. D. Anderson Cancer Center (Dr. Stanley Hamilton, Department of Pathology). On the basis of histology, three areas on the slides: normal mucosa, adenoma, and carcinoma, were defined for each case. Two of these cases: Patient 8 and 10, are presented in FIGURE 3.2.

3.1.2 IF and IHC analyses

3.1.2.1 Altered NHERF1 expression in adenoma and carcinoma

For all 11 cases (100%), NHERF1 localization as assessed by confocal IF and/or IHC was at the apical membrane in normal mucosa. In adjacent adenoma and carcinoma, however, this apical membrane staining was lost and NHERF1 was very low or not detectable in 10 of 11 (91%) of adenoma and 6 of 11 (55%) carcinoma cases. In the remaining 1 of 11 (9%) of adenoma and 5 of 11 (45%) carcinoma areas, NHERF1 was strongly re-expressed in the cytoplasm. A graphical summary for these area categorical

	All patients (n=11)	Patient 8	Patient 10
Sex, M:F	4:7	M	F
Age, y (range)	63.0 \pm 3.3 (50-79)	79	53
Primary tumor site, C:A:T:D:S:R	2:2:1:0:4:2	S	S
TNM Stage, T1:T2:T3:T4	2:6:3:0	T2	T3
AJCC Stage, I:II:III:IV	8:1:1:1	I	III

TABLE 3.1 Demographic characteristics of patients in CRC case study. n=11. Primary tumor sites are: C, cecum; A, ascending colon; T, transverse colon; D, descending colon; S, sigmoid colon; R, rectum. T scores only of the TNM staging system are shown. Patient 8 and 10, respectively, represent the cases depicted in FIGURE 3.4 and FIGURE 3.5.

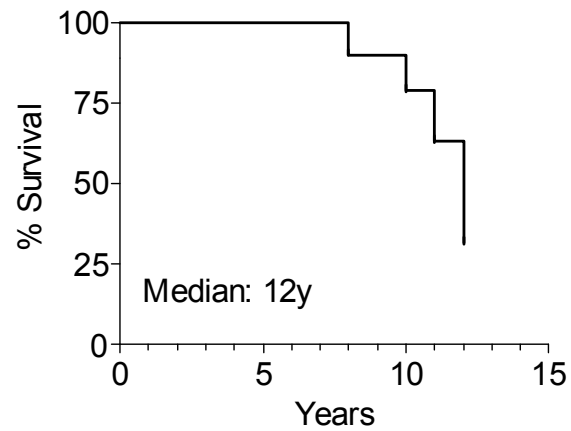
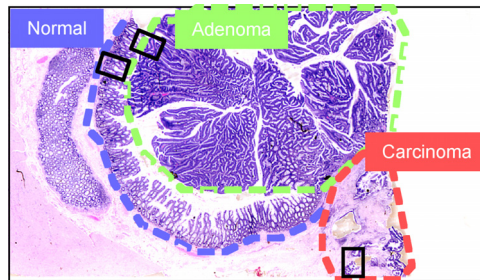


FIGURE 3.1 Post-CRC diagnosis survival status of patients in CRC case study. Median survival was 12 years. n=11. Disease-specificity of the deaths is unknown.

Patient 8



Patient 10

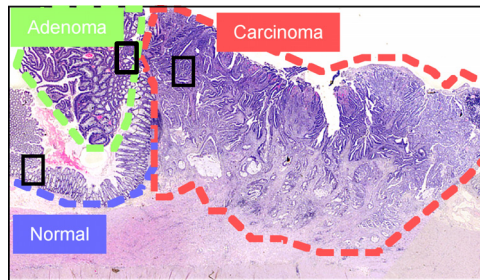


FIGURE 3.2 Normal, adenoma, and carcinoma areas in CRC resection specimens. H&E sections of two representative cases (Patient 8 and 10) are shown. Note the areas of normal colonic mucosa (blue lining), adjacent adenoma (green lining), and invasive carcinoma (red lining) for each case. Boxes indicate selected regions of these three areas for which IF and IHC analyses are presented in FIGURE 3.4 (Patient 8) and FIGURE 3.5 (Patient 10).

comparisons is presented in FIGURE 3.3. The observed differences in NHERF1 staining pattern were statistically significant ($\chi^2=38.5$, d.f.=4; $P < 0.001$). The two split patterns of NHERF1 expressions in carcinomas –the first pattern in which there is low/ no expression of NHERF1, and second pattern in which it is re-expressed in cytoplasm– are represented by two cases (Patient 8 and 10) in FIGURE 3.4 and FIGURE 3.5, respectively. Quantitative analyses of these IF data are presented in FIGURE 3.6 and FIGURE 3.7, respectively.

3.1.2.2 Nuclear NHERF1 at the invasive front of carcinoma

In seeking tumor cells deeper in the mucosa, a small cluster of cells displaying NHERF1 in the nucleus was found. These cells appeared to be moving away from a nearby tumor mass, and were larger than, and shaped differently from, NHERF1-negative stromal cells in the surrounding neighborhood (FIGURE 3.8). While this was the only area in this section where nuclear NHERF1 could be detected, re-inspection of other 10 IHC sections showed that, indeed, nuclear species of NHERF1 are present in many other protruding areas or isolated masses of invasive tumors (FIGURE 3.9).

3.1.2.3 NHERF1-positive T lymphocytes

Unexpectedly, we also found some strongly NHERF1-positive non-epithelial cells that infiltrated some areas of normal colonic mucosa (FIGURE 3.10). As the IHC analyses of serial sections showed, these were likely CD3 (T lymphocyte) and CD4

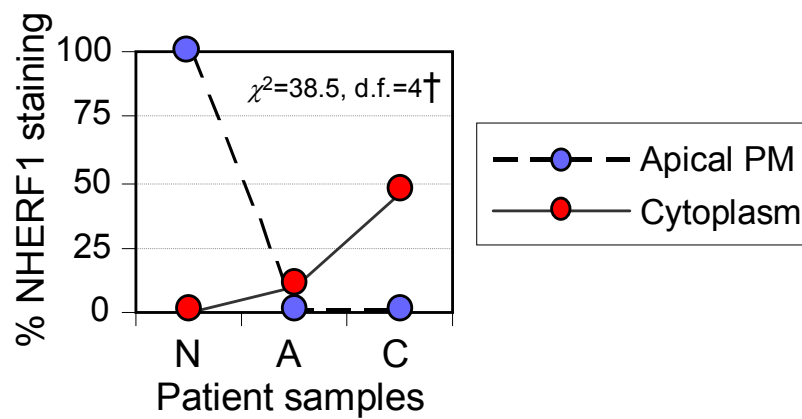


FIGURE 3.3 Area comparisons of NHERF1 intracellular distribution. A graphical summary of IF and/or IHC staining results is shown. n=11. N, normal mucosa; A, adenoma; C, carcinoma. PM, plasma membrane. d.f. = degree of freedom. $^\dagger P < 0.001$.

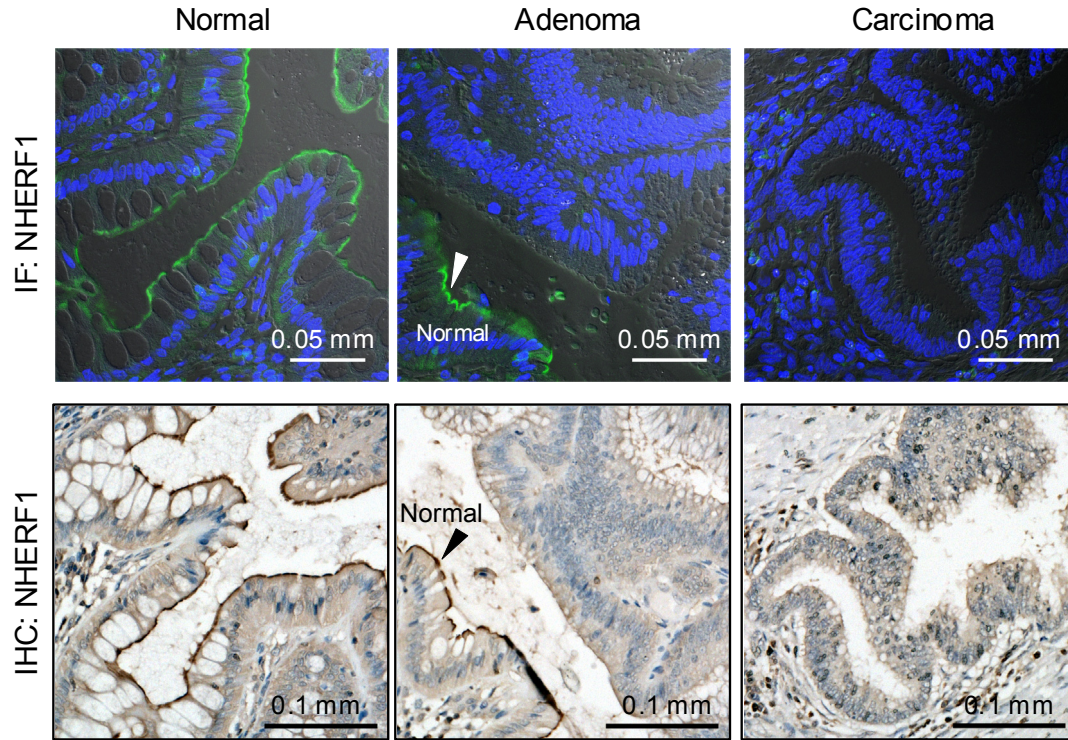


FIGURE 3.4 Loss of NHERF1 expression in carcinoma. IF and IHC analyses with NHERF1 antibody show loss of apical membrane NHERF1 in normal mucosa (left panels) from both adenoma (middle panels) and carcinoma (right panels) areas. A representative case (Patient 8) is shown. Arrowheads in middle panels indicate normal mucosa. Cell nuclei were marked with ToPro-3 (blue for IF) and hematoxylin (blue for IHC).

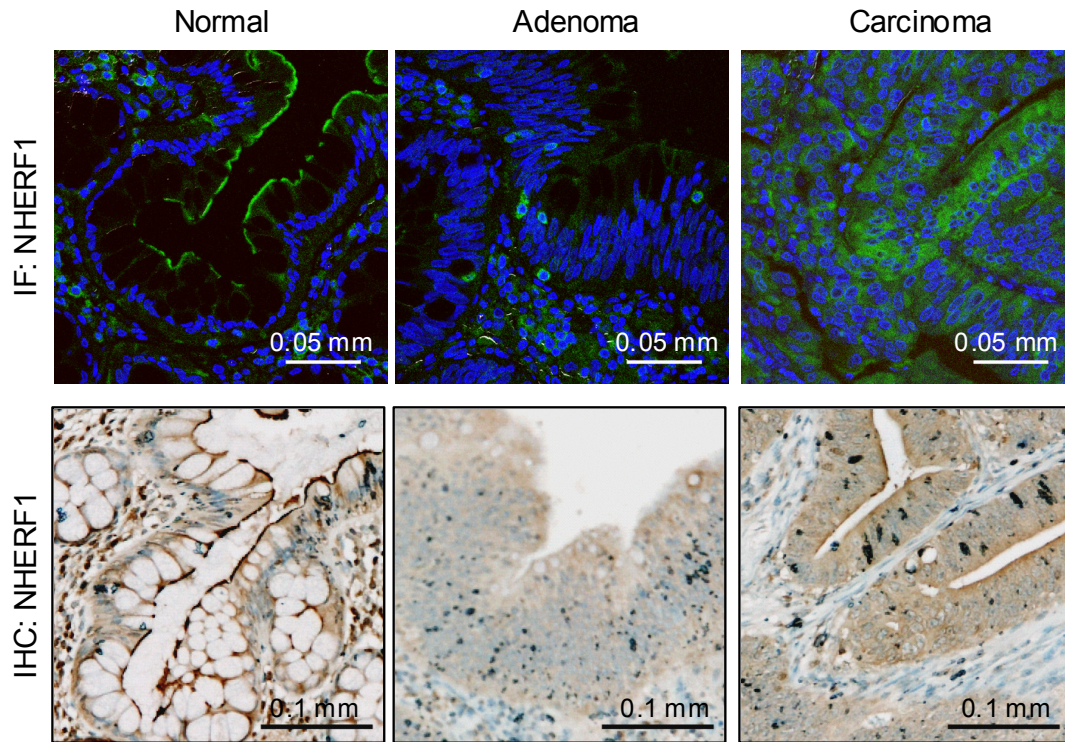


FIGURE 3.5 Cytoplasmic overexpression of NHERF1 in carcinoma. IF and IHC analyses with NHERF1 antibody show strong cytoplasmic expression of NHERF1 in carcinoma (right panels). The corresponding NHERF1 staining in normal mucosa is apically localized (left panels), with loss in adenoma (middle panel) as seen in FIGURE 3.4. A representative case (Patient 10) is shown. Cell nuclei were marked with ToPro-3 (blue for IF)- and hematoxylin (blue for IHC).

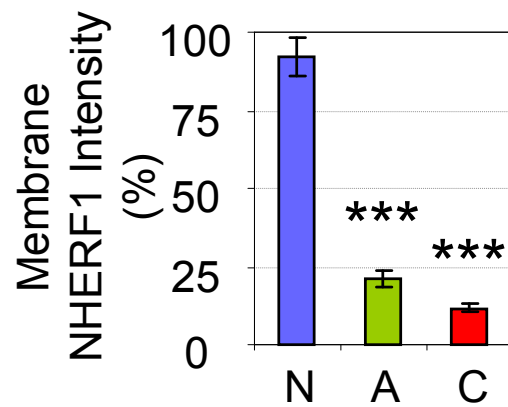


FIGURE 3.6 Quantitative analysis of IF data for NHERF1 loss. Densitometric analysis of membrane NHERF1 intensity is shown. N, normal mucosa; A, adenoma; C, carcinoma. Data are means \pm SEM of the triplicate measurements for Patient 8. *** $P < 0.001$ vs. N.

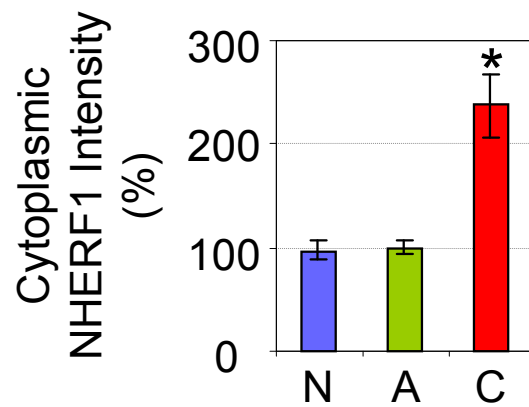


FIGURE 3.7 Quantitative analysis of IF data for cytoplasmic NHERF1 overexpression. Densitometric analysis of cytoplasmic NHERF1 intensity is shown. N, normal mucosa; A, adenoma; C, carcinoma. Data are means \pm SEM of the triplicate measurements for Patient 10. * $P < 0.05$ vs. N.

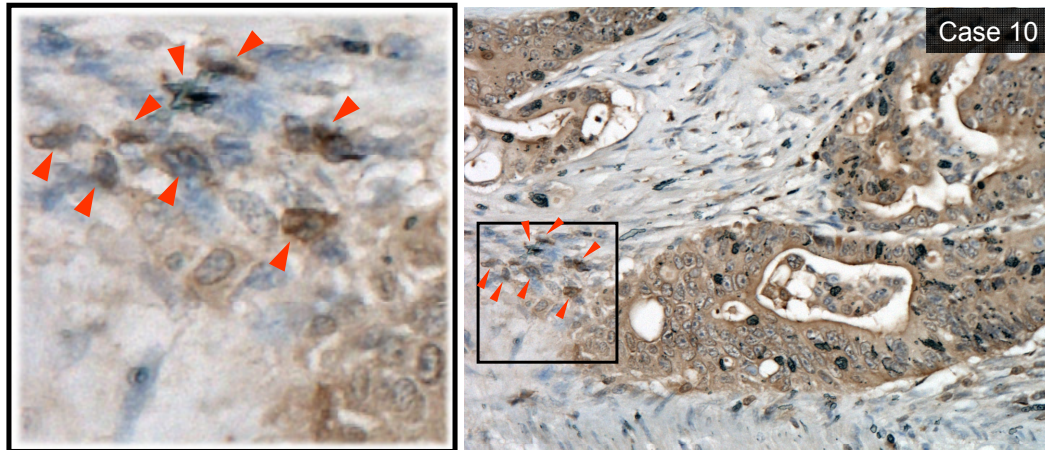


FIGURE 3.8 Nuclear NHERF1 at the leading edges of invasive tumor cells. IHC analysis with NHERF1 antibody as in FIGURE 3.5 (Patient 10) shows nuclear expression of NHERF1 in small groups of tumor cells at the leading edge of invasion (arrowheads in inset). Cell nuclei were marked with hematoxylin (blue).

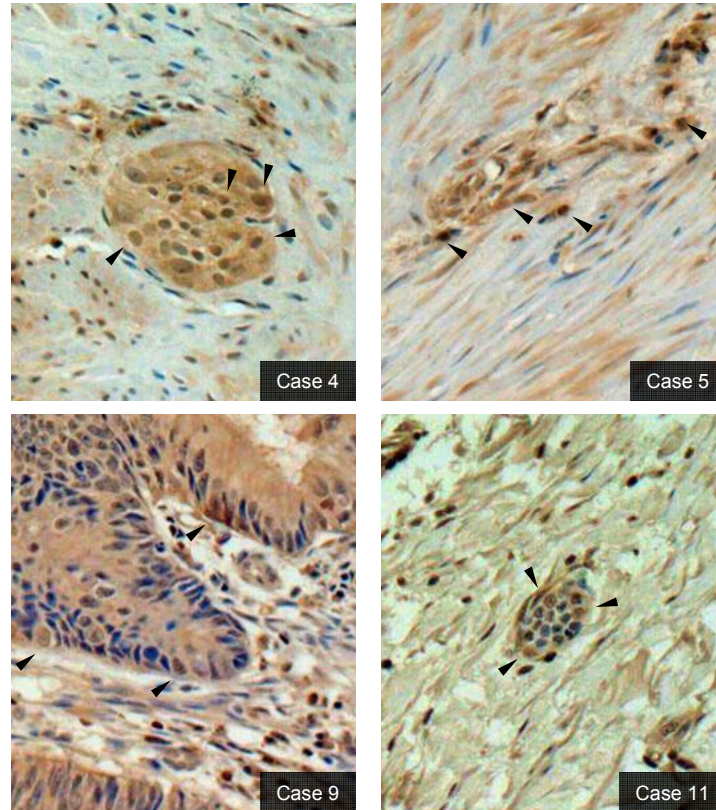


FIGURE 3.9 More nuclear NHERF1 at the leading edges of invasive tumor cells. IHC analysis of additional CRC cases as in FIGURE 3.8 shows nuclear expression of NHERF1 in many protruding areas or isolated masses of invasive carcinomas (arrowheads). Cell nuclei were marked with hematoxylin (blue).

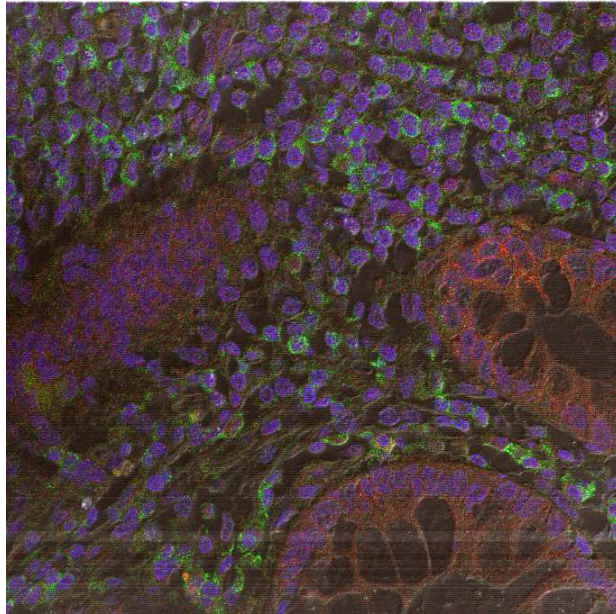


FIGURE 3.10 NHERF1-positive immune cells infiltrate the colonic mucosa. Confocal IF analysis of NHERF1 (green)-stained section shows massive infiltration of NHERF1-positive non-epithelial cells in some areas of colonic mucosa. β -catenin (red) co-stained. Cell nuclei were marked with ToPro-3 (blue).

(helper T lymphocyte)-positive T lymphocytes that stained, as did NHERF1, most intensely in the cortex of lymphoid nodule and in intraepithelial regions (FIGURE 3.11). Other markers, such as CD20 (B lymphocyte), CD68 (macrophage), and CD8 (cytotoxic T lymphocyte) stained more prominently in the germinal center or else did not stain in these areas.

3.1.3 Immunoblot analysis

Supplemental immunoblot analysis of liquid nitrogen-frozen CRC specimens was performed with seven additional cases. In five of these cases (cases 12-16) (71%), NHERF1 expression was notably decreased in both adenoma and carcinoma as compared with normal mucosa. In the remaining two cases (cases 17-18) (29%), NHERF1 was detected in both adenoma and carcinoma but as the lower molecular weight form (FIGURE 3.12). All lanes of samples showed multiple molecular weight forms of NHERF1, with the highest form in the normal tissue, and the lower forms in both adenoma and carcinoma. The low molecular weight form of NHERF1, as compared to the apical membrane associated higher molecular weight form, is likely hypophosphorylated and localized in the cytoplasm (Saotome et al., 2004). We noted truncated oncogenic form of β -catenin in adenoma and carcinoma in two of seven cases (cases 14 and 16).

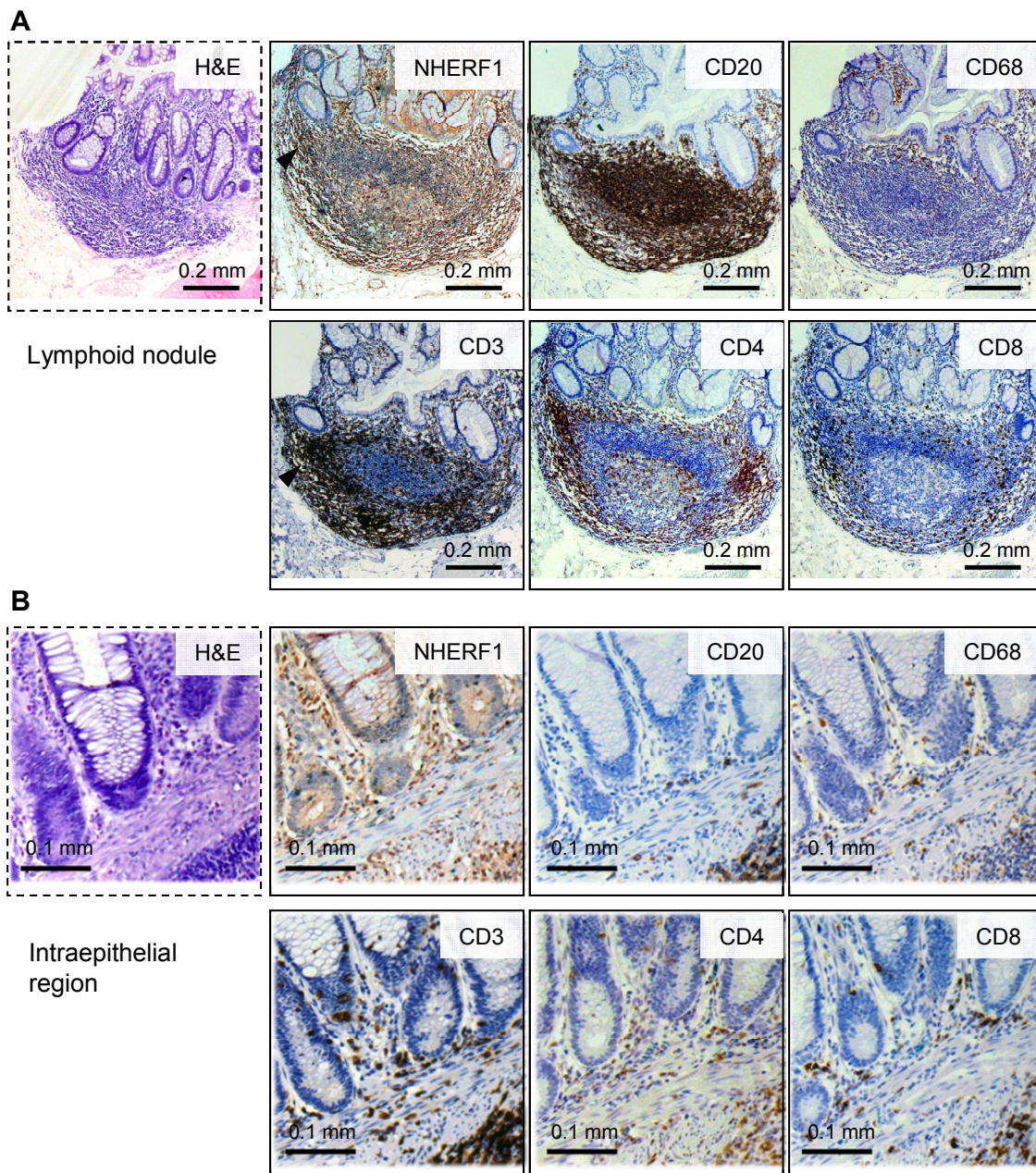


FIGURE 3.11 Characterization of NHERF1-positive immune cells. **(A)** A lymphoid nodule with NHERF1-positive cells is shown in the cortical area (arrowhead). Serial IHC analysis with immune cell markers showed CD3 (T lymphocytes) and CD4 (helper T lymphocytes) as the best matches to NHERF1. Also used were: CD20 (B lymphocytes), CD68 (macrophages), and CD8 (cytotoxic T lymphocytes). **(B)** Intraepithelial region showing NHERF1-positive cells. The best match to NHERF1 was again indicated with CD3 and CD4.

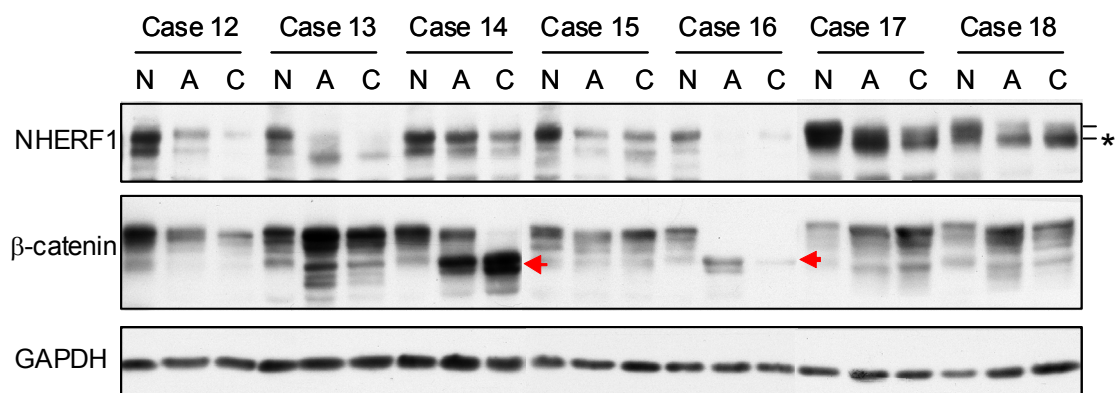


FIGURE 3.12 Low molecular weight form of NHERF1 in carcinoma. Immunoblot analysis of whole tissue lysates is shown. Proteins were loaded at 20 μ g per lane. N, normal; A, adenoma; C, carcinoma. The lines mark the high and low molecular weight forms of NHERF1 and the star the lower form, likely representing hypo-phosphorylated and cytoplasmically localized NHERF1. Also note truncated β -catenin mutants in Cases 14 and 16 (arrowheads). GAPDH was used as a loading control.

3.2 CRC tissue microarray study

3.2.1 IHC analysis

To examine NHERF1 expression in a larger number of CRC samples, we obtained T-CL-1-TARP colon TMA to repeat the IHC analysis with NHERF1 antibody. A scanned section of this IHC-stained TMA is presented in FIGURE 3.13. As the indication was clear that individual TMA samples varied in their IHC reactivity, densitometric quantification was obtained for each of these samples.

3.2.1.1 *Analysis by three groups of tumor grade*

The colon section of this TMA had limited patient data: gender (51/89 of samples), age (51/89 of samples), and tumor grade (31/89 of samples, not matched to gender or age data). Although initial efforts were directed at examining these limited data for possible association with densitometric values of IHC-NHERF1 intensity, all results lacked sufficient power to not reject the null hypothesis, due to unmatched datasets, less usable tissues, and larger data variability (TABLE 3.2). An alternative data reduction approach was therefore taken, as below.

3.2.1.2 *Analysis by four groups of IHC-NHERF1 intensity scores*

The histogram showing the distribution of IHC-NHERF1 intensity scores for the TMA samples is presented in FIGURE 3.14. The IHC-NHERF1 intensity scores ranged from 46 to 142 in an 8-bit scale of 0 to 255, with a mean (\bar{x}) of 99.0 and standard

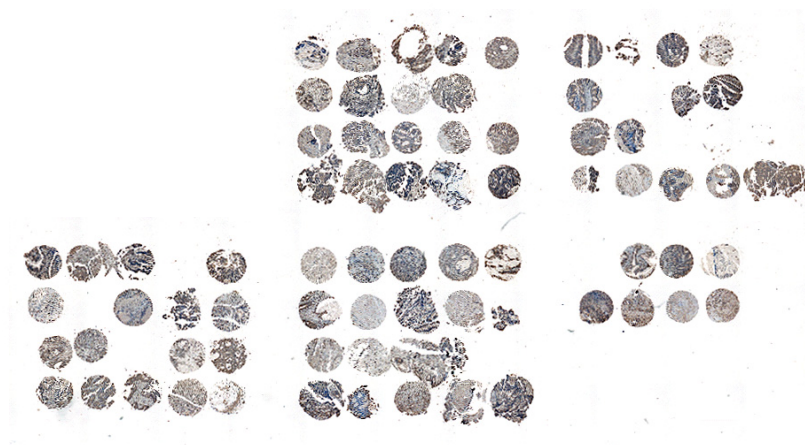


FIGURE 3.13 IHC-stained CRC TMA section with NHERF1 antibody. A scanned section of the TMA samples is shown. Note marked inter-sample differences in IHC reactivity to NHERF1 antibody. Cell nuclei were marked with hematoxylin (blue).

		Well- differentiated	Moderately differentiated	Poorly differentiated
Sex, M:F	Data missing	Data missing	Data missing	Data missing
Age, y	Data missing	Data missing	Data missing	Data missing
n	24	6	15	3
NHERF1 score	92.8 ± 4.7	86.3 ± 12.0	96.3 ± 5.8	88.2 ± 6.9

TABLE 3.2 IHC-NHERF1 intensity scores of TMA samples by tumor grade. n=24 (seven less usable data). Descriptive statistics could not be computed for patient sex and age, as data points for these variables were unmatched to tumor grade. The resultant small sample size and larger data variability.

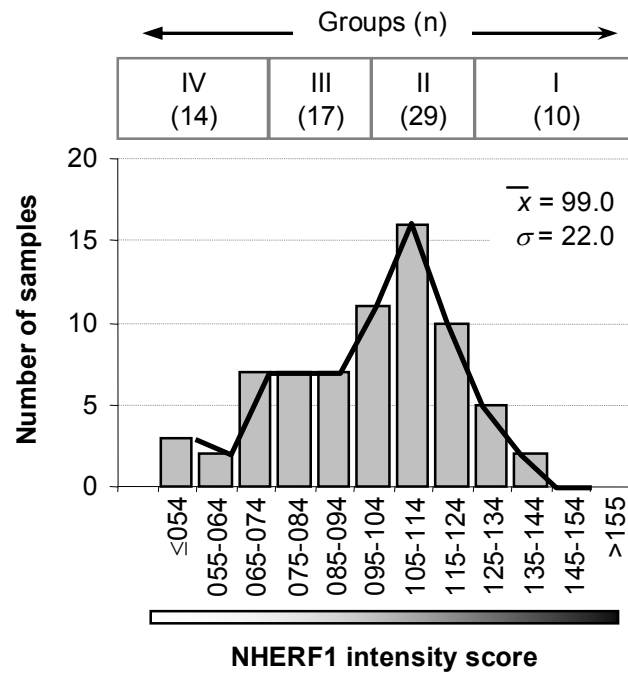


FIGURE 3.14 Distribution of NHERF1 intensity scores in CRC TMA samples. n=70. Defined score range is 0 (white) to 255 (black). Groups were assigned to each TMA sample according to their IHC intensity scores. Cut-off values for the groups were derived from the descriptive statistics mean (\bar{x}) and SD (σ).

deviation (σ) of 22.0. On the basis of these descriptive statistics, four groups were defined in equal decrements of IHC-NHERF1 intensity scores: Group I (scores >121), Group II (scores 100-121), Group III (scores 78-99), and Group IV (scores ≤ 77). The mean differences in NHERF1 intensity scores, as defined, for Group I and II (130.8 ± 2.2 vs. 109.0 ± 1.1 , $P < 0.001$), II and III (109.0 ± 1.1 vs. 89.3 ± 1.5 , $P < 0.001$), and III and IV (89.3 ± 1.5 vs. 67.2 ± 3.3 , $P < 0.001$), are presented in FIGURES 3.15. The four groups of TMA samples differed in several parameters. Namely, there was a decreasing trend for both epithelial tissue content and tumor differentiation between Group I, II, III, and IV. There was also a converse increasing tendency in the surrounding stromal content, and a shifting tendency for NHERF1 subcellular localization in which predominant cytoplasmic localization of NHERF1 in Group I became increasingly nuclear toward Group IV (FIGURE 3.16). The re-analysis of TMA sample distribution in this grouping scheme is presented in TABLE 3.2.

3.2.1.3 Serial analyses with β -catenin, E-cadherin, and cytokeratin

Serial analyses of TMA sections with three epithelial markers: β -catenin, E-cadherin, and cytokeratin were then performed. Although none of these epithelial markers showed significant differences in their IHC intensity scores between Group I and II (β -catenin, 125.0 ± 10.6 vs. 113.6 ± 3.8 ; E-cadherin, 109.6 ± 8.7 vs. 110.4 ± 4.4 ; cytokeratin, 91.3 ± 5.4 vs. 86.0 ± 2.2 ; all $P = \text{NS}$), they did all indicate stepwise decreases from Group II to III (β -catenin, 113.6 ± 3.8 vs. 84.6 ± 5.6 ; E-cadherin, 110.4 ± 4.4 vs. 79.4 ± 4.6 ; cytokeratin, 86.0 ± 2.2 vs. 71.4 ± 3.8 ; all $P < 0.001$) and from Group III to IV (β -catenin, 84.6 ± 5.6 vs. 52.9 ± 3.2 ; E-cadherin, 79.4 ± 4.6 vs. 51.3 ± 4.1 ;

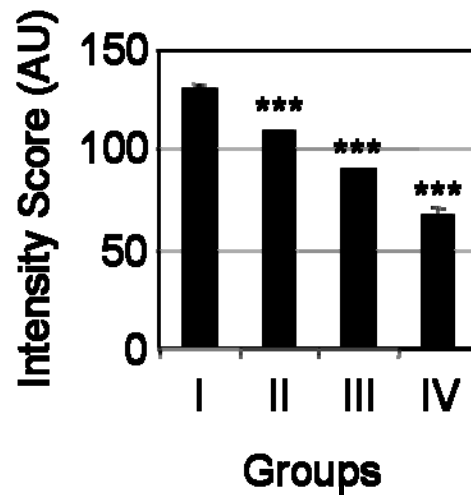


FIGURE 3.15 IHC-NHERF1 intensity scores of TMA samples by groups. Mean intensity scores for NHERF1 are shown by the groups. *** $P < 0.001$ vs. left neighbor group.

NHERF1

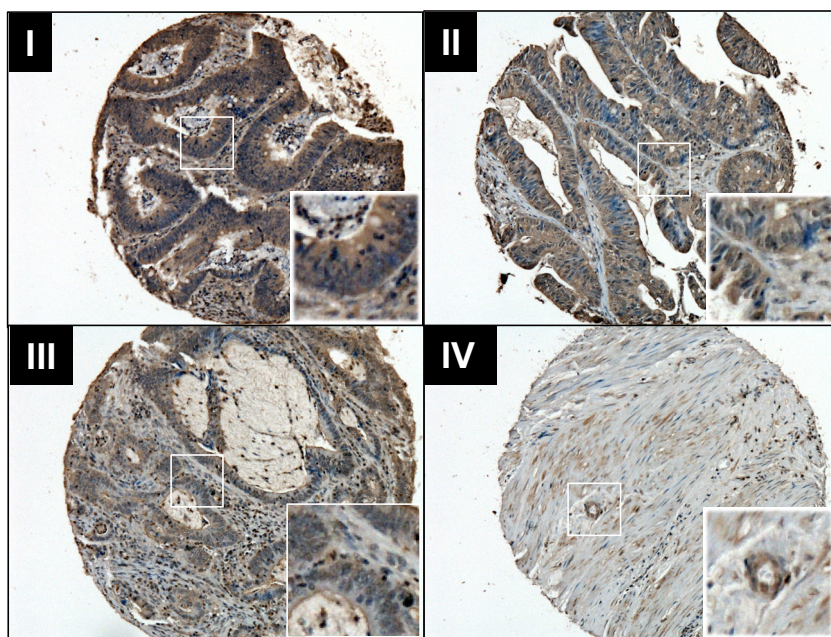


FIGURE 3.16 IHC-NHERF1 staining of TMA samples by groups. Representative staining is shown. Note the overall decreases in IHC staining intensity for NHERF1 by groups, as defined; and a shifting trend of NHERF1 subcellular localization from strong cytoplasmic to strong nuclear from Group I to Group IV, respectively.

	All patients (n=39)	Group I	Group II	Group III	Group IV
Sex, M:F	18:21	2:3	12:6	2:9	2:3
Age, y (range)	67.5 ± 2.4 (37-90)	70.8 ± 2.8 (61-78)	66.1 ± 4.1 (37-86)	70.4 ± 4.8 (39-90)	62.2 ± 5.4 (41-72)
Tumor grade (n=24)					
1	6 (25%)	0 (0%)	2 (29%)	2 (22%)	2 (33%)
2	15 (63%)	2 (100%)	5 (71%)	5 (56%)	3 (50%)
3	3 (13%)	0 (0%)	0 (0%)	2 (22%)	1 (17%)

TABLE 3.3 IHC-NHERF1 intensity scores of TMA samples by groups and patient data. Sex, age, and tumor grade data are non-matched. Tumor grades are: 1, well differentiated; 2, moderately differentiated; 3, poorly differentiated.

cytokeratin, 71.4 ± 3.8 vs. 50.9 ± 3.4 ; all $P < 0.001$) (FIGURES 3.17, 3.18, and 3.19, respectively). It may be taken that the grouping scheme used in this study specifically selected for epithelial tissue-rich tumor core (Groups I and II) against tissue-scarce invasive edges (Groups III and IV). The differences in NHERF1 intensity scores for all except between Group I and II may then reflect the differences in epithelial tissue content in the changing carcinoma background environment. The IHC-stained β -catenin, E-cadherin, and cytokeratin sections are shown in FIGURE 3.20, 3.21, and 3.22, respectively. β -catenin staining was mostly cytoplasmic, with variable but increased nuclear staining toward Group II, III, and IV. E-cadherin and cytokeratin did not have coherent staining patterns; many tissues lacked staining completely, whereas others stained strongly at membrane, or less frequently in the cytoplasm.

3.2.2 IF analysis

3.2.2.1 Nuclear localization analyses of NHERF1

As the results of IHC analyses from both CRC cases and CRC TMA suggested that there may be nuclear species of NHERF1 in invasive carcinoma, quantitative confocal IF analysis was performed for co-localization between NHERF1, nuclear marker ToPro-3, and β -catenin. The results of this analysis are presented in FIGURE 3.23. Nuclear localization of NHERF1 as indicated by % co-localized voxels between NHERF1 and ToPro-3 was doubled between Group I and III ($12.6 \pm 4.3\%$ vs. $24.2 \pm 2.8\%$, $P < 0.05$) and remained elevated in Group IV ($12.6 \pm 4.3\%$ vs. $26.4 \pm 3.3\%$, $P < 0.05$), whereas nuclear localization of β -catenin increased only non-significantly overall

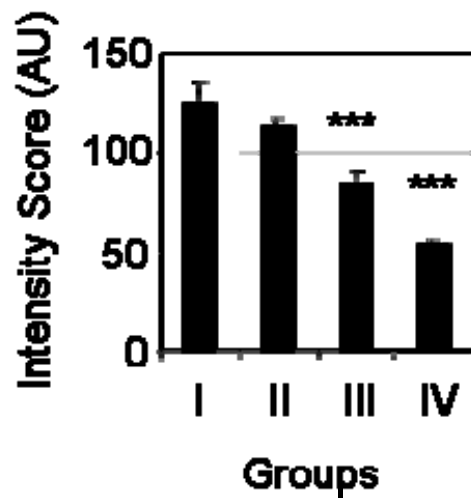


FIGURE 3.17 IHC-β-catenin intensity scores of TMA samples by groups. Mean intensity scores for β-catenin are shown. *** $P < 0.001$ vs. left neighbor group.

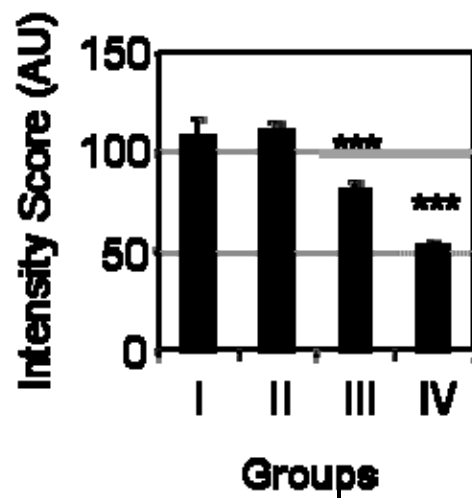


FIGURE 3.18 IHC-E-cadherin intensity scores of TMA samples by groups. Mean intensity scores for E-cadherin are shown. *** $P < 0.001$ vs. left neighbor group.

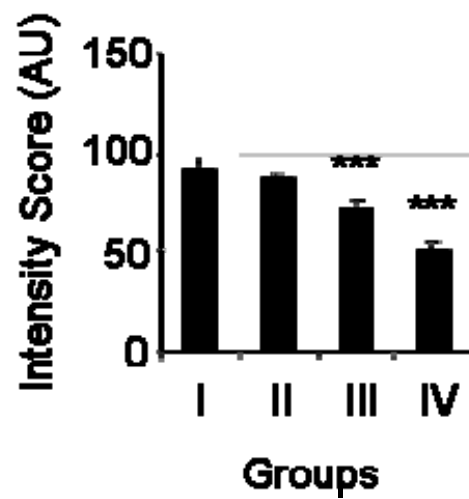


FIGURE 3.19 IHC-cytokeratin intensity scores of TMA samples by groups. Mean intensity scores for cytokeatin are shown. *** $P < 0.001$ vs. left neighbor group.

β -catenin

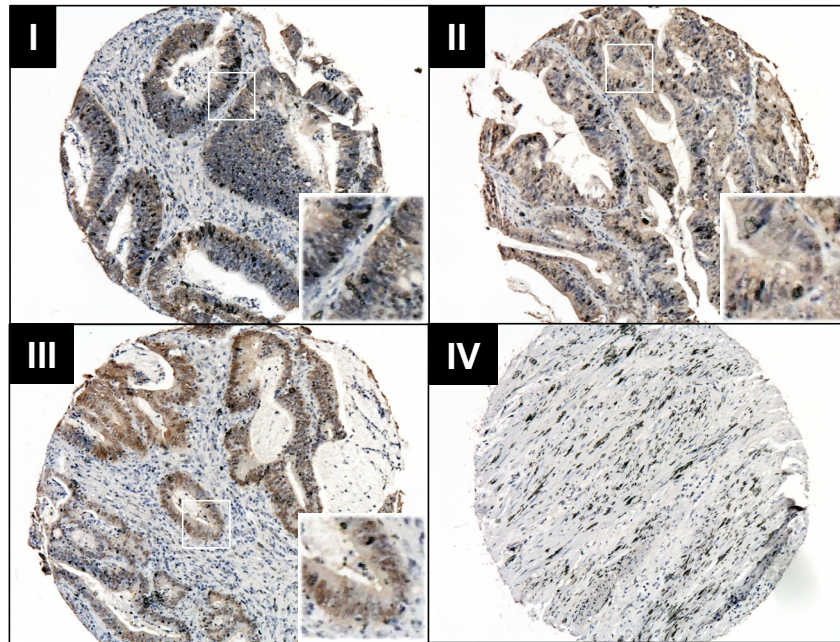


FIGURE 3.20 IHC- β -catenin staining of TMA samples by groups. Serial sections to those presented in FIGURE 3.16 are shown.

E-cadherin

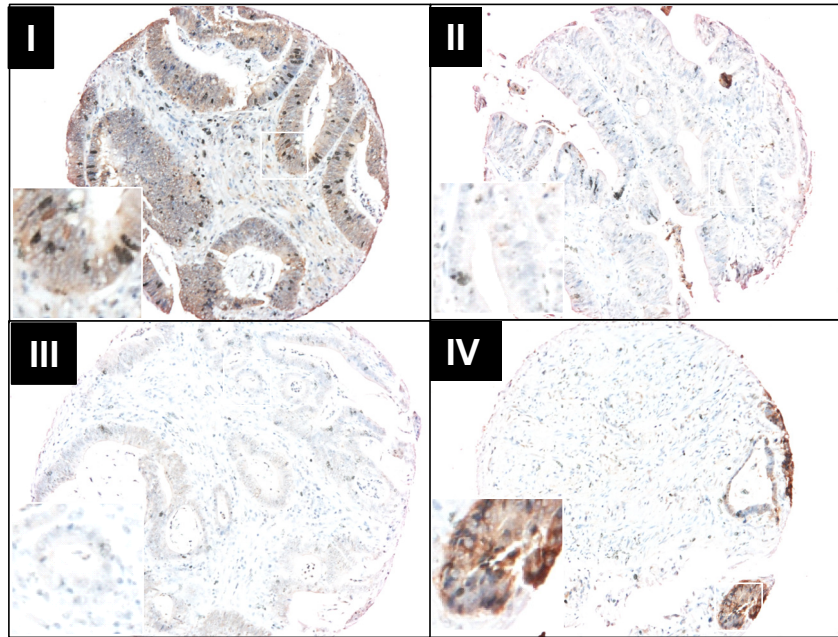


FIGURE 3.21 IHC-E-cadherin staining of TMA samples by groups. Serial sections to those presented in FIGURE 3.16 are shown.

Cytokeratin

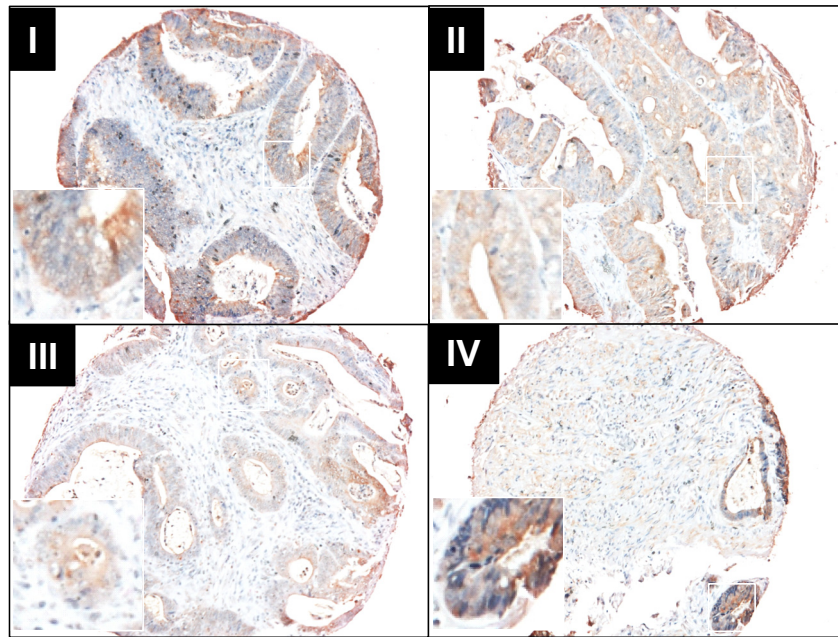


FIGURE 3.22 IHC-cytokeratin staining of TMA samples by groups. Serial sections to those presented in FIGURE 3.16 are shown.

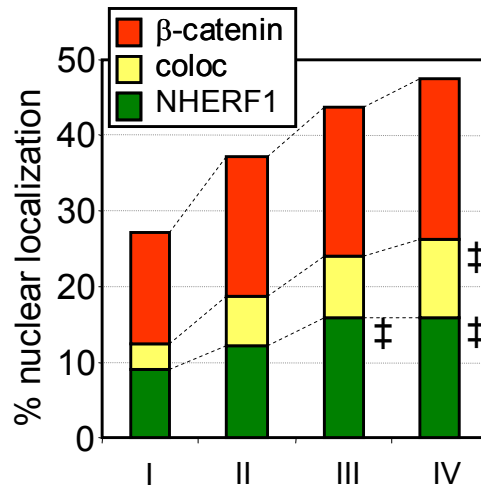


FIGURE 3.23 Nuclear localization analysis of NHERF1 and β -catenin in TMA samples. Quantitative analysis of confocal IF imaging data is shown. Note increases in nuclear NHERF1 localization and in nuclear NHERF1/ β -catenin co-localization in Groups III and IV. ‡ $P < 0.05$ vs. Group I.

(Group I: $18.2 \pm 4.7\%$ vs. Group IV: $31.5 \pm 4.0\%$, $P = \text{NS}$). Nuclear co-localization of NHERF1 and β -catenin, on the other hand, increased significantly from Group I to IV ($3.6 \pm 1.8\%$ vs. $10.4 \pm 2.0\%$, $P < 0.05$), and the tissue morphology was rather clear that those carcinomas in Group III and IV were increasingly more invasive than those in Group I and II. Selected few confocal images of double-stained TMA samples by NHERF1 and β -catenin are presented in FIGURE 3.24.

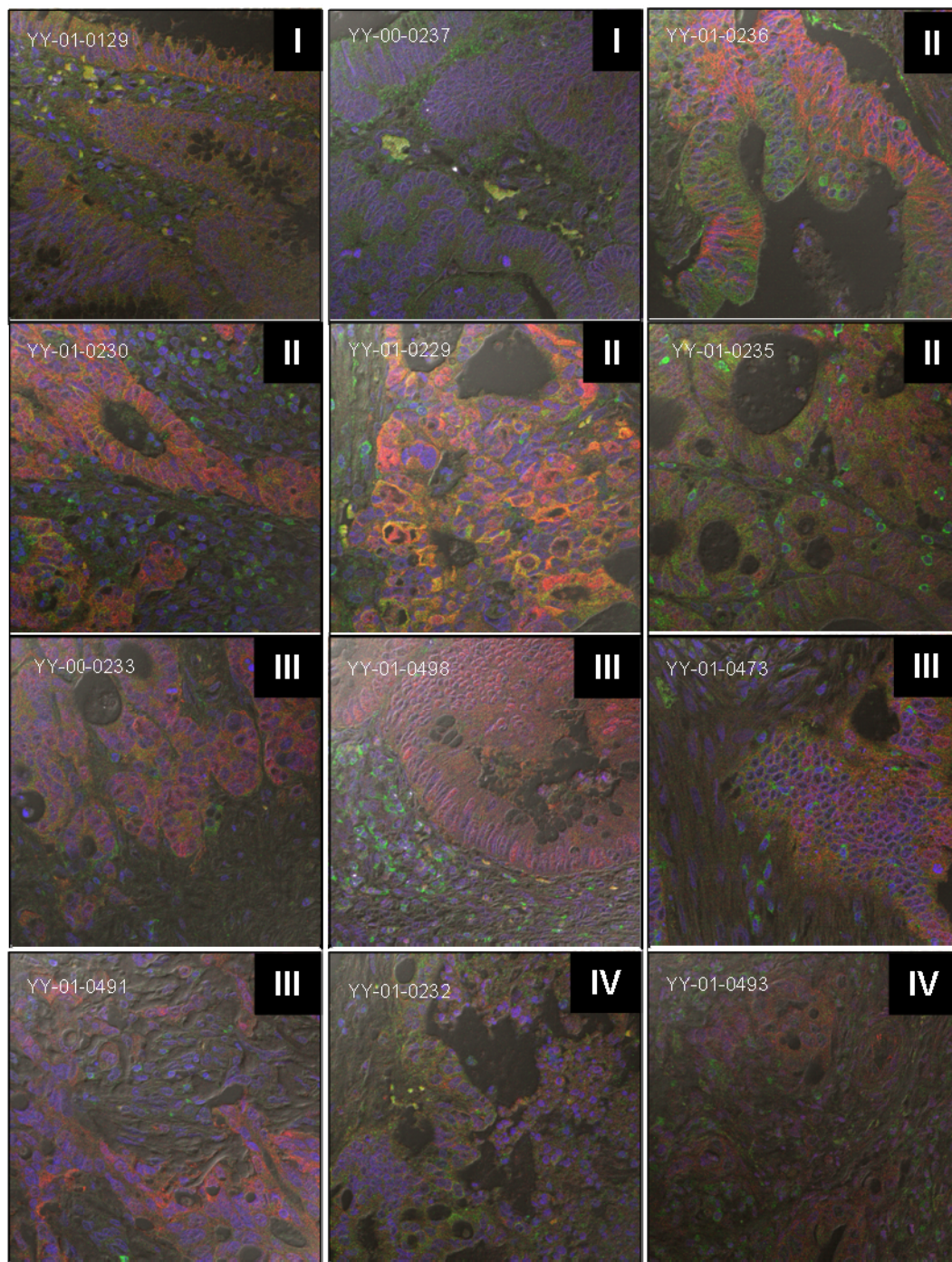


FIGURE 3.24 NHERF1 IF staining of TMA samples by groups. Confocal analysis is shown. NHERF1 (green) and β -catenin (red) co-stained. Cell nuclei were marked with ToPro-3 (blue).

3.3 CRC cell study

3.3.1 Screening of human intestinal cells

To model the observed NHERF1 alterations in CRC specimens, a panel of six human intestinal cell lines was screened for NHERF1 expression (FIGURE 3.25). Subcellular fractionation analyses were also performed for each of these cell lines (data not shown); the results suggested that Caco-2, but none of the other cell lines, have polarized distribution of NHERF1 at the apical microvilli. Confocal IF analysis was then performed with Caco-2 cells in the confluent 2D monolayer; NHERF1 was indeed at the apical microvilli in these cells, as contrasted to E-cadherin which was localized at the basolateral membranes (FIGURE 3.26).

3.3.2 NHERF1 knockdown in Caco-2 cells

To mimic the NHERF1 loss in human colonic adenoma, NHERF1 in Caco-2 cells were depleted by two constructs of shRNAs (sh1 and sh4). Efficient knockdown of NHERF1 induced notable cell scattering in both of the NHERF1-depleted cells (FIGURE 3.27); and, as the changes in cell shape suggested epithelial-mesenchymal transition (EMT) in NHERF1-depleted cells as compared to the vector control, total cell lysates were probed for the epithelial marker E-cadherin and the mesenchymal marker fibronectin. We found moderate reduction in E-cadherin level, with a gain in fibronectin, in NHERF1-depleted cells (FIGURE 3.28). While total β -catenin level was unchanged in these cells, IF analysis of 2D monolayer showed significant reduction of membrane β -catenin (vector: 100.0 ± 4.4 %, sh1: 58.4 ± 2.5 %, sh4: 46.4 ± 2.1 %, $P < 0.05$); and

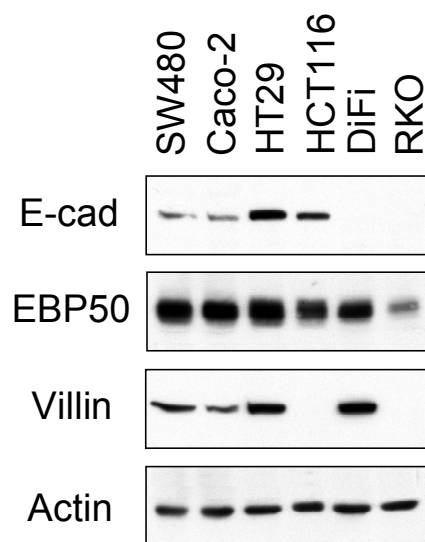


FIGURE 3.25 Screening of six CRC cell lines for NHERF1 expression. Western blot analysis of total cell lysates is shown. Proteins were loaded at 30 μ g per lane.

Caco-2: NHERF1 & E-cadherin

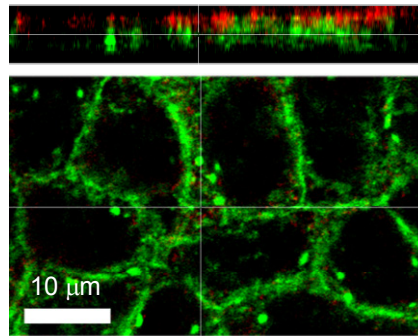


FIGURE 3.26 Subcellular localization of NHERF1 in Caco-2 cells. Confocal IF analysis is shown. NHERF1 (red) and E-cadherin (green) co-stained. Note NHERF1 localized apically to E-cadherin E-cadherin is shown at the lateral cell-cell junctions in both XY (bottom) and Z sections (top).

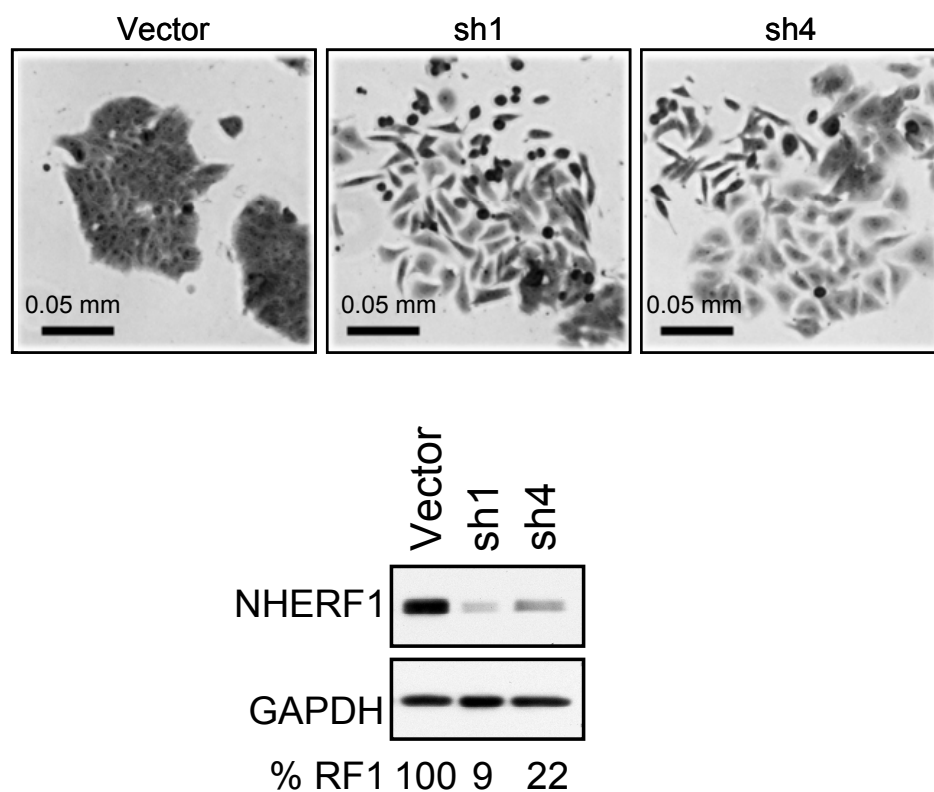


FIGURE 3.27 NHERF1 depletion by two shRNAs (sh1 and sh4) in Caco-2 cells. Crystal violet staining and immunoblot analysis are shown. Note EMT-like morphological changes in NHERF1-depleted cells. Numbers under the lanes of immunoblot indicate NHERF1 levels relative to GAPDH.

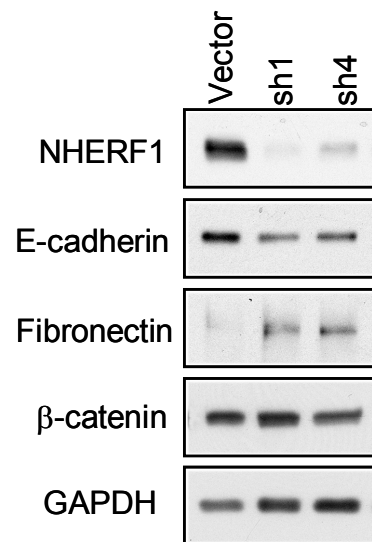


FIGURE 3.28 EMT for NHERF1-depleted Caco-2 cells. Immunoblot analysis is shown with indicated EMT markers. Proteins were loaded at 30 μ g per lane.

nuclear β -catenin was concomitantly increased (vector: 100.0 ± 6.8 %, sh1: 235.2 ± 9.7 %, sh4: 215.1 ± 9.2 %, $P < 0.05$) (FIGURE 3.29). In wound-healing assay, NHERF1-depleted cells showed significantly faster migration than their vector control cells (vector: 112 ± 8 $\mu\text{m}/48\text{h}$, sh1: 154 ± 9 $\mu\text{m}/48\text{h}$, sh4: 158 ± 6 $\mu\text{m}/48\text{h}$, $P < 0.05$) (FIGURE 3.30). They also showed increased invasive activity in transwell matrigel assay (vector: 54.0 ± 11.8 cells/field, sh1: 139.3 ± 15.4 cells/field, $P < 0.05$) (FIGURE 3.31), and increased activities of secreted MMPs as shown by gelatin zymography (FIGURE 3.32).

3.3.3 Re-establishment of epithelial phenotypes by Myr-NHERF1

To rescue the phenotypes of NHERF1-depleted Caco-2 cells, we expressed three variants of NHERF1 constructs: wild-type NHERF1, membrane-targeted Myr-NHERF1, and nuclear-targeted NLS-NHERF1. Western blot, confocal IF analysis, and corresponding proliferation assay for the cells expressing these three constructs are shown in FIGURE 3.33, FIGURE 3.34, and FIGURE 3.35, respectively. Reconstitution of NHERF1-depleted Caco-2 cells with membrane-targeted Myr-NHERF1 restored E-cadherin at lateral cell-cell contacts, whereas both nuclear-targeted NLS-NHERF1 and wild-type wt-NHERF1 failed to restore E-cadherin. The corresponding immunoblot analysis also showed restoration of E-cadherin level only by Myr-NHERF1. Whereas no change in cell proliferation was induced by reconstitution with Myr-NHERF1, both NLS- and wt-NHERF1 increased cell proliferation significantly. Migration, invasion, and secreted MMP activities were also examined, but no increase could be detected beyond the already elevated level achieved by NHERF1 depletion.

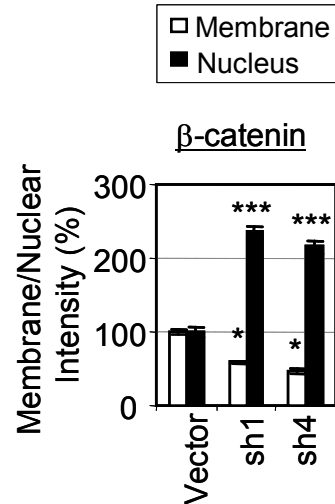
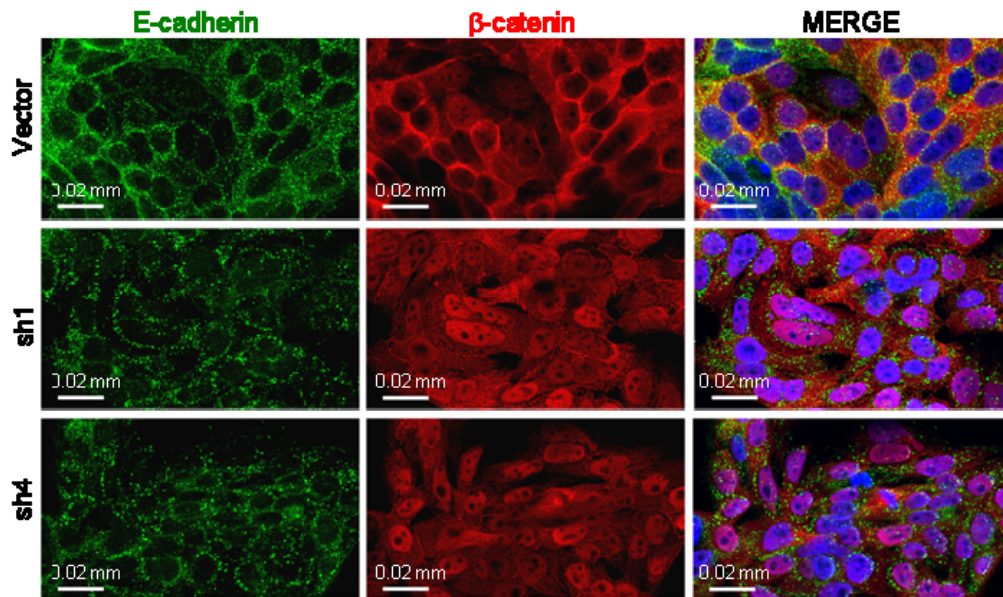


FIGURE 3.29 Nuclear β-catenin in NHERF1-depleted Caco-2 cells. Confocal IF images and densitometric analysis of β-catenin intensity are shown. β-catenin (red) and E-cadherin (green) co-stained. Cell nuclei were marked with ToPro-3 (blue). n=25. * $P < 0.05$; *** $P < 0.001$ vs. Vector.

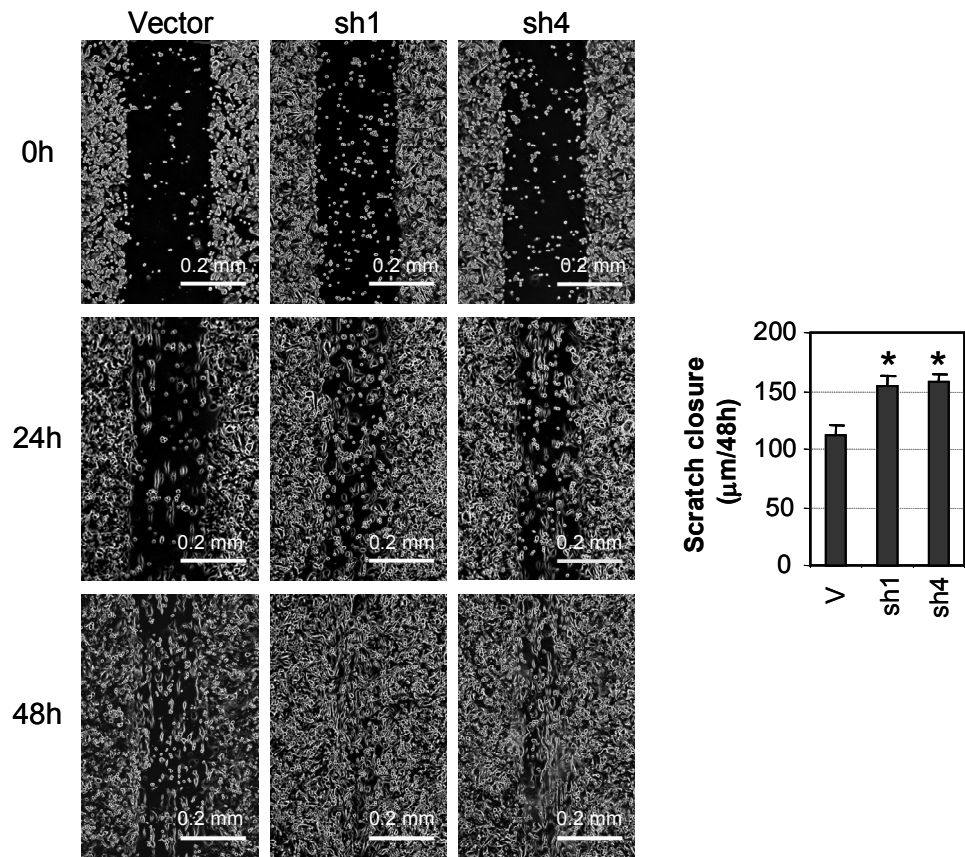


FIGURE 3.30 Migration assay in NHERF1-depleted Caco-2 cells. Quantitative analysis of scratch closures at 48h is shown. n=3. * $P < 0.05$ vs. Vector.

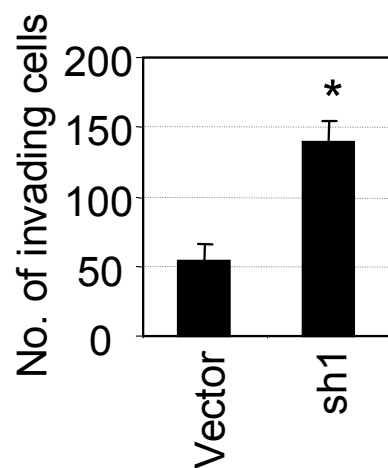


FIGURE 3.31 Invasion assay in NHERF1-depleted Caco-2 cells. Quantitative analysis of invading cells through the matrigel substrate at 48h is shown. n=3. * $P < 0.05$ vs. Vector.

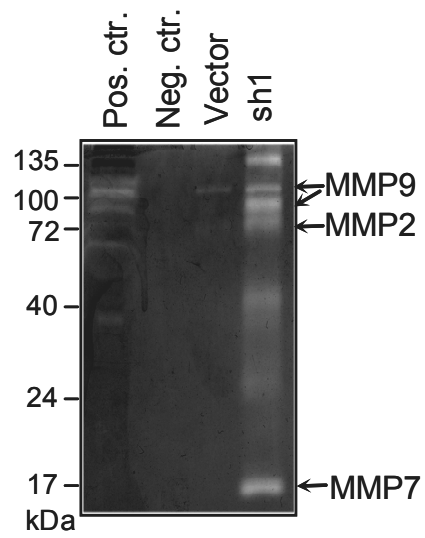


FIGURE 3.32 Gelatin zymography for NHERF1-depleted Caco-2 cells. Positive and negative controls are DMEM with and without FCS, respectively. Sample loading was normalized to cell numbers.

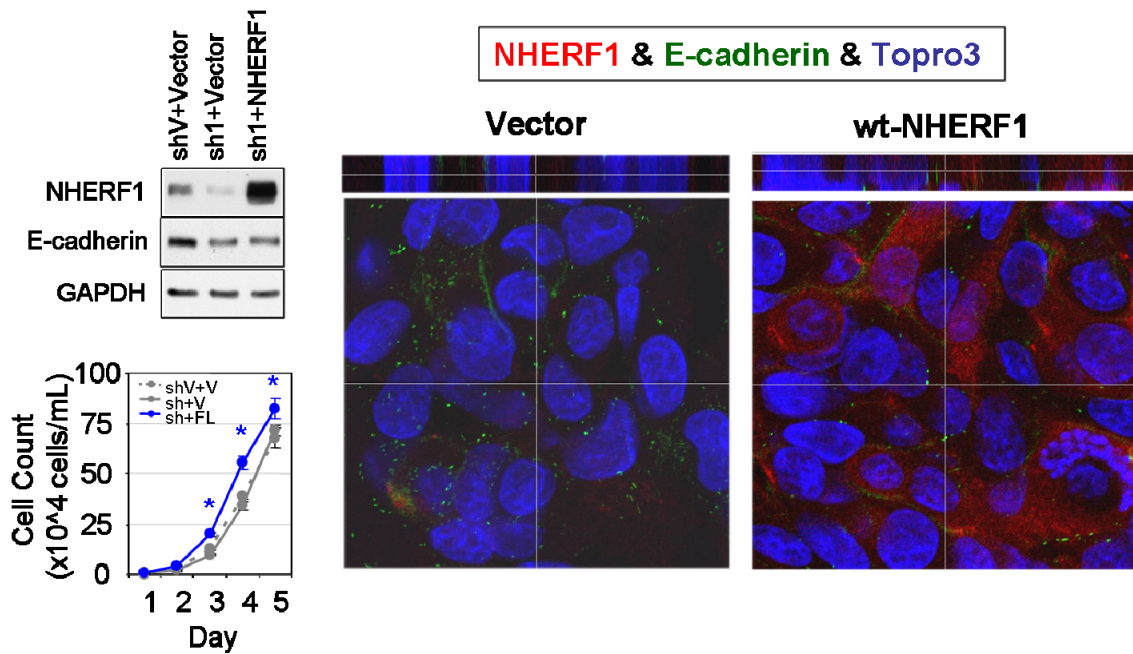


FIGURE 3.33 Wild-type NHERF1 overexpression in NHERF1-depleted Caco-2 cells. Confocal IF analysis showing reconstituted wild-type NHERF1 (red) in the cytoplasm, failing to restore E-cadherin (green) expression at the lateral membrane. Cell nuclei were marked with ToPro-3 (blue). Note corresponding increase in cell proliferation in cells overexpressing wild-type NHERF1. * $P < 0.05$. vs Vector.

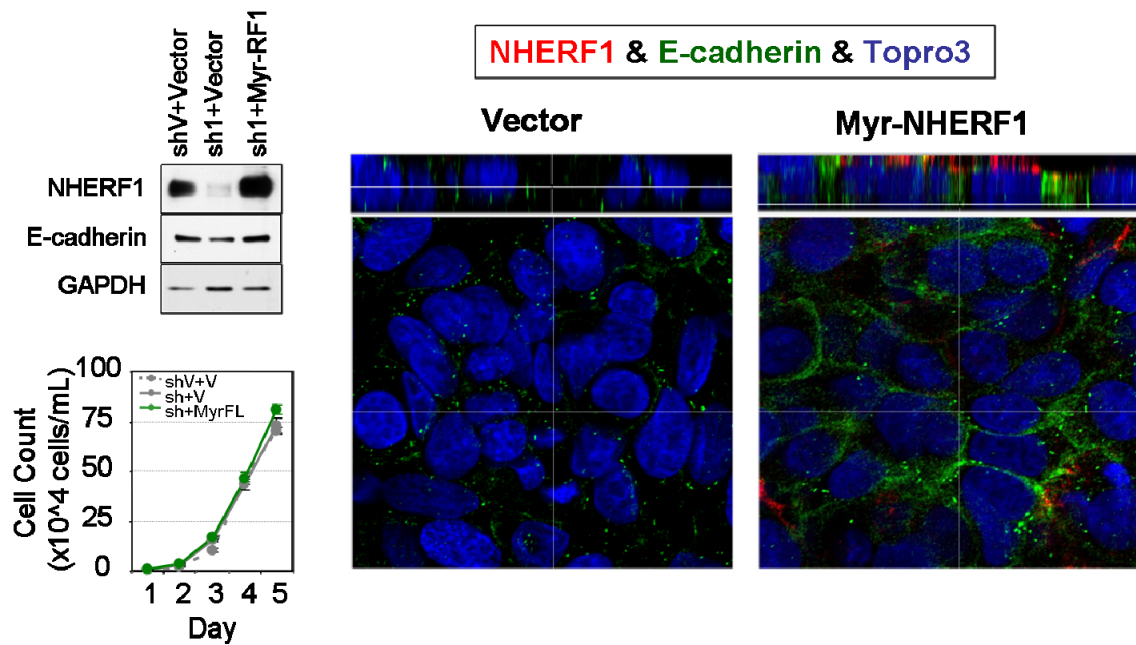


FIGURE 3.34 Myr-NHERF1 overexpression in NHERF1-depleted Caco-2 cells. Confocal IF analysis showing reconstituted membrane-targeted Myr-NHERF1 (red) at the apical membrane, and E-cadherin (green) re-expression at the lateral membrane. Cell nuclei were marked with ToPro-3 (blue).

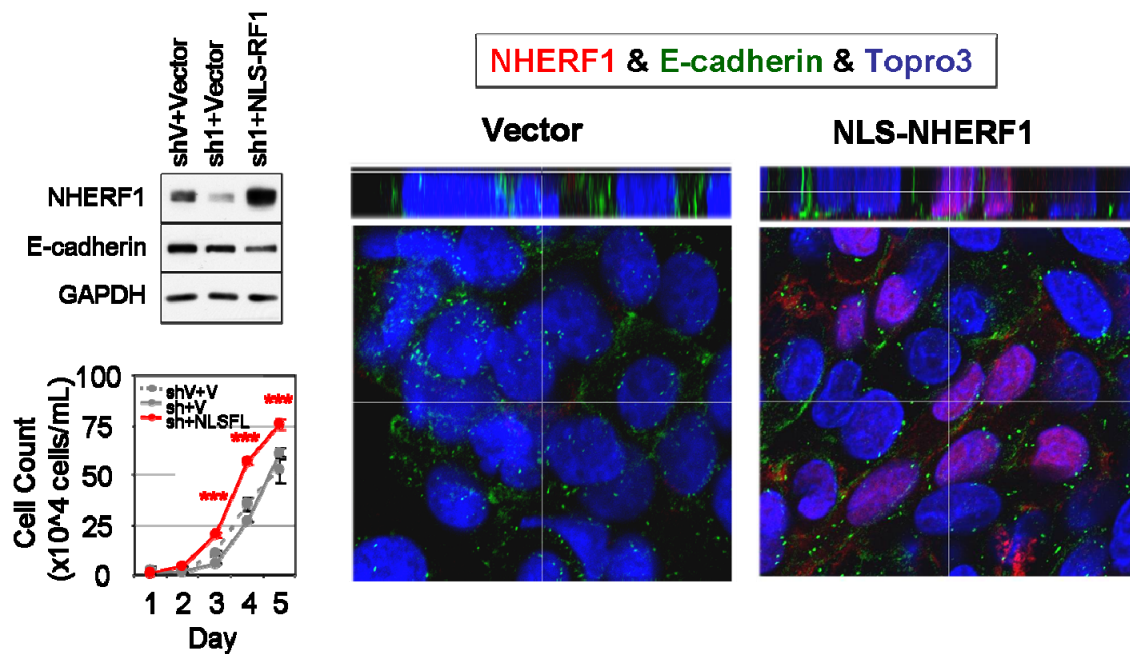


FIGURE 3.35 NLS-NHERF1 overexpression in NHERF1-depleted Caco-2 cells. Confocal IF analysis showing reconstituted nuclear-targeted NLS-NHERF1 (red) in the cytoplasm, failing to restore E-cadherin (green) expression at the lateral membrane. Cell nuclei were marked with ToPro-3 (blue). Note corresponding increase in cell proliferation in cells overexpressing wild-type NHERF1. *** $P < 0.001$. vs Vector.

FIGURE 3.36 shows the crystal violet staining of Myr-NHERF1-reconstituted Caco-2 cells. Myr-NHERF1-reconstituted cells reverted to wild-type-like cell showing tight clustering of cells and dense nuclear staining by crystal violet, as compared to the more scattered and faintly-stained NHERF1-depleted cells. FIGURE 3.37 shows the wound-healing migration assay of Myr-NHERF1-and vector reconstituted cells. At 48h post-scratching, Myr-NHERF1-reconstituted cells migrated significantly less than vector control cells (vector: $176 \pm 19 \mu\text{m}/48\text{h}$, +Myr-NHERF1: $107 \pm 13 \mu\text{m}/48\text{h}$, $P < 0.05$). FIGURE 3.38 shows confocal IF analysis of β -catenin distribution in Myr-NHERF1-reconstituted Caco-2 cells. Nuclear β -catenin decreased (vector: $100.0 \pm 4.7 \%$, +Myr-NHERF1: $43.4 \pm 8.2 \%$, $P < 0.001$), whereas membrane β -catenin increased (vector: $100.0 \pm 6.2 \%$, +Myr-NHERF1: $146.3 \pm 5.1 \%$, $P < 0.001$), in Myr-NHERF1 reconstituted cells as compared to vector control. Concomitant increase in E-cadherin was also noted for Myr-NHERF1-reconstituted cells.

3.3.4 Apical targeting of Myr-NHERF1 requires tail EB-region

FIGURE 3.39 shows confocal IF analysis of Myr-NHERF1 and Myr-PDZ1-2 (carboxyl-terminal EB region deleted) expression in NHERF1-depleted Caco-2 cells. Whereas Myr-NHERF1 was localized exclusively at the apical membrane, Myr-PDZ1-2 was concentrated at the lateral membranes, suggesting the requirement of EB region for targeting of NHERF1 to the apical plasma membrane. Differences in confluent cell monolayer morphology were also noted for these cells; phase contrast images are presented in FIGURE 3.40.

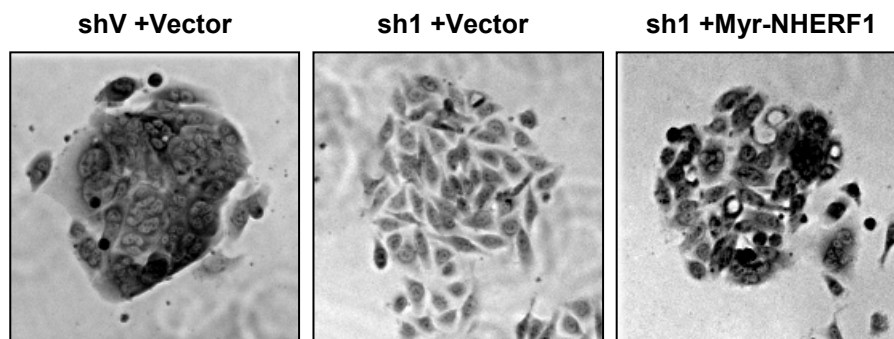


FIGURE 3.36 Epithelial-like morphology of Myr-NHERF1-reconstituted Caco-2 cells. Crystal violet staining is shown. Note tighter cell clustering and denser nuclear staining for sh1+Myr-NHERF1 cells than sh1+Vector cells.

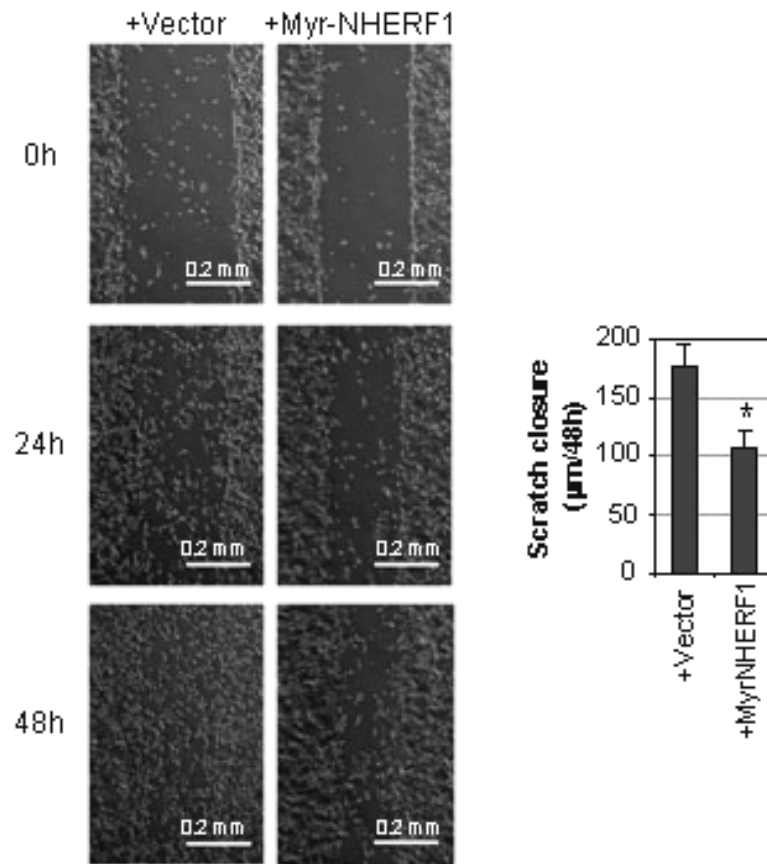


FIGURE 3.37 Migration assay of Myr-NHERF1-reconstituted Caco-2 cells. Quantitative analysis of scratch closures at 48h is shown. $n=3$. * $P < 0.05$ vs. Vector.

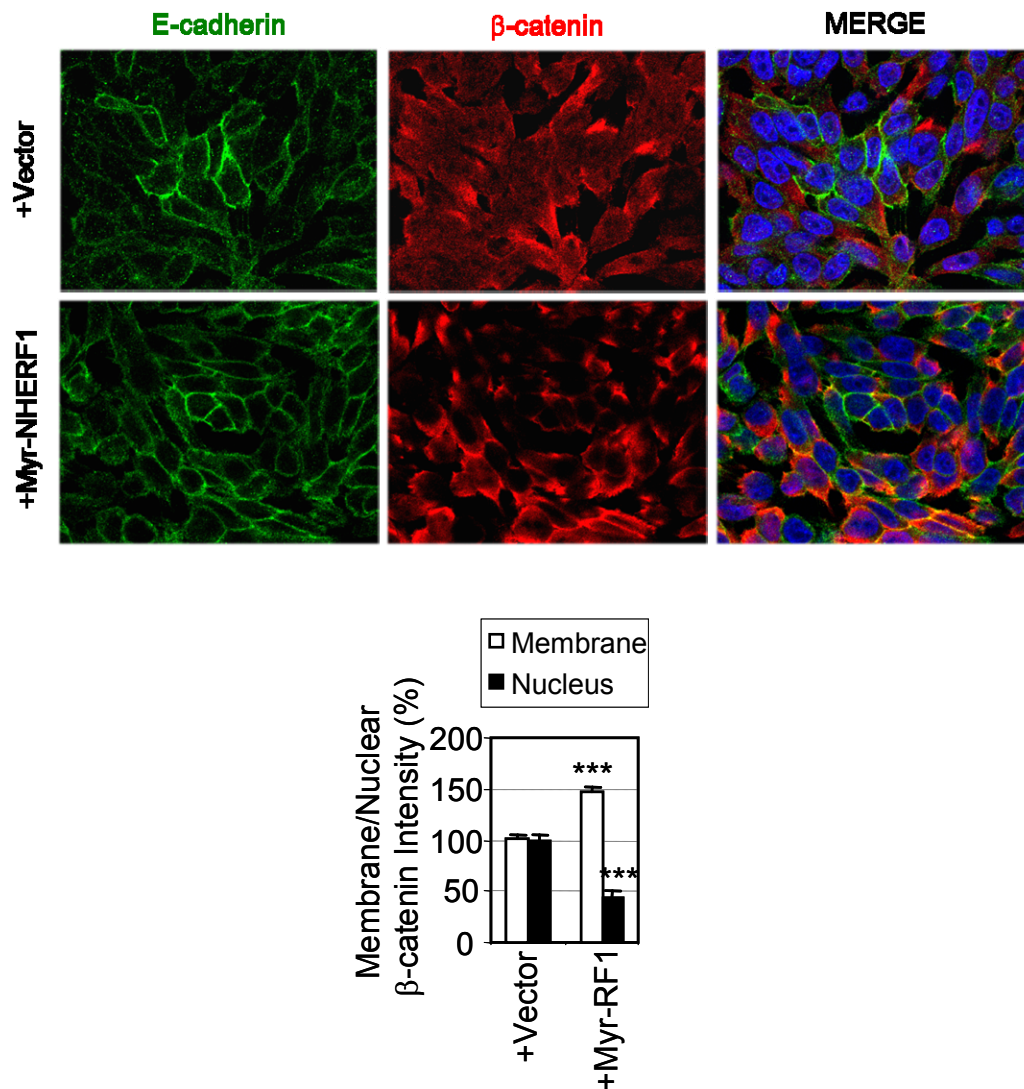


FIGURE 3.38 β-catenin redistribution in Myr-NHERF1-reconstituted Caco-2 cells. Confocal IF images and densitometric analysis of β-catenin intensity are shown. β-catenin (red) and E-cadherin (green) co-stained. Cell nuclei were marked with ToPro-3 (blue). n=25. *** $P < 0.001$ vs. Vector.

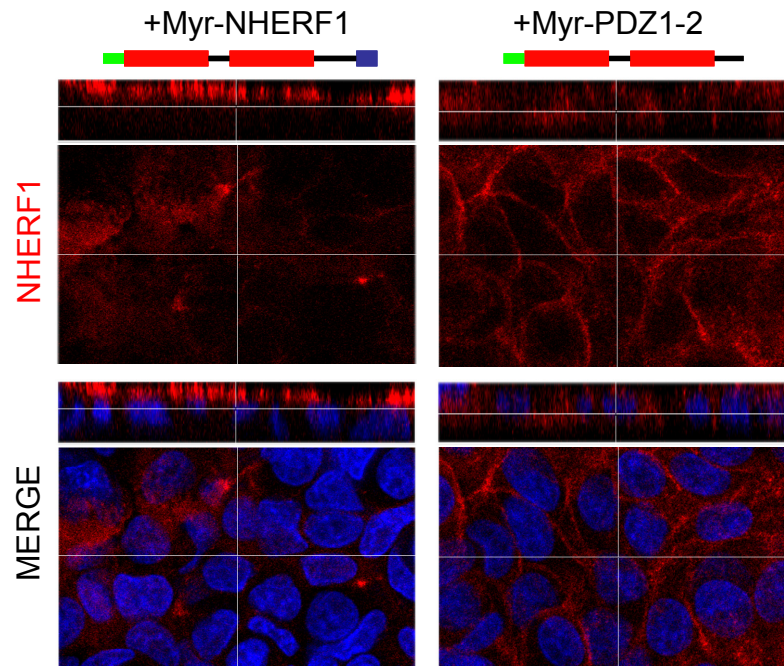


FIGURE 3.39 Apical vs. lateral distribution of Myr-NHERF1 and Myr-PDZ1-2. Confocal IF analysis is shown. NHERF1 (red)-stained. Cell nuclei were marked with ToPro-3 (blue).

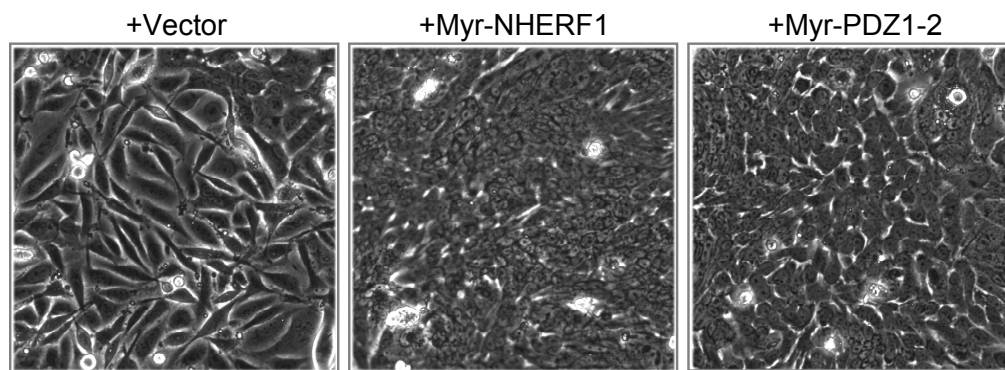


FIGURE 3.40 Confluent cell morphology with Myr-NHERF1 and Myr-PDZ1-2. Phase contrast analysis is shown. Note partial restoration of confluent cell morphology by Myr-PDZ1-2 as compared to Myr-NHERF1.

3.3.5 NHERF1-depleted Caco-2 cysts

To investigate further the role of NHERF1 in epithelial morphogenesis, we collaborated with Dr. Alan Hall (Memorial Sloan-Kettering Cancer Center, NY) to establish the 3D morphogenesis assay. When embedded as single cell suspensions in matrigel, Caco-2 3D cysts formed a polarized spherical monolayer through successive divisions for 8-12 days (FIGURE 3.41). NHERF1 was only weakly expressed in the cytoplasm at single-cell stage, but it began to concentrate along the metaphase plate during mitosis, and even more strongly concentrated in a disc around the center of cell-cell interface at the beginning of two-cell stage. It then remained tightly associated with this disc space until the lumen formed in the mature cyst (FIGURE 3.42).

NHERF1 depletion by shRNA induced severe disruption of the cyst morphology, with formation of large asymmetrical spheroids lacking the lumen, varying in individual cell shape, size, and alignment. Although these spheroids retained lateral cell junctions as marked by E-cadherin (adherens junctions protein), apical polarity as marked by Ezrin (actin-binding protein), aPKC (Par complex component), and ZO-1 (tight junctions protein) were all lost or inverted to outer periphery of the cyst structure. Apical (supranuclear) orientation of the Golgi apparatus as marked by GM130 (*cis*-Golgi matrix protein) was also randomly re-distributed throughout the spheroids. Basal polarity as marked by Laminin (basement membrane protein) was lost or detached from the basement membrane (FIGURE 3.43). β -catenin was markedly accumulated in the nucleus of these NHERF1-depleted spheroids (FIGURE 3.44).

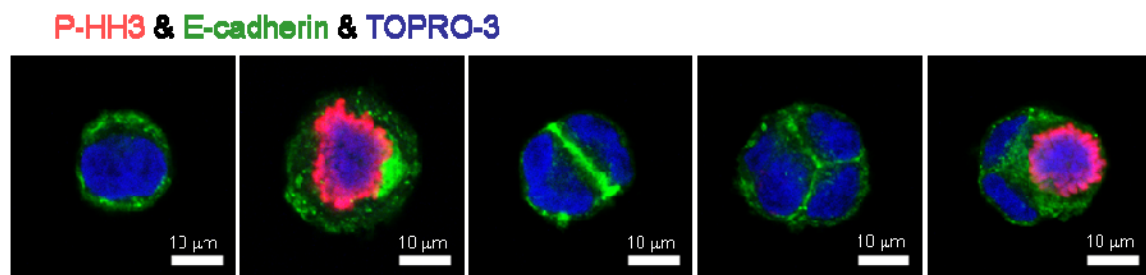


FIGURE 3.41 Development of Caco-2 3D cyst. Confocal IF analysis is shown. The cells were fixed and stained, at 2-8 days post-plating in matrigel. Phospho-Histone H3-S10 (red) and E-cadherin (green) co-stained. Cell nuclei were marked with ToPro-3 (blue).

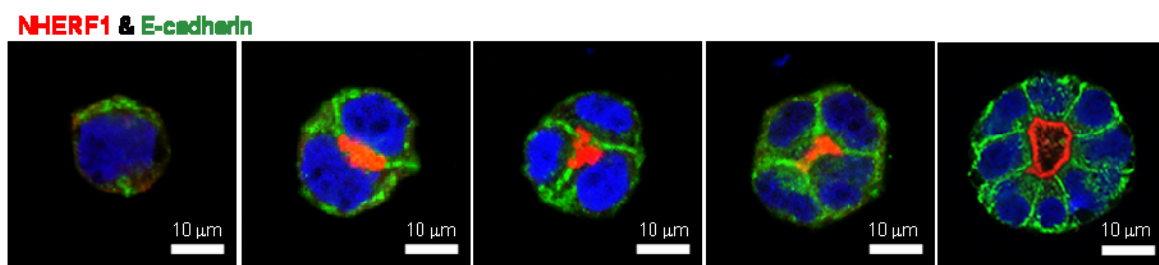


FIGURE 3.42 Apical PM formation in Caco-2 cysts. Confocal IF analysis is shown. The cells were fixed and stained, at 2-8 days post-plating in matrigel. NHERF1 (red) and E-cadherin (green) co-stained. Cell nuclei were marked with ToPro-3 (blue).

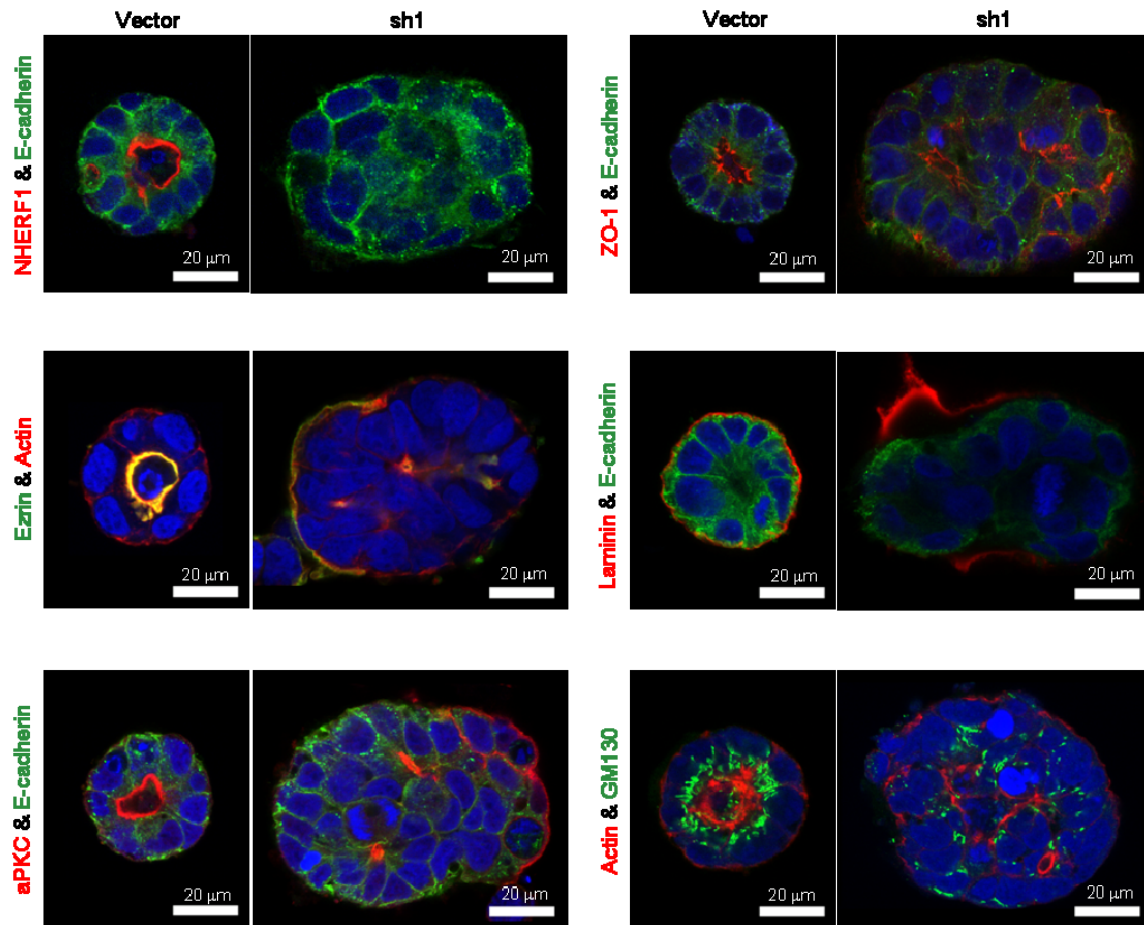


FIGURE 3.43 Loss of cell polarity in NHERF1-depleted Caco-2 spheroids. Confocal IF analysis with indicated polarity markers is shown. Cell nuclei were marked with ToPro-3 (blue).

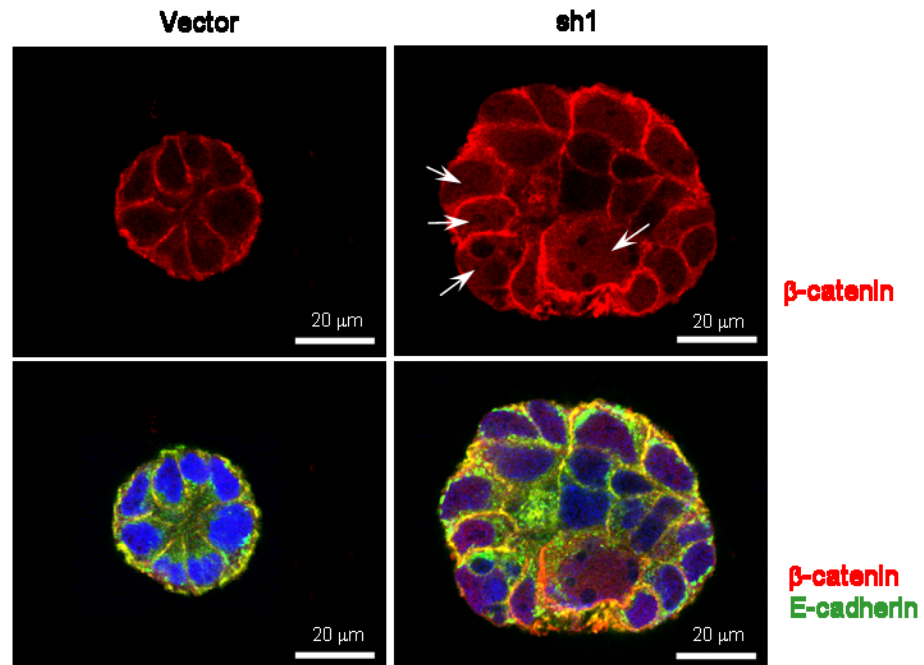


FIGURE 3.44 Nuclear β-catenin in NHERF1-depleted Caco-2 spheroids. Confocal IF analysis is shown. β-catenin (red) and E-cadherin (green) co-stained. Cell nuclei were marked with ToPro-3 (blue). Arrowheads indicate nuclear β-catenin.

3.3.6 Polarized distributions of AKT and PTEN in Caco-2 cysts

Immunoblot analysis of HA-tagged AKT overexpression and corresponding IF analysis of HA-AKT distribution in Caco-2 cysts are presented in FIGURE 3.45. Contrasting to apical NHERF1, HA-AKT was partly localized in the cytoplasm, with some noticeable concentrations at the basal membrane. Similar analyses of Caco-2 cysts with overexpressed Myc-tagged PTEN and PTEN- Δ PDZ (last three amino acids of PTEN deleted) are presented in FIGURE 3.46. While most of Myc-PTEN was localized in the cytoplasm and nucleus, a small fraction in some cysts was concentrated at the apical PM. Myc-PTEN- Δ PDZ tended to eliminate this apical concentration, with its increased concentrations in cell nuclei. In NHERF1-depleted spheroids, PTEN was localized predominantly in the cytoplasm.

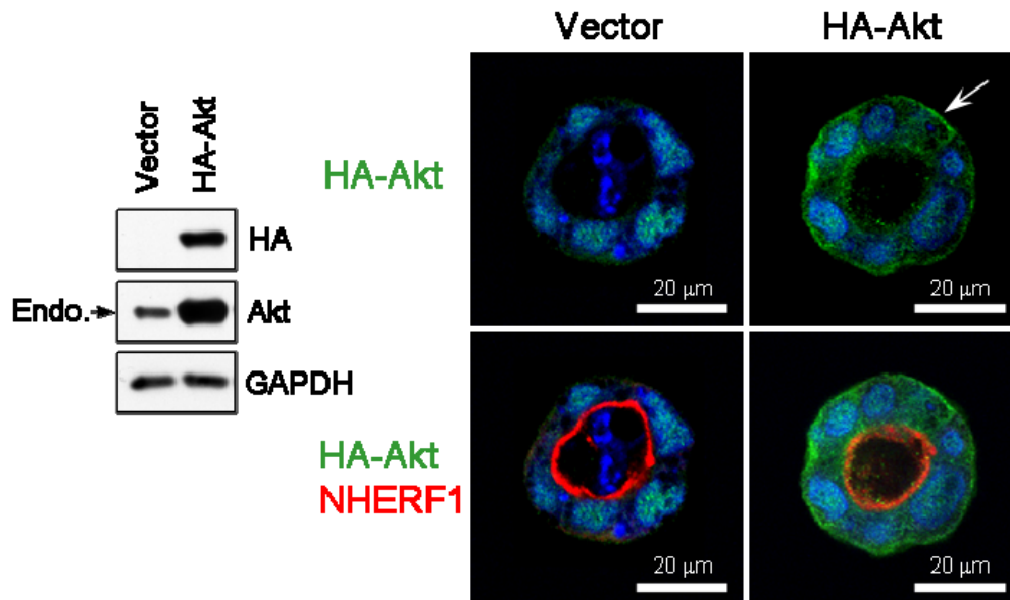


FIGURE 3.45 Basal distribution of HA-AKT in Caco-2 cysts. Immunoblot of whole cell lysates shows HA-tagged AKT expression in Caco-2 cells. Proteins were loaded at 30 μg per lane. Endogenous (Endo.) AKT is indicated. Corresponding confocal IF analysis of Caco-2 cysts with HA (green) and NHERF1 (red) antibodies is shown. Note basal membrane distribution of HA-AKT (arrow).

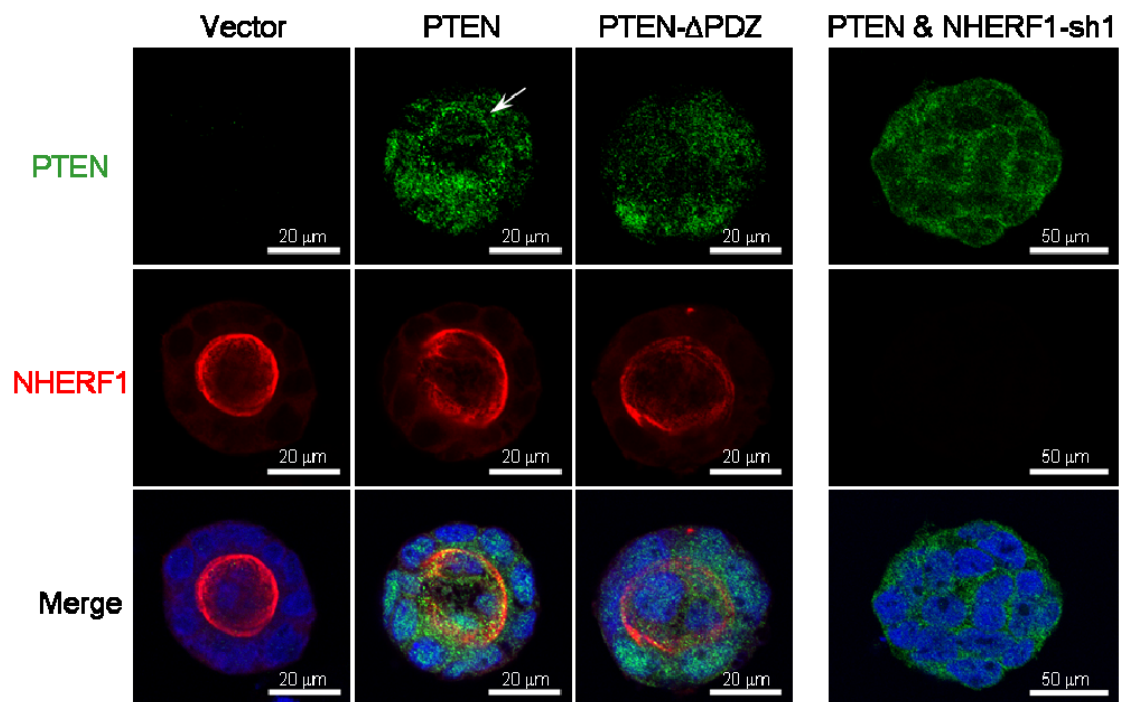
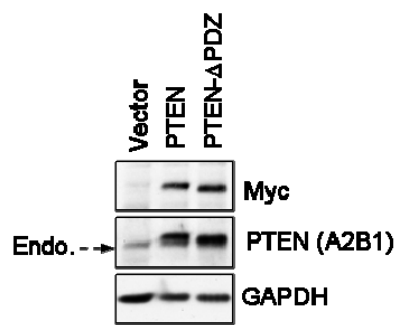


FIGURE 3.46 Apical distribution of Myc-PTEN in Caco-2 cysts. Immunoblot of whole cell lysates shows Myc-tagged PTEN and PTEN- Δ PDZ expression in Caco-2 cells. Proteins were loaded at 30 μ g per lane. Endogenous (Endo.) PTEN is indicated. Corresponding confocal IF analysis of Caco-2 cysts with PTEN (green) and NHERF1 (red) antibodies, and similar analysis of NHERF1-depleted spheroids, is shown. Note apical membrane localization of Myc-PTEN in Caco-2 cyst (arrow).

CHAPTER 4

DISCUSSION

4.1 Initial summary

This study was undertaken to test the hypothesis that NHERF1 acts as a tumor suppressor in normal human colon, and therefore that it may be lost or altered in CRC. The results of our study indicate that the expression of NHERF1 protein and the development of CRC are indeed closely intertwined. NHERF1 is selectively localized at the apical membrane in normal human colonic mucosa, and may be a regulator of epithelial morphogenesis. NHERF1 loss, in this way, plays a role in the loss of normal epithelial phenotypes, and may contribute to colorectal tumorigenesis. NHERF1 is also ectopically overexpressed in some colonic carcinomas. This appears to increase tumor aggressiveness beyond the loss of NHERF1 alone, and may thereby contribute to CRC progression. The findings presented here provide insights not only in the general field of biology concerning cell polarity and junctional complex formation, but also have implications for the detection of colonic adenoma and the therapeutic management of advanced carcinoma. These points will be discussed in the paragraphs below.

4.2 NHERF1 and epithelial morphogenesis

NHERF1 was localized at the apical membrane in normal human colonic mucosa, but not in adjacent adenoma or carcinoma areas (see FIGURE 3.2-3.7). The noted selective expression of NHERF1 in these human specimens confirms the previous results in mice in which NHERF1 was detected at the apical microvilli of intestinal BBM (Ingraffea et al., 2002; Reczek et al., 1997). Given the primary function of apical microvilli to increase the surface area for fluid and electrolyte transport, defects in these

structures due to NHERF1 deficiency may be expected to incur disturbances in the dynamics of the associated transport processes. It has been previously described that the pH profile is altered in many tumors, and this has been, so far, attributed to deregulated proton secreting activities of the Na⁺/H⁺ exchanger (NHE1) (Cardone et al., 2005). A topic that may be of future interest is the role of NHERF1 in the pH dynamics of intestinal enterocytes. NHERF1 as a co-regulator of NHE3 (Weinman et al., 1993; Weinman et al., 1995) may well have a functional involvement in this process.

In a complementary cell-based study to examine the role of NHERF1 in CRC, we used human intestinal Caco-2 cells that express NHERF1 at the apical microvilli (see FIGURE 3.26). Depletion of NHERF1 in 2D cell monolayers induced characteristic migratory appearance and scattering of the cells suggestive of EMT, with loss of E-cadherin, gain of fibronectin, and increase in nuclear β -catenin (see FIGURE 3.27-3.29). Our group has previously obtained similar results in a study of NHERF1-deficient MEFs (Kreimann et al., 2007). The finding in MEFs appeared to reflect the loss of direct interaction between NHERF1 and β -catenin. However, the same two proteins in Caco-2 cells are sequestered in distant cellular compartments; the likeliness of their direct interaction is thereby limited in this case. It is possible that NHERF1 deficiency indirectly induces tyrosine phosphorylation of β -catenin for uncoupling from E-cadherin (Lilien and Balsamo, 2005). An alternative possibility is the cross-activation of β -catenin by the activation of Akt and/or inhibition of glycogen synthase kinase-3 β (GSK3 β) (Larue and Bellacosa, 2005). Whatever is the case, β -catenin release may then induce E-cadherin downregulation through endocytosis (Bryant and Stow, 2004), or perhaps

through activation of the TCF/LEF complex to increase E-cadherin transcriptional repressors such as Snail and Slug (Nelson and Nusse, 2004).

Unlike those cells in 2D monolayers, NHERF1-depleted cells in 3D morphogenesis assay did not decrease E-cadherin level, yet nuclear shift of β -catenin was still evident (see FIGURE 3.44). The discrepancy in the results of 2D and 3D assays is difficult to explain, but may be taken that the change in β -catenin, rather than in E-cadherin, is the more primary and less variable consequence of NHERF1 deficiency in CRC cells. From a technical standpoint, the noted absence of E-cadherin in NHERF1-depleted cells in 3D assay is a single disqualifying criterion for these cells in the classic EMT (Thiery, 2002). Importantly, however, the fact has been often underscored that many of the epithelial cell features are also retained even in the most advanced carcinoma specimens. It is of interest that a semi-quantitative scoring system was recently proposed for the evaluation of EMT in epithelial carcinomas; this is represented by the scale of 0 (minimal transition) to 3 (full transition), based on cell polarity, cell cohesiveness, and the expressions of keratin and vimentin filaments (Klymkowsky and Savagner, 2009). The phenotypes of NHERF1-depleted cells in our 3D morphogenesis assay fitted remarkably well in the level 1 category: that “most tumor cells display loss of cell polarity, but retain cohesive cell-cell contacts and keratin expression”.

NHERF1-depleted cells in 3D morphogenesis assay displayed indeed severe loss of cell polarity. In this loss, apical-tight junction markers such as ezrin, aPKC, and ZO-1 were all shifted “inside-out” to the periphery of the cyst structures, whereas basement membrane marker, laminin, was detached from the basal surface out to ECM medium

(see FIGURE 3.43). Somewhat unexpectedly, our results were most comparable with two of those previous studies that addressed the collagen I- β 1-integrin-Rac1 pathway in Madin-Darby canine kidney (MDCK) cells (O'Brien et al., 2001; Yu et al., 2005). In these studies, inhibition of the pathway by the addition of β 1-integrin blocking antibody or by the expression of a dominant negative mutant of Rac1 led to the failure of laminin assembly and, as in our study, resulted in the “inside-out” loss of apical-basal polarity. Although NHERF1, laminin, and the components of the collagen I- β 1-integrin-Rac1 pathway are all too distant from one to another to have direct mechanism of interactions, many possibilities remain open for indirect mechanism. We will first seek the consequence of NHERF1 interaction with PTEN (see FIGURE 3.45-3.46), which itself has been required for the establishment of apical polarity (Martin-Belmonte et al., 2007). This may be, in turn, indirectly involved with Rac1 (Martin-Belmonte and Mostov, 2007).

4.3 NHERF1 loss and ectopic overexpression

Over 90% of adenomas in this study had losses of NHERF1 expression as compared to normal mucosa, yet approximately half of the matched carcinomas had overt NHERF1 overexpression in the cytoplasm (see FIGURE 3.5). It appears that NHERF1 synthesis and/or its degradation is profoundly altered during colorectal tumorigenesis, but the mechanism of this alteration is not presently known. NHERF1 overexpression has been previously reported in several studies of human tumors, namely breast cancer (Cardone et al., 2007; Mangia et al., 2009; Song et al., 2007; Stemmer-Rachamimov et al., 2001), hepatocellular carcinoma (Shibata et al., 2003), and

Schwannoma (Fraenzer et al., 2003). In our cell-based study, NHERF1 overexpression in cells already depleted with NHERF1 conferred additional growth advantage (see FIGURE 3.33-3.35). It is possible that ectopically overexpressed NHERF1 forms a complex in this new compartment with molecule(s) that promotes cell growth. One such candidate is β -catenin, to which NHERF1 associates directly in vivo (Kreimann et al., 2007; Shibata et al., 2003). This idea was supported by our preliminary study which co-immunoprecipitated β -catenin with NHERF1 in CRC cells that expressed NHERF1 in the cytoplasm (data not shown). As also noted in the present study, these two proteins were co-localized in up to one-third of nuclear β -catenin pool in CRC TMA (see FIGURE 3.23).

4.4 Theoretical and clinical considerations

The findings from our study provide several insights to the field of cell biology at large; central to this theme is the role of NHERF1 as a regulator of epithelial morphogenesis. It is striking, even somewhat unexpected, that peripheral presence of this small adaptor protein with no known enzymatic activities has such profound effect on a fundamental cellular process as cell polarization. It is also surprising, though the indications are clear, that there is no functional redundancy for this small yet important protein. Possible answers to these questions may lie in the idea that NHERF1 as a PDZ protein is capable of multimerization (Harris and Lim, 2001), that gives it both complexity and uniqueness of context not easily replicated by even most closely related NHERF family proteins. Another consideration is that many coordinate PDZ proteins are, like NHERF1, targeted to different membrane domains of polarized epithelial cells (Fanning and Anderson, 1999a; Fanning and Anderson, 1999b; Nourry et al., 2003). It

appears that these scaffolds would then functionally interact, and are integrated into a single polarity pathway (Bilder et al., 2003; Tanentzapf and Tepass, 2003). The role of NHERF1 in this pathway remains yet to be uncovered. In this interest, Sip1, a *Drosophila* homolog of NHERF1, was recently identified (Hughes et al., 2010). A possible screening approach for the interacting partners of NHERF1 will be to use the genetic tools available in this *Drosophila* model.

On a more clinical note, EMT that appears to be induced by NHERF1 deficiency can be considered an attractive target for cancer therapy. The traditional expectation would have been that inhibition of EMT might intervene with cancer metastasis and with problematic chemoresistance that is characteristic of this transdifferentiation process (Polyak and Weinberg, 2009). Lately, however, EMT is also increasingly discussed in the context of acquired cell stemness (Brabletz et al., 2005; Mani et al., 2008). Cancer cell stemness by the definition of the term is the cell's ability to seed new tumors (Reya et al., 2001). In this modified term, inhibition of EMT would intervene with tumorigenesis, in fact exactly as we observed in our experimental context.

4.5 Future aims

4.5.1 Mechanism of NHERF1 loss in colorectal tumorigenesis

The mechanism of NHERF1 loss during colorectal tumorigenesis remains unclear. Two scenarios, that this either involves genomic or epigenetic instability, are probably most likely (Grady and Carethers, 2008). It is of our interest that the preliminary sequence analysis of human genomic *NHERF1* (NG_013022) indicated

dense CpG islands in the 5' promoter region (data not shown). This promoter region may be subject to aberrant DNA methylation during colorectal tumorigenesis, as are a panel of other markers that have shown clinical potential in being used non-invasively as fecal DNA-based screening tests (Chan et al., 2002; Li et al., 2003; Petko et al., 2005; Rashid et al., 2001). One might approach this experiment in three ways: first, to verify that NHERF1 silencing does indeed occur epigenetically; that is, silencing occurs at the transcript level and that this involves no changes in the coding region of *NHERF1*. Next, the location of methylated cytosines will be identified in CRC specimens and/or CRC cell lines by bisulfite sequencing. DNA demethylating agent can then be used to treat CRC cells, and changes in cell phenotype to be evaluated.

4.5.2 Role of cytoplasmic and nuclear NHERF1 in colorectal cancer invasion

On the basis of results from histological studies in CRC specimens, we postulate that the cells with nuclear NHERF1 and to a less extent cytoplasmic NHERF1, too, are more invasive, metastatic, and stem-cell like than those without NHERF1 alone. However, in vitro migration and invasion experiments have not been thus far conducive in discriminating NHERF1-depleted cells from those ectopically overexpressing NHERF1 (data not shown). The failure of these experiments might reflect the limitation in sensitivity of these in vitro assays, and/or in difficulty of the cell culture system to adequately reproduce the components of tumor microenvironment. Additional battery of tumorigenesis and metastasis assays will be attempted next, including soft agar assay to examine anchorage-independent growth; implantation and tail vein injection of the cells in immunodeficient mice to examine tumorigenesis and metastasis *in vivo*; and 2D

and/or 3D chemoresistance/apoptosis assay with 5-fluorouracil (5-FU). As we also postulate that nuclear NHERF1 associates with β -catenin to cooperate in the activation of the Wnt/ β -catenin pathway, double-IF staining will be performed to evaluate co-localization between these two proteins. Cell nuclear fraction will be also extracted to evaluate complex formation by co-immunoprecipitation; and TOP/FOP luciferase assay will be performed to evaluate β -catenin-specific transcriptional activity.

4.5.3 Cooperation between NHERF1 and β -catenin in $Apc^{Min/+}$ mouse model

We began to cross C57BL/6J $Apc^{Min/+}$ mice from the Jackson Laboratory with our NHERF1(-/-) mice inbred in the same background. The Min mice develop multiple intestinal neoplasia due to a truncating mutation at T2549A, similarly to those in FAP and sporadic CRC patients, and are thus commonly used as the mouse model of intestinal cancer (Moser et al., 1990; Su et al., 1993). The analysis of the first 53 mice showed that median survival was significantly reduced in NHERF1(-/-)/ $Apc^{Min/+}$ mice as compared to NHERF1(+/-)/ $Apc^{Min/+}$ and NHERF1(+/-)/ $Apc^{Min/+}$ mice (19 vs. 29 and 30 weeks, $P < 0.001$). Efforts are now directed at characterization of the tumor development in these mice by the assessment of location, number, size, grade, and metastatic potential of the tumors. To evaluate also the contribution of the Wnt/ β -catenin pathway to the pathogenesis of these tumors, tissue staining will be performed with Wnt/ β -catenin-specific markers. Tissue will be additionally profiled by the known β -catenin target genes by quantitative RT-PCR of crypt-villus axis fractions.

4.6 Conclusions

This study shows that the development of human CRC is closely associated with progressive changes in the expression of NHERF1 protein (FIGURE 4.1). NHERF1 appears as an important regulator of epithelial morphogenesis when localized at the apical membrane. NHERF1 loss and ectopic expression that induce massive disruption of epithelial polarity may, thereby, contribute to CRC progression. Future studies will aim to clarify the mechanism of NHERF1 downregulation in adenoma, and characterize greater phenotypic details of ectopic NHERF1 overexpression in advanced carcinoma. As part of complementary effort to these, studies are also under way to address the cooperation between NHERF1 deficiency and the Wnt/ β -catenin pathway activation in the Apc^{Min/+} mouse model of colorectal cancer.

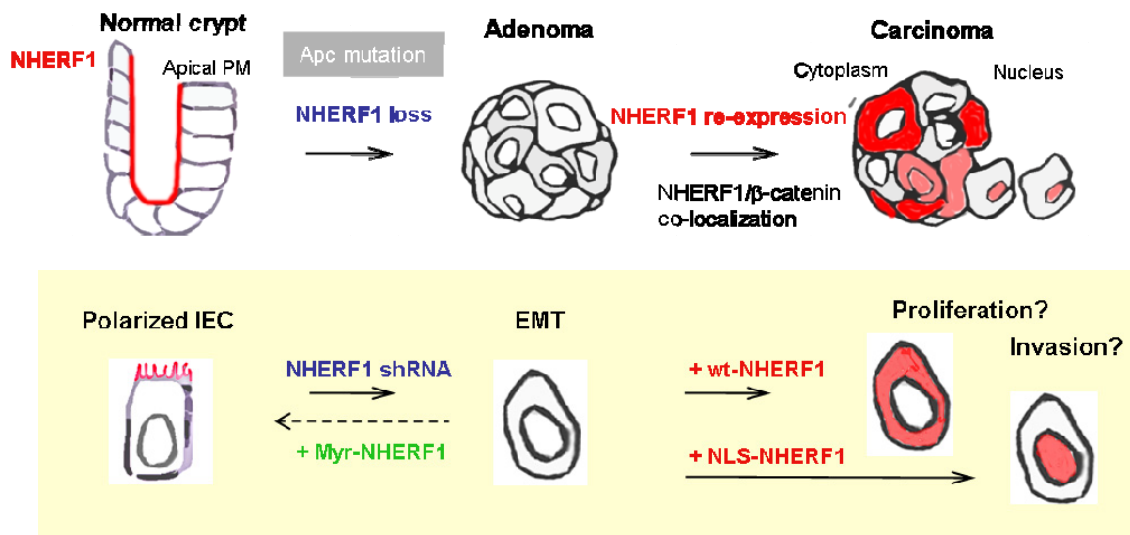


FIGURE 4.1 Model of NHERF1 role in CRC development. Note the initiating loss of NHERF1 from apical plasma membrane in normal colonic mucosa to induce the formation of benign adenoma. Ectopic re-expression of NHERF1 in the cytoplasm and nucleus further promotes CRC progression, possibly through cooperative interaction between NHERF1 and β -catenin. The lower panel scheme depicts the experimental strategies used in this thesis to model NHERF1 loss and re-expression in cultured intestinal epithelial cells (IECs).

REFERENCES

Aranda, V., Nolan, M. E., and Muthuswamy, S. K. (2008). Par complex in cancer: a regulator of normal cell polarity joins the dark side. *Oncogene* 27, 6878-6887.

Armitage, P., and Doll, R. (1954). The age distribution of cancer and a multi-stage theory of carcinogenesis. *Br J Cancer* 8, 1-12.

Ashton-Rickardt, P. G., Dunlop, M. G., Nakamura, Y., Morris, R. G., Purdie, C. A., Steel, C. M., Evans, H. J., Bird, C. C., and Wyllie, A. H. (1989). High frequency of APC loss in sporadic colorectal carcinoma due to breaks clustered in 5q21-22. *Oncogene* 4, 1169-1174.

Bienz, M., and Clevers, H. (2000). Linking colorectal cancer to Wnt signaling. *Cell* 103, 311-320.

Bilder, D., Li, M., and Perrimon, N. (2000). Cooperative regulation of cell polarity and growth by *Drosophila* tumor suppressors. *Science* 289, 113-116.

Bilder, D., Schober, M., and Perrimon, N. (2003). Integrated activity of PDZ protein complexes regulates epithelial polarity. *Nat Cell Biol* 5, 53-58.

Bodmer, W. F., Bailey, C. J., Bodmer, J., Bussey, H. J., Ellis, A., Gorman, P., Lucibello, F. C., Murday, V. A., Rider, S. H., Scambler, P., and et al. (1987). Localization of the gene for familial adenomatous polyposis on chromosome 5. *Nature* 328, 614-616.

- Brabletz, T., Jung, A., Spaderna, S., Hlubek, F., and Kirchner, T. (2005). Opinion: migrating cancer stem cells - an integrated concept of malignant tumour progression. *Nat Rev Cancer* 5, 744-749.
- Bryant, D. M., and Stow, J. L. (2004). The ins and outs of E-cadherin trafficking. *Trends Cell Biol* 14, 427-434.
- Cardone, R. A., Bellizzi, A., Busco, G., Weinman, E. J., Dell'Aquila, M. E., Casavola, V., Azzariti, A., Mangia, A., Paradiso, A., and Reshkin, S. J. (2007). The NHERF1 PDZ2 domain regulates PKA-RhoA-p38-mediated NHE1 activation and invasion in breast tumor cells. *Mol Biol Cell* 18, 1768-1780.
- Cardone, R. A., Casavola, V., and Reshkin, S. J. (2005). The role of disturbed pH dynamics and the Na⁺/H⁺ exchanger in metastasis. *Nat Rev Cancer* 5, 786-795.
- Chan, A. O., Broaddus, R. R., Houlihan, P. S., Issa, J. P., Hamilton, S. R., and Rashid, A. (2002). CpG island methylation in aberrant crypt foci of the colorectum. *Am J Pathol* 160, 1823-1830.
- Dai, J. L., Wang, L., Sahin, A. A., Broemeling, L. D., Schutte, M., and Pan, Y. (2004). NHERF (Na⁺/H⁺ exchanger regulatory factor) gene mutations in human breast cancer. *Oncogene* 23, 8681-8687.
- Donowitz, M., Cha, B., Zachos, N. C., Brett, C. L., Sharma, A., Tse, C. M., and Li, X. (2005). NHERF family and NHE3 regulation. *J Physiol* 567, 3-11.

- Ediger, T. R., Kraus, W. L., Weinman, E. J., and Katzenellenbogen, B. S. (1999). Estrogen receptor regulation of the Na⁺/H⁺ exchange regulatory factor. *Endocrinology* *140*, 2976-2982.
- Fanning, A. S., and Anderson, J. M. (1996). Protein-protein interactions: PDZ domain networks. *Curr Biol* *6*, 1385-1388.
- Fanning, A. S., and Anderson, J. M. (1999a). PDZ domains: fundamental building blocks in the organization of protein complexes at the plasma membrane. *J Clin Invest* *103*, 767-772.
- Fanning, A. S., and Anderson, J. M. (1999b). Protein modules as organizers of membrane structure. *Curr Opin Cell Biol* *11*, 432-439.
- Fearon, E. R., and Vogelstein, B. (1990). A genetic model for colorectal tumorigenesis. *Cell* *61*, 759-767.
- Feigin, M. E., and Muthuswamy, S. K. (2009). Polarity proteins regulate mammalian cell-cell junctions and cancer pathogenesis. *Curr Opin Cell Biol* *21*, 694-700.
- Fouassier, L., Duan, C. Y., Feranchak, A. P., Yun, C. H., Sutherland, E., Simon, F., Fitz, J. G., and Doctor, R. B. (2001). Ezrin-radixin-moesin-binding phosphoprotein 50 is expressed at the apical membrane of rat liver epithelia. *Hepatology* *33*, 166-176.
- Foulds, L. (1954). The experimental study of tumor progression: a review. *Cancer Res* *14*, 327-339.

- Fraenzer, J. T., Pan, H., Minimo, L., Jr., Smith, G. M., Knauer, D., and Hung, G. (2003). Overexpression of the NF2 gene inhibits schwannoma cell proliferation through promoting PDGFR degradation. *Int J Oncol* 23, 1493-1500.
- Georgescu, M. M., Kirsch, K. H., Akagi, T., Shishido, T., and Hanafusa, H. (1999a). The tumor-suppressor activity of PTEN is regulated by its carboxyl-terminal region. *Proc Natl Acad Sci U S A* 96, 10182-10187.
- Georgescu, M. M., Kirsch, K. H., Shishido, T., Zong, C., and Hanafusa, H. (1999b). Biological effects of c-Mer receptor tyrosine kinase in hematopoietic cells depend on the Grb2 binding site in the receptor and activation of NF-kappaB. *Mol Cell Biol* 19, 1171-1181.
- Georgescu, M. M., Morales, F. C., Molina, J. R., and Hayashi, Y. (2008). Roles of NHERF1/EBP50 in cancer. *Curr Mol Med* 8, 459-468.
- Grady, W. M., and Carethers, J. M. (2008). Genomic and epigenetic instability in colorectal cancer pathogenesis. *Gastroenterology* 135, 1079-1099.
- Harris, B. Z., and Lim, W. A. (2001). Mechanism and role of PDZ domains in signaling complex assembly. *J Cell Sci* 114, 3219-3231.
- He, T. C., Sparks, A. B., Rago, C., Hermeking, H., Zawel, L., da Costa, L. T., Morin, P. J., Vogelstein, B., and Kinzler, K. W. (1998). Identification of c-MYC as a target of the APC pathway. *Science* 281, 1509-1512.

- Huang, L., and Muthuswamy, S. K. (2010). Polarity protein alterations in carcinoma: a focus on emerging roles for polarity regulators. *Curr Opin Genet Dev* 20, 41-50.
- Hughes, S. C., Formstecher, E., and Fehon, R. G. (2010). Sip1, the *Drosophila* orthologue of EBP50/NHERF1, functions with the sterile 20 family kinase Slik to regulate Moesin activity. *J Cell Sci* 123, 1099-1107.
- Ingraffea, J., Reczek, D., and Bretscher, A. (2002). Distinct cell type-specific expression of scaffolding proteins EBP50 and E3KARP: EBP50 is generally expressed with ezrin in specific epithelia, whereas E3KARP is not. *Eur J Cell Biol* 81, 61-68.
- Jaffe, A. B., Kaji, N., Durgan, J., and Hall, A. (2008). Cdc42 controls spindle orientation to position the apical surface during epithelial morphogenesis. *J Cell Biol* 183, 625-633.
- Jemal, A., Siegel, R., Ward, E., Hao, Y., Xu, J., and Thun, M. J. (2009). Cancer statistics, 2009. *CA Cancer J Clin* 59, 225-249.
- Klymkowsky, M. W., and Savagner, P. (2009). Epithelial-mesenchymal transition: a cancer researcher's conceptual friend and foe. *Am J Pathol* 174, 1588-1593.
- Korinek, V., Barker, N., Morin, P. J., van Wichen, D., de Weger, R., Kinzler, K. W., Vogelstein, B., and Clevers, H. (1997). Constitutive transcriptional activation by a beta-catenin-Tcf complex in APC^{-/-} colon carcinoma. *Science* 275, 1784-1787.
- Kreimann, E. L., Morales, F. C., de Orbeta-Cruz, J., Takahashi, Y., Adams, H., Liu, T. J., McCrea, P. D., and Georgescu, M. M. (2007a). Cortical stabilization of beta-catenin contributes to NHERF1/EBP50 tumor suppressor function. *Oncogene* 26, 5290-5299.

Kreimann, E. L., Morales, F. C., de Orbeta-Cruz, J., Takahashi, Y., Adams, H., Liu, T. J., McCrea, P. D., and Georgescu, M. M. (2007b). Cortical stabilization of beta-catenin contributes to NHERF1/EBP50 tumor suppressor function. *Oncogene*.

Larue, L., and Bellacosa, A. (2005). Epithelial-mesenchymal transition in development and cancer: role of phosphatidylinositol 3' kinase/AKT pathways. *Oncogene* 24, 7443-7454.

Lee, M., and Vasioukhin, V. (2008). Cell polarity and cancer--cell and tissue polarity as a non-canonical tumor suppressor. *J Cell Sci* 121, 1141-1150.

Lengauer, C., Kinzler, K. W., and Vogelstein, B. (1998). Genetic instabilities in human cancers. *Nature* 396, 643-649.

Leppert, M., Dobbs, M., Scambler, P., O'Connell, P., Nakamura, Y., Stauffer, D., Woodward, S., Burt, R., Hughes, J., Gardner, E., and et al. (1987). The gene for familial polyposis coli maps to the long arm of chromosome 5. *Science* 238, 1411-1413.

Li, H., Myeroff, L., Smiraglia, D., Romero, M. F., Pretlow, T. P., Kasturi, L., Lutterbaugh, J., Rerko, R. M., Casey, G., Issa, J. P., *et al.* (2003). SLC5A8, a sodium transporter, is a tumor suppressor gene silenced by methylation in human colon aberrant crypt foci and cancers. *Proc Natl Acad Sci U S A* 100, 8412-8417.

Lilien, J., and Balsamo, J. (2005). The regulation of cadherin-mediated adhesion by tyrosine phosphorylation/dephosphorylation of beta-catenin. *Curr Opin Cell Biol* 17, 459-465.

Loeb, L. A. (1991). Mutator phenotype may be required for multistage carcinogenesis. *Cancer Res* 51, 3075-3079.

Mangia, A., Chiriatti, A., Bellizzi, A., Malfettone, A., Stea, B., Zito, F. A., Reshkin, S. J., Simone, G., and Paradiso, A. (2009). Biological role of NHERF1 protein expression in breast cancer. *Histopathology* 55, 600-608.

Mani, S. A., Guo, W., Liao, M. J., Eaton, E. N., Ayyanan, A., Zhou, A. Y., Brooks, M., Reinhard, F., Zhang, C. C., Shipitsin, M., *et al.* (2008). The epithelial-mesenchymal transition generates cells with properties of stem cells. *Cell* 133, 704-715.

Martin-Belmonte, F., Gassama, A., Datta, A., Yu, W., Rescher, U., Gerke, V., and Mostov, K. (2007). PTEN-mediated apical segregation of phosphoinositides controls epithelial morphogenesis through Cdc42. *Cell* 128, 383-397.

Martin-Belmonte, F., and Mostov, K. (2007). Phosphoinositides control epithelial development. *Cell Cycle* 6, 1957-1961.

Miyoshi, Y., Nagase, H., Ando, H., Horii, A., Ichii, S., Nakatsuru, S., Aoki, T., Miki, Y., Mori, T., and Nakamura, Y. (1992). Somatic mutations of the APC gene in colorectal tumors: mutation cluster region in the APC gene. *Hum Mol Genet* 1, 229-233.

Morales, F. C., Takahashi, Y., Kreimann, E. L., and Georgescu, M. M. (2004). Ezrin-radixin-moesin (ERM)-binding phosphoprotein 50 organizes ERM proteins at the apical membrane of polarized epithelia. *Proc Natl Acad Sci U S A* 101, 17705-17710.

- Morin, P. J., Sparks, A. B., Korinek, V., Barker, N., Clevers, H., Vogelstein, B., and Kinzler, K. W. (1997). Activation of beta-catenin-Tcf signaling in colon cancer by mutations in beta-catenin or APC. *Science* 275, 1787-1790.
- Moser, A. R., Pitot, H. C., and Dove, W. F. (1990). A dominant mutation that predisposes to multiple intestinal neoplasia in the mouse. *Science* 247, 322-324.
- Mullin, J. M. (2004). Epithelial barriers, compartmentation, and cancer. *Sci STKE* 2004, pe2.
- Munemitsu, S., Albert, I., Souza, B., Rubinfeld, B., and Polakis, P. (1995). Regulation of intracellular beta-catenin levels by the adenomatous polyposis coli (APC) tumor-suppressor protein. *Proc Natl Acad Sci U S A* 92, 3046-3050.
- Murthy, A., Gonzalez-Agosti, C., Cordero, E., Pinney, D., Candia, C., Solomon, F., Gusella, J., and Ramesh, V. (1998). NHE-RF, a regulatory cofactor for Na(+)-H+ exchange, is a common interactor for merlin and ERM (MERM) proteins. *J Biol Chem* 273, 1273-1276.
- Nelson, W. J., and Nusse, R. (2004). Convergence of Wnt, beta-catenin, and cadherin pathways. *Science* 303, 1483-1487.
- Nolan, M. E., Aranda, V., Lee, S., Lakshmi, B., Basu, S., Allred, D. C., and Muthuswamy, S. K. (2008). The polarity protein Par6 induces cell proliferation and is overexpressed in breast cancer. *Cancer Res* 68, 8201-8209.

Nourry, C., Grant, S. G., and Borg, J. P. (2003). PDZ domain proteins: plug and play! *Sci STKE* 2003, RE7.

O'Brien, L. E., Jou, T. S., Pollack, A. L., Zhang, Q., Hansen, S. H., Yurchenco, P., and Mostov, K. E. (2001). Rac1 orientates epithelial apical polarity through effects on basolateral laminin assembly. *Nat Cell Biol* 3, 831-838.

Pan, Y., Wang, L., and Dai, J. L. (2006). Suppression of breast cancer cell growth by Na⁺/H⁺ exchanger regulatory factor 1 (NHERF1). *Breast Cancer Res* 8, R63.

Petko, Z., Ghiassi, M., Shuber, A., Gorham, J., Smalley, W., Washington, M. K., Schultenover, S., Gautam, S., Markowitz, S. D., and Grady, W. M. (2005). Aberrantly methylated CDKN2A, MGMT, and MLH1 in colon polyps and in fecal DNA from patients with colorectal polyps. *Clin Cancer Res* 11, 1203-1209.

Polakis, P., Hart, M., and Rubinfeld, B. (1999). Defects in the regulation of beta-catenin in colorectal cancer. *Adv Exp Med Biol* 470, 23-32.

Polyak, K., and Weinberg, R. A. (2009). Transitions between epithelial and mesenchymal states: acquisition of malignant and stem cell traits. *Nat Rev Cancer* 9, 265-273.

Powell, S. M., Zilz, N., Beazer-Barclay, Y., Bryan, T. M., Hamilton, S. R., Thibodeau, S. N., Vogelstein, B., and Kinzler, K. W. (1992). APC mutations occur early during colorectal tumorigenesis. *Nature* 359, 235-237.

Rashid, A., Shen, L., Morris, J. S., Issa, J. P., and Hamilton, S. R. (2001). CpG island methylation in colorectal adenomas. *Am J Pathol* 159, 1129-1135.

Reczek, D., Berryman, M., and Bretscher, A. (1997). Identification of EBP50: A PDZ-containing phosphoprotein that associates with members of the ezrin-radixin-moesin family. *J Cell Biol* 139, 169-179.

Reczek, D., and Bretscher, A. (1998). The carboxyl-terminal region of EBP50 binds to a site in the amino-terminal domain of ezrin that is masked in the dormant molecule. *J Biol Chem* 273, 18452-18458.

Regala, R. P., Weems, C., Jamieson, L., Khor, A., Edell, E. S., Lohse, C. M., and Fields, A. P. (2005). Atypical protein kinase C iota is an oncogene in human non-small cell lung cancer. *Cancer Res* 65, 8905-8911.

Reya, T., Morrison, S. J., Clarke, M. F., and Weissman, I. L. (2001). Stem cells, cancer, and cancer stem cells. *Nature* 414, 105-111.

Saotome, I., Curto, M., and McClatchey, A. I. (2004). Ezrin is essential for epithelial organization and villus morphogenesis in the developing intestine. *Dev Cell* 6, 855-864.

Saras, J., and Heldin, C. H. (1996). PDZ domains bind carboxy-terminal sequences of target proteins. *Trends Biochem Sci* 21, 455-458.

Shenolikar, S., Voltz, J. W., Cunningham, R., and Weinman, E. J. (2004). Regulation of ion transport by the NHERF family of PDZ proteins. *Physiology (Bethesda)* 19, 362-369.

Shenolikar, S., Voltz, J. W., Minkoff, C. M., Wade, J. B., and Weinman, E. J. (2002). Targeted disruption of the mouse NHERF-1 gene promotes internalization of proximal tubule sodium-phosphate cotransporter type IIa and renal phosphate wasting. *Proc Natl Acad Sci U S A* 99, 11470-11475.

Shibata, T., Chuma, M., Kokubu, A., Sakamoto, M., and Hirohashi, S. (2003). EBP50, a beta-catenin-associating protein, enhances Wnt signaling and is over-expressed in hepatocellular carcinoma. *Hepatology* 38, 178-186.

Solomon, E., Voss, R., Hall, V., Bodmer, W. F., Jass, J. R., Jeffreys, A. J., Lucibello, F. C., Patel, I., and Rider, S. H. (1987). Chromosome 5 allele loss in human colorectal carcinomas. *Nature* 328, 616-619.

Song, J., Bai, J., Yang, W., Gabrielson, E. W., Chan, D. W., and Zhang, Z. (2007). Expression and clinicopathological significance of oestrogen-responsive ezrin-radixin-moesin-binding phosphoprotein 50 in breast cancer. *Histopathology* 51, 40-53.

Stemmer-Rachamimov, A. O., Wiederhold, T., Nielsen, G. P., James, M., Pinney-Michalowski, D., Roy, J. E., Cohen, W. A., Ramesh, V., and Louis, D. N. (2001). NHERF, a merlin-interacting protein, is primarily expressed in luminal epithelia, proliferative endometrium, and estrogen receptor-positive breast carcinomas. *Am J Pathol* 158, 57-62.

Su, L. K., Vogelstein, B., and Kinzler, K. W. (1993). Association of the APC tumor suppressor protein with catenins. *Science* 262, 1734-1737.

Tanentzapf, G., and Tepass, U. (2003). Interactions between the crumbs, lethal giant larvae and bazooka pathways in epithelial polarization. *Nat Cell Biol* 5, 46-52.

Tetsu, O., and McCormick, F. (1999). Beta-catenin regulates expression of cyclin D1 in colon carcinoma cells. *Nature* 398, 422-426.

Thiery, J. P. (2002). Epithelial-mesenchymal transitions in tumour progression. *Nat Rev Cancer* 2, 442-454.

Vogelstein, B., Fearon, E. R., Hamilton, S. R., Kern, S. E., Preisinger, A. C., Leppert, M., Nakamura, Y., White, R., Smits, A. M., and Bos, J. L. (1988). Genetic alterations during colorectal-tumor development. *N Engl J Med* 319, 525-532.

Vogelstein, B., and Kinzler, K. W. (1993). The multistep nature of cancer. *Trends Genet* 9, 138-141.

Wade, J. B., Liu, J., Coleman, R. A., Cunningham, R., Steplock, D. A., Lee-Kwon, W., Pallone, T. L., Shenolikar, S., and Weinman, E. J. (2003). Localization and interaction of NHERF isoforms in the renal proximal tubule of the mouse. *Am J Physiol Cell Physiol* 285, C1494-1503.

Wade, J. B., Welling, P. A., Donowitz, M., Shenolikar, S., and Weinman, E. J. (2001). Differential renal distribution of NHERF isoforms and their colocalization with NHE3, ezrin, and ROMK. *Am J Physiol Cell Physiol* 280, C192-198.

Waite, K. A., and Eng, C. (2002). Protean PTEN: form and function. *Am J Hum Genet* 70, 829-844.

Walsh, J. M., and Terdiman, J. P. (2003). Colorectal cancer screening: scientific review. *JAMA* 289, 1288-1296.

Weinman, E. J., Hall, R. A., Friedman, P. A., Liu-Chen, L. Y., and Shenolikar, S. (2006). The association of NHERF adaptor proteins with g protein-coupled receptors and receptor tyrosine kinases. *Annu Rev Physiol* 68, 491-505.

Weinman, E. J., Steplock, D., and Shenolikar, S. (1993). CAMP-mediated inhibition of the renal brush border membrane $\text{Na}^+\text{-H}^+$ exchanger requires a dissociable phosphoprotein cofactor. *J Clin Invest* 92, 1781-1786.

Weinman, E. J., Steplock, D., and Shenolikar, S. (2003). NHERF-1 uniquely transduces the cAMP signals that inhibit sodium-hydrogen exchange in mouse renal apical membranes. *FEBS Lett* 536, 141-144.

Weinman, E. J., Steplock, D., Wang, Y., and Shenolikar, S. (1995). Characterization of a protein cofactor that mediates protein kinase A regulation of the renal brush border membrane $\text{Na}^+\text{-H}^+$ exchanger. *J Clin Invest* 95, 2143-2149.

Yeatman, T. (2003). Colon cancer. In *Encyclopedia of Life Sciences*, (John Wiley & Sons, Ltd.).

Yu, W., Datta, A., Leroy, P., O'Brien, L. E., Mak, G., Jou, T. S., Matlin, K. S., Mostov, K. E., and Zegers, M. M. (2005). Beta1-integrin orients epithelial polarity via Rac1 and laminin. *Mol Biol Cell* 16, 433-445.

Yun, C. H., Lamprecht, G., Forster, D. V., and Sidor, A. (1998). NHE3 kinase A regulatory protein E3KARP binds the epithelial brush border $\text{Na}^+\text{/H}^+$ exchanger NHE3 and the cytoskeletal protein ezrin. *J Biol Chem* 273, 25856-25863.

Zen, K., Yasui, K., Gen, Y., Dohi, O., Wakabayashi, N., Mitsufuji, S., Itoh, Y., Zen, Y., Nakanuma, Y., Taniwaki, M., *et al.* (2009). Defective expression of polarity protein PAR-3 gene (PARD3) in esophageal squamous cell carcinoma. *Oncogene* 28, 2910-2918.